Final Report

Hydrologic and hydraulic modeling for floodplain inundation mapping under future climate change scenarios: A case study of Tawi River, India

NATIONAL INSTITUTE OF HYDROLOGY

Western Himalayan Regional Centre

Irrigation and Flood Control Complex,

Satwari, Jammu Cantt. Jammu -180003

May 2022

PREFACE

The Tawi River basin is continuously subjected to water related disaster such as heavy torrential rainstorms, frequent cloud bursts along with its high precipitous relief. Most recently, the high flood event of September 2014 was perhaps unique and unprecedented in terms of the colossal damages it had caused to the life and property. This flood event triggered government and civil organizations to plan better flood management as well reduction strategies to fight water-related disasters in the Tawi River basin under glooming future climate change scenarios.

Therefore, the need of hour is to come with promising scientific tools to assist in planning of efficient water-related disasters management and reduction strategies. In this context, the present study entitled as "Hydrologic and hydraulic modeling for floodplain inundation mapping under future climate change scenarios: A case study of Tawi River, India" which attempt to develop the flood inundation and hazard maps for Tawi river basin using well accepted physically based hydrological and hydraulic modelling tools like HEC-HMS and HEC-RAS etc. and the GIS based flood mapping techniques using satellite data products under future climate change scenarios is very essential as well as important.

We are grateful to Indus Basin Organization, (IBO) Central Water Commission (CWC), Chandigarh, CWC Jammu, Indian Meteorological Department, Srinagar & Jammu, Jammu & Kashmir Water Resources Regulatory Authority, Jammu (JKWRRA), Irrigation & Flood Control Department (IFCD), Jammu, Jammu Development Authority for providing the necessary hydro-meteorological data to conduct this study. We are grateful to Sh. G. S. Jha, Chairman, JKWRRA, Sh. Shiv Nandan Kumar, Chief Engineer, IBO, CWC, Chandigarh, Dr. Mahender Singh, Senior Scientist, Sher-e-Kashmir University of Agricultural Sciences and Technology Jammu, Sh. Ravi Ranjan, Director, CWC, Jammu, Sh. Sonam Lotus, Director, Meteorological Centre, IMD Srinagar, Sh. Rishi Kumar, Dy. Director, CWC, Jammu sh. V. K. Pandita, CWC Jammu for providing fruitful suggestion and healthy discussions during this study.

This report has been prepared by Dr. Ravindra V. Kale, Scientist D, WHRC, NIH Jammu, and Dr. P. G. Jose, Scientist D, WHRC, NIH Jammu.

(Jaivir Tyagi)

DIRECTOR

ABSTRACT

The Tawi River basin is continuously subjected to water related disaster such as heavy torrential rainstorms, frequent cloud bursts along with its high precipitous relief. The historic record of floods occurred over Jammu and Kashmir region indicates that this region is subjected to eight severe flood events in the 20th century while in last 18 years period the region has witnessed major seven floods' events. This fact clearly brought out the role of changing climate pattern and its impact on occurrence of severe flood events in this region with increased frequency. This is particularly true about possible changes at a regional or local level and changes in the climate extremes that produce catchment flooding. Such changes might include more frequent short-duration, high-intensity rainfall (i.e., cloud burst events) or more frequent periods of long-duration and widespread sustained rainfall. In order to assess the flood risk due to uncertain climatic conditions, there is a need to study the climate change impacts on future floods by using improved modelling capabilities and climate change scenarios. Particularly in the Tawi River basin, recently an unprecedented, widespread and long duration sustained high rainfall occurred in year 2014. This precipitation event proved to be triggering event which triggered government and civil organizations to plan better flood assessment and management as well reduction strategies to fight water-related disasters in the Tawi River basin under glooming future climate change scenarios.

To address these issues, this study has been taken up with following objectives: (i) To set-up HEC-HMS model for the Tawi River basin for the rainfall-runoff simulation (ii) To set-up HEC-RAS model for the Tawi River basin for flood inundation mapping (iii) Flood frequency analysis for the Tawi River basin under current climatic conditions (iv) Assessment of flood inundation under current and changing climatic conditions.

The HEC-HMS modelling schematic is prepared to simulate the runoff at three G&D namely Udhampur (Salmay Bridge), Sidhara (Jammu) and Jammu (Bikram Chowk) stations as well as other subbasins up to the Jammu (Bikram Chowk bridge) G&D station. During calibration, the simulated hourly flood hydrographs (e.g. High flood event of September 2014) by developed event-based HEC-HMS model for the Tawi basin up to Jammu (Bikram Chowk) gauging station were very well comparable with the observed flood hydrographs. The performance of the event-based HEC-HMS model in simulation of discharge and stage hydrographs using various performance criteria like NSE, R^2, RMSE, PBIAS, Error in peak discharge estimation (%) and Error in time to peak (hr) was found to be very good. As during calibration, the observed and computed peak discharges were 12569 m^3/s & 12201 m^3/s (E_p=

3.9% & E_{pt}= -0.16%, NSE = 0.79, R^2 = 0.86, RMSE = 0.47 and PBIAS = 36.48%), and 13552.4 m^3/s and 12232 m^3/s (E_p= 10.8%, E_{pt}= -0.83 hr, NSE = 0.82, R^2 = 0.87, RMSE = 0.42 and PBIAS = 28.55%), respectively at Udhampur (Salmay Bridge), Sidhara (Jammu) and Jammu (Bikram Chowk) gauging stations. During validation, performance of calibrated event-based HEC-HMS model for Tawi River basin in was verified by comparing the simulated discharge and stage hydrograph with observed discharge and stage hydrographs at Sidhara (Jammu) gauging station for the 1-10 August 2016 flood event and the model performance was found to very good in simulation of discharge hydrograph and good in stage hydrograph. Although, the event-based HEC-HMS model evaluated with 2.76-time higher flood peak (6th September, 2014), it is performed very well in production of hydrograph shape as well as all other required parameters of performance evaluation criteria.

Further, the steady state HEC-RAS model was set-up to obtain flood inundation mapping in lower Tawi basin downstream of the Sidhara G&D site up to its confluence with Chenab just upstream of Marla Barrage using Energy Equations. It was found that for September 2014 high flood event, the total inundated flood depth was varying between 0 to 12.64 m including depth in the river. The flood inundation depth over the flood plain area varying between 0 to 8.3 m with maximum flood height observed at Indo-Pak border region.

Flood Frequency Analysis (FFA) were conducted at Bikram chowk, Sidhara and Salmay Bridge G&D stations using nine types of the frequency distribution recommended in the CWC guidelines. Based on the results of the FFA, the flood inundation map for different return year period were obtained using the developed HEC-RAS model for the Tawi river basin. Further, NEX-GDDP and COREDEX RCM datasets were used to generate future scenarios using Climate Perturbation Tool. Based on this analysis, it was found that winter precipitation will increase by 25 to 50% as predicted by all the RCMs considered. To analyze future flood under climate change impact, four scenarios with 5% (CC5), 15% (CC15), 25% (CC25) and 35% (CC35) increase in the extreme rainfall event assuming baseline period event of September 2014 were considered for simulation of flood hydrographs using event-based HEC-HMS model. The obtained future extreme floods for climate change scenarios CC5, CC15, CC25 and CC35 were used as input in the HEC-RAS model to generate future flood inundation depth map and flood hazard maps for lower Tawi basin downstream of the Sidhara gauging station.

Table of Contents

List of Figures

List of Tables

1 INTRODUCTION

1.1 General

Floods are the most common natural disasters that often cause significant economic losses, and human and social tragedies. In the recent years, the flood management challenges have been raised multidimensionally with unprecedented climate change and land use change issues. Staggered development in flood plain and changing climate pattern resulting in the exponential increase in inundation of flood plain and associated risks due to increased potential floods. The analysis of the climate change impact on flood frequency represents an important issue for water resources management and flood risk mitigation. Global warming is predicted to cause significant changes to the world's climate, but uncertainties remain about the precise nature of these changes. This is particularly true with regard to possible changes at a regional or local level and to changes in the climate extremes that produce catchment flooding. Such changes might include more frequent short-duration, high-intensity rainfall (i.e. cloud burst events) or more frequent periods of long-duration and widespread sustained rainfall. In order to assess the flood risk due to uncertain climatic conditions, there is a need to study the climate change impacts on future floods by using improved modelling capabilities and climate change scenarios.

Recently, over the J&K State and particularly in the Tawi River basin, an unprecedented, widespread and long duration sustained high rainfall occurred in year 2014. This precipitation event proved to be triggering event to relook at flood assessment and mitigation strategies in the Indus River basin and particularly, in the Tawi river basin. As per the information from Government records suggest that 6th September 2014 flood event in the Tawi river basin caused death of around 190 peoples, full damage of 9814 residential houses and partial damage to 23763 residential houses in Jammu region. Over 234 relief camps were set up in the state and 23900 people were rehabilitated from the Jammu region only. Again, on 8th August 2016, a continuous heavy rain caused flash floods in Jammu region. During floods in the Tawi River, it receives heavy rainfall and causing its water to flow above danger mark at some areas. The local area in the Jammu city and BSF troops and their posts at boarder area suffers due to heavy floods.

1.2 The Scope of the Study

The demarcation of flood prone areas has wide range of applications, ranging from engineering to climate change studies, and for planning of effective emergency response activities. Information about potential changes to flood risk is valuable to a range of decision makers confronted with mitigation and/or adaptation options. At the catchment scale, it is crucial to water resources managers who may be responsible for conserving water resources while mitigating the effects of heavy rainfall events. At the metropolitan scale, information about flood risks is crucial to local planners who must consider the vulnerability of increased population and assets located in flood-prone areas.

The flood projections studies include large number of challenges such as sparse observations make statistical methods application difficult, significant uncertainties can arise due to a wide range of climate model projections at regional scales, there are additional uncertainties associated with downscaling techniques that are used to transform the model outputs into usable information at smaller (i.e. catchment) scales and also the hydrological models that are used to transform rainfall estimates into flow estimates are imperfect, and therefore increase the level of uncertainty. Although, projections of extreme rainfall and future flooding are one of the most challenging areas, however, the spread of possible outcomes is large. Considering all above points, in this study, an attempt will be made to describe an integrated hydrological and hydraulic modeling approach for the assessment of flood-prone areas as well as the potential changes in the flood inundation for Tawi River basin up to Indian border by combining the evidence for recent trends in extreme weather events with the projections of climate models.

1.3 The Objectives of the Study

This study has been taken up with following objectives

a. To set-up well known hydrological model such as HEC-GeoHMS for the Tawi River basin for the rainfall-runoff simulation
b. To set-up river hydraulic model such as HEC-RAS for the Tawi River basin for flood inundation mapping
c. Flood frequency analysis for the Tawi River basin under current and changing climatic conditions
d. Assessment of flood inundation under current and changing climatic conditions.

2 STUDY AREA

2.1 General

The Tawi River is an important tributary of the Chenab River in the Western Himalayan region. Tawi river originates from the lap of Kailash Kund glacier and adjoining area southwest of Bhadarwah in Doda district of the Union Territory of Jammu and Kashmir, India. The catchment area of the Tawi river basin is bounded by latitude 32° 35' 20"-33° 6' 6" N and longitude 74° 29' 8"-75° 40' 54" E which varies between 239 and 4331 m as illustrated in Figure 2.1. The total catchment area up to its confluence with the Chenab River is around 2964 km². In Indian territory, this river basin falls in the districts of Jammu, Udhampur and a small part of Doda. The length of Tawi river is about 141 km. This basin has an elongated shape in the upper part while it is broad circular shaped in the lower part. This river basin is characterized by rugged mountainous topography in the upper reaches while its lower reaches consist of low hills and aggradational plains. The river in general flows through steep hills on either side excepting the lower reach for about 35 km. The river is about 300 m (980 ft) wide at the bridge in Jammu city. The slope of the basin is from east to west in the upper part and northeast to southwest in the lower part. Being a mountainous river Tawi has more than 2000 numbers of tributaries and sub-tributaries. However, there are nine numbers of predominant tributaries of the river Tawi. The Tawi River is comprised of streams of 1-6 orders.

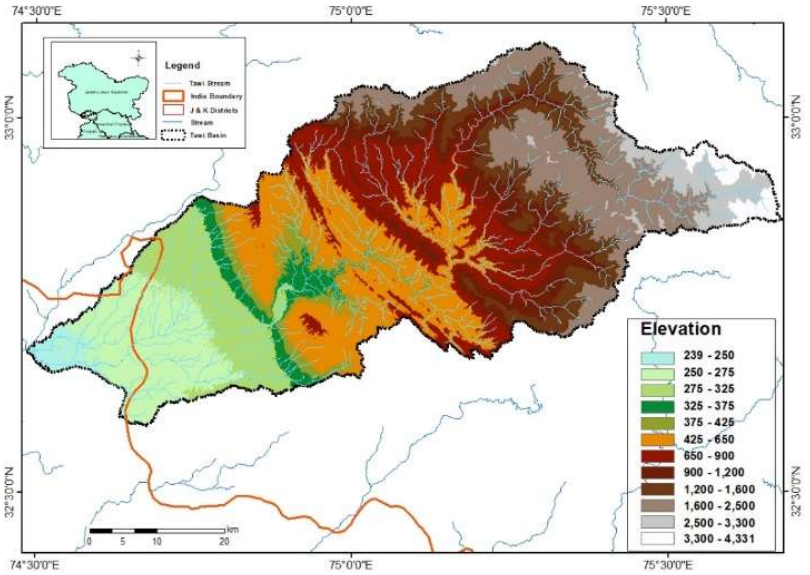

Figure 2.1 Location map of Tawi River basin up to its confluence with Chenab River.

2.2 Climatology and Physiology

In this section the information climatic condition, soil, LULC and catchment physiology is described.

2.2.1 Climate

The Tawi River basin is mainly falling under a subtropical monsoonal climate regime. The summer monsoon is more active in the plains, while winter monsoon rainfall is received in the hilly terrains. Near its origin, only a small portion of Tawi catchment is snow fed. The middle portion of the Tawi River records the heaviest rainfall over the catchments. The annual rainfall varies from 900 to 1900 mm. The summer monsoon is more active in the plains, while winter monsoon rainfall is received in the hilly terrains. The average annual rainfall is 926 mm in the mountainous terrain of Bhaderwah town 1490.33 mm in the hilly terrain of Udhampur (CGWB, 2014), and 1116 mm over the Jammu plains (Ray et al., 2015).

2.2.2 Elevation and Slope

A majority of the terrain of the Tawi catchment consists of hilly tract becoming plain areas after Jammu town and before its confluence with the Chenab River. As shown in Figure 2.1, the elevation of Tawi ranges between 239 m at confluence to 4331 m at its origin. The catchment area covered in different elevation band is presented in Table 2.1. As it is well known fact that the elevation plays a very important and effective role in flood susceptibility. The lower the elevation is more likely the area is to be flooded, as low-lying areas are the points of convergence of the various rivers. According to several literature, it has been found that elevation is the most dominating factor that directs flood occurrence. Because of the gravitational force, water moves rapidly moves from upland to lowland areas and the water gets spread over the lower elevated plains and causes inundation. Although the variation of relief in Tawi basin is 239 to 4330 m. But about 70% of the total area falls under an altitude of 1200 m in including around 20.2% below 325 m elevation, and around 28% of area falls under and altitude of range 1200-3300m and less than 2% of area have altitude greater than 3300m.

Slopes influence surface runoff and rainwater infiltration. Areas having low slopes can have flood more quickly because of the low surface runoff velocity. Areas with high slopes, on the other hand, have high runoff velocity that is incompatible with flooding. Surface runoff and water accumulation process in any geomorphic setting relies upon its

surface slope appropriation. The slope map of Tawi river basin is presented in Figure 2.2. In the Tawi basin region, very high and continuous regional slope is found along the upper region of the basin which mainly lies in Udhampur area while the slope in low-laying areas have less value which indicates large area prone to flood as for most of Jammu region as slope varies from 0 to 6.62. In the Tawi basin, we have slope divided the into five classes on the basis of equal intervals (see Figure 2.2). The range of slope varies from 0 to 1.43, 1.44 to 6.31, 6.32 to 12, 12.1 to 19.5 and 19.6 to 70.4.

Table 2.1 *Area covered under different elevation band in the Tawi River basin.*

Elevation Band	Catchment Area (km^2)	Percentage of total area (%)
0-239	0.00	0.00
239-275	348.45	12.20
275-325	231.02	8.09
325-375	96.23	3.37
375-425	96.58	3.38
425-650	546.46	19.13
650-900	407.77	14.27
900-1200	245.05	8.58
1200-1600	277.56	9.71
1600-2500	440.45	15.42
2500-3300	117.43	4.11
3300-4330	50.09	1.75

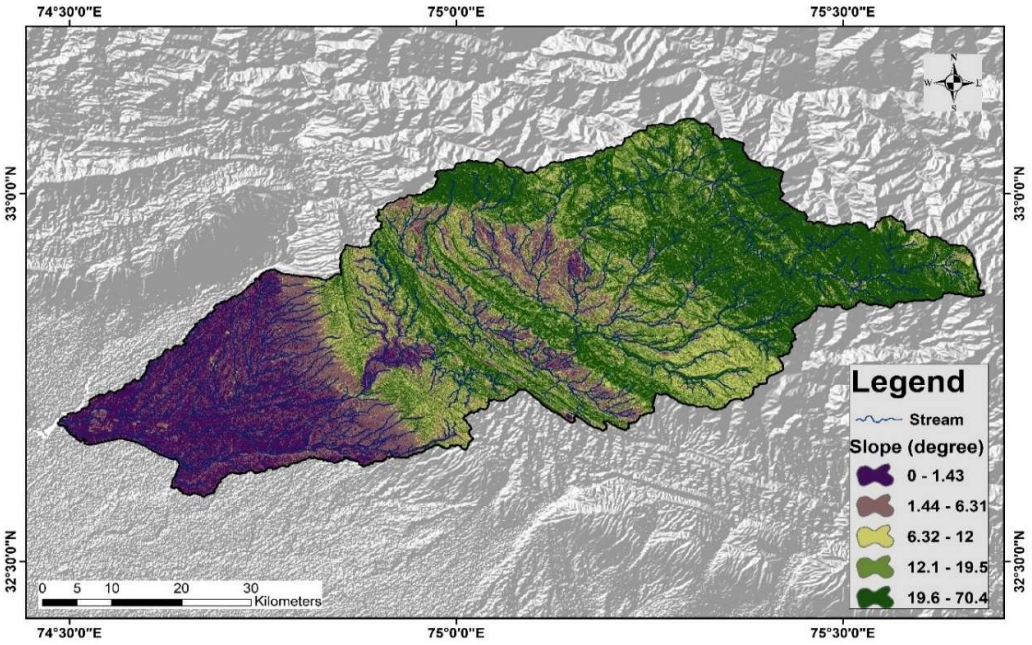

Figure 2.2 Slope map of Tawi River basin up to its confluence with Chenab River.

2.2.3 Soil

The soil texture has great control over the infiltration mechanism. In general, soil composed of a large proportion of fine particles has higher runoff generation as water can't infiltrate through the fine pores. The soil texture map of Tawi river basin is presented in Figure 2.3. It can be seen that there are eight major soil textures classes in Tawi basin which are as follows: 1. Dystric Eutrochrepts, 2. Udic Ustochrepts, 3. Fluventic Ustochrepts 4. Typic Ustifluvents 5. Typic Udorthents 6. Typic Eutrochrepts 7. Lithic Udorthents 8. Lithic Hapludolls.

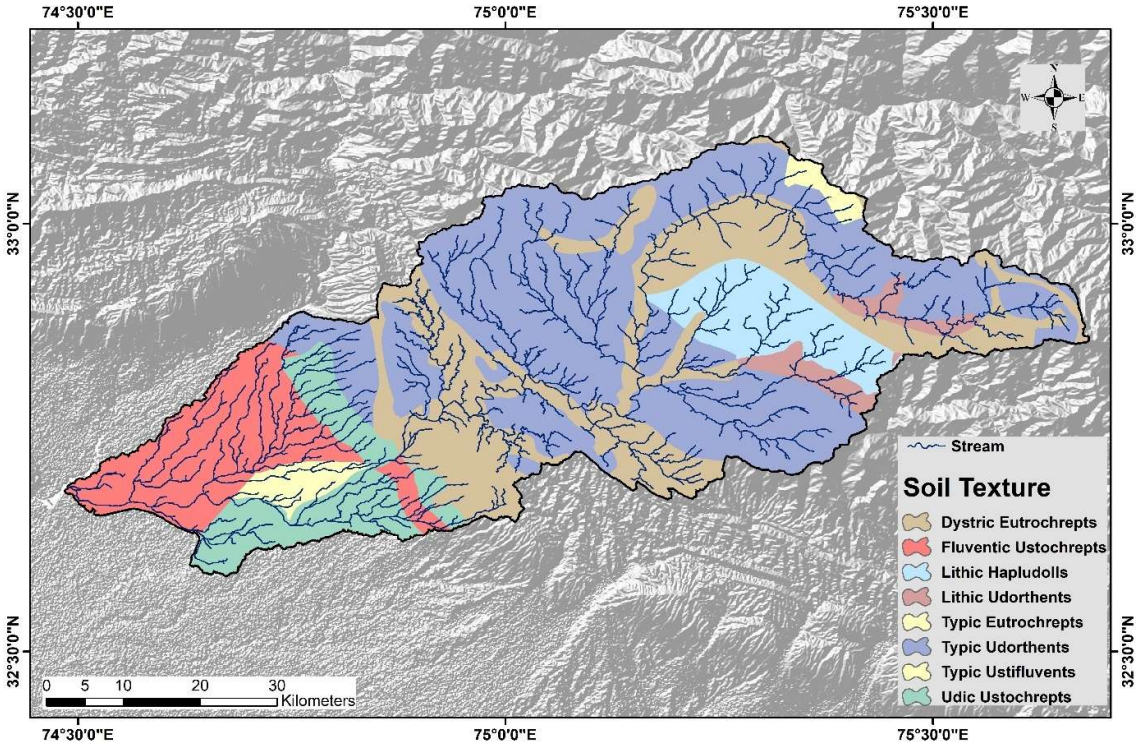

Figure 2.3 Soil texture map of Tawi River basin up to its confluence with Chenab River.

2.2.4 Land Use Land Cover

The land-use pattern of an area plays an important role in hydrological processes such as surface runoff, rate of infiltration, and evapotranspiration. As a result of this, in flood susceptibility mapping this is considered as one of the important parameters. The Land use land cover map prepared for year 2014 using Landsat 8 imagery data by supervised classification approach for the study area is shown in Figure 2.4. It can be seen that, the major land-use in the study area are river, settlement, forest, snow, agriculture and wasteland. The percentage area under each class is presented in Table 2.2.

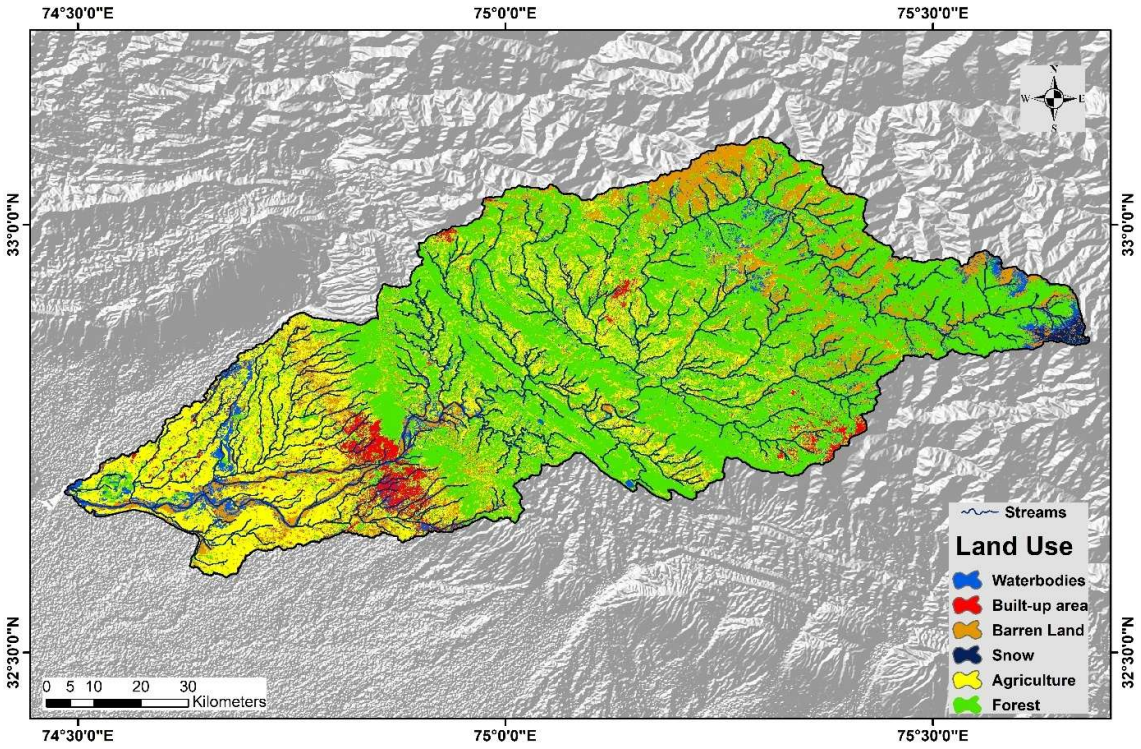

Figure 2.4 Land use land cover map of Tawi River basin up to its confluence with Chenab River.

Table 2.2 Percentage of catchment area covered under each LLUC class in the Tawi River basin.

S.NO	Class	Catchment area	Area percentage (%)
1	Waterbodies	226.06	7.63
2	Build-up area	79.37	2.68
3	Forest	1442.12	48.66
4	Snow	12.54	0.42
5	Agriculture	796.51	26.87
6	Barren Land	407.21	13.74

2.2.5 Catchment Physiology

Tawi river basin consists mainly of metamorphic terrain in the higher reaches associated with granite intrusions and sedimentary rocks in the lower reaches. The Tawi catchments have three meso-geomorphic regions; the upper one is in the north of the Panjal Thrust with a maximum elevation of 4331m, the middle one is between the Panjal thrust to the Udhampur thrust with an elevation of 700 m to 1900 m and the lower one is comprised of low-lying hillocks between Udhampur and Jammu. Table 2.3 details the major nallahs draining the Tawi River basin.

Table 2.3 The major nallahs in Tawi River Basin

Sr. No.	Major Nallah	Catchment Area (Km^2)	Approx. Length (Km)	Source	Confluence point	Gradient
1	Duddar	275	34	Near Ladda mountain	With Tawi at Sunal	Upper steep Valley up to 11%; Near Jasdar Kote reduces to around 2% with is constant and continuous up to the confluence point
2	Ramnagar Wali Khad	487	31.5	Up to Resian	With left bank of Tawi near Dchhapar	Upper extremely Steep up to 18% which reduces to 2% up to the confluence
3	Gambir	112	17	In Rang mountain (near Thial village)	With right bank of Tawi near Kothar	Average of 1.5%
4	Jhajjar	148	30.5	Near Kothri	With right bank of Tawi near Kanalah	Upper steep Valley up to 18% along 2 Km; Middle steep sloping valley with 6% gradient up to Chandwa/ Talen and from d/s of Talen relatively constant gradient of 1% along 20 Km up to confluence point
5	Sardan	87	17.5	Near Sagon	With left bank of Tawi near Bhed Gran village	Average of 1.0%
6	Ballini	97	23	Near Bamyal village	With right bank of Tawi near Nagrota	Along upper approx. 2 Km stretch 2% and afterward nearly constant slope of 0.8% up to confluence
7	Chirwa	37	13	Near Pangali	With right bank of Tawi near Nandor	Upper valley with 1.6 % from source to Jagti village and afterward nearly constant slope of

						0.8% up to confluence
8	Sohagni	320	28.5	Near Bhata	With right bank of Waddi Tawi near just upstream of LOC	Along upper approx. 6 Km stretch 4% and afterward nearly constant slope of 0.4 % up to confluence
9	Balole	155	30.5	Near Deawan	With left bank of Nikki Tawi near Sapuran Pur (Around 9 Km upstream of LOC)	Upper steep valley with 3% gradient (from source to 1.5 Km d/s); Middle steep valley with average 0.6% up to Bandurakh; and from d/s of Bandurakh relatively constant gradient of 0.2 % along 15 Km up to confluence point

2.3 Data procurement / collection

For flood inundation study, the different datasets used in this work can be categorised as elevation datasets, stage-discharge data at different gauging stations, meteorological data of historical, present and future period, soil and land use-land cover information.

In the present study, the five freely available DEM datasets with different spatial resolution namely ASTER 30 m, SRTM 30 m, ALOS (AW3D30) 30 m, CartoDEM 30 m and ALOS PALSAR – RTC 12.5 m have been used. It is well accepted that different indicators of the drainage network give an inference about the basin's hydrological and geological characteristics (Singh et al. 2013). Therefore, these DEMs have been investigated by extracting geometric features like tributaries and topographic features and estimation of various drainage morphometric parameters. The drainage network extracted by using these DEM datasets is compared with those of the topographic map by Survey of India (SoI) LULC map and with google earth maps. The main characteristics of all the above-mentioned DEM datasets are provided briefly in the following section.

- **ASTER DEM with 30 m resolution**: ASTER Global Digital Elevation Model first version (GDEM-V1) with 30 m resolution and absolute accuracy of 20 m (95% confidence interval) were released in 2009. The second version (GDEM-V2) was released in 2011 and the third version (GDEM-V3) released in 2019 and available from NASA's Land Processes Distributed Active Archive Center (LP DAAC). Its land surface coverage extent range between 83°N and 83°S. The ASTER GDEM Version 3 was produced through automated processing of 2.3 million scenes (1 arc-second) from the ASTER archive in GeoTIFF format, with 30-meter spatial resolution and 1°x1° tiles. It uses WGS84 geoid projection.
- **SRTM DEM with 30 m resolution**: SRTM 1 arc-second DEM with global coverage was first made available worldwide for public use by the US government on 23 September 2014. The National Aeronautics and Space Administration (NASA) and the National Geospatial-Intelligence Agency (NGA) participated in the international project to acquire radar data through the Shuttle Radar Topography Mission (SRTM) which was flown aboard the space shuttle Endeavour February 11-22, 2000. Its land surface coverage extent range between 60° N and 56° S which cover about 80% of the Earth's surface.
- **CartoDEM with 30 m resolution**: Indian National DEM generated by Indian Space Research Organization (ISRO) on May 5, 2005. Cartosat-1 or IRS-P5 is a stereoscopic Earth observation satellite in a sun-synchronous orbit satellite globally capture along-track stereo images (Forward +26o, Aft -5o) with 2.5m spatial resolution (ground sampling distance) with 27km swath and the base-height ratio of 0.63 using two panchromatic charge-coupled device sensors. These stereo images (2.5m resolution) were used for DEM generation using augmented stereo strip triangulation (ASST) with 10m posting for Indian landmass. Freely Available CartoDEM V3.1 (30m resolution) covering a geographical area of India for public use can be downloaded from the BHUVAN portal (https://bhuvan.nrsc.gov.in) of ISRO.
- **ALOS (AW3D30) DEM with 30 m resolution**: AW3D30 is a global digital surface model (DSM) released by the Japan Aerospace Exploration Agency (JAXA) on Jan 24, 2006, with a spatial resolution of approx. 30 m (1 arc-second). The AW3D30 dataset covering the global land surfaces was produced using 3 million scene archives acquired by the PRISM panchromatic optical sensor on the Advanced Land Observing Satellite "DAICHI" (ALOS) operated from 2006 to 2011. The AW3D30 is a resampling of the

2.5-meter mesh version of the "World 3D Topographic Data". This DSM global dataset was made freely available for public use in May 2016. Presently, the AW3D30 version 3.1/3.2 can be downloaded from the JAXA website.

- **ALOS PALSAR- RTC Dem with 12.5 m resolution**: The Alaska Satellite Facility Distributed Active Archive Data Center (ASF DAAC) released geometrically and radiometrically terrain corrected data products derived from ALOS PALSAR, processed using the Gamma Remote Sensing software package in October 2014. ALOS PALSAR- RTC RT1 product with 12.5 m spatial resolution is produced using 1⁄3 arc-second National Elevation (NED) Dataset for the USA and 1 arc-second SRTM GL1 datasets for the rest of the globe excluding Antarctica, Greenland, Iceland, and northern Eurasia. The dataset is available in the GeoTIFF format. The detailed information about the data sources used in the present study is shown in Table 2.4 and 2.5.

Table 2.4 General information about DEMs and topographical data used in this study

Sr. no.	Production authority	Topographic maps and DEMs details	Survey year/date of release	Spatial resolution/ scale	Source
1	Alaska Satellite Facility, USA	**ALOS PALSAR-RTC DEM**: AP_12569_FBD_F0640_RT1.dem.tif AP_04342_FBS_F0640_RT1.dem.tif	2014	12.5 m	https://asf.alaska.edu/data-sets/derived-data-sets/alos-palsar-rtc/alos-palsar-radiometric-terrain-correction/
2	NASA, USA	**ASTER DEM**: ASTGTMV003_N32E074 ASTGTMV003_N32E075 ASTGTMV003_N33E074 ASTGTMV003_N33E075	2011	30 m	https://e4ftl01.cr.usgs.gov/
3	EORC, JAXA	**AW3D30 DEM**: N032E074_AVE_DSM.tif N032E075_AVE_DSM.tif N033E074_AVE_DSM.tif N033E075_AVE_DSM.tif	2016	30 m	https://www.eorc.jaxa.jp/ALOS/en/aw3d30/data/index.htm
4	ISRO, INDIA	**CARTO DSM**: C1_DEM_16B_2005-2014_v3_R-1_74E32N_i43u C1_DEM_16B_2005-2014_v3_R-1_74E33N_i43o C1_DEM_16B_2005-2014_v3_R-1_75E32N_i43v C1_DEM_16B_2005-2014_v3_R-1_75E33N_i43p	2005	30 m	https://bhuvan-app3.nrsc.gov.in/data/download/index.php?c=s&s=C1&p=cdv2
5	NASA, USA	**SRTM DEM**: n33_e075_1arc_v3.tif n33_e074_1arc_v3.tif n32_e075_1arc_v3.tif	2000	30 m	https://earthexplorer.usgs.gov/

		n32_e074_1arc_v3.tif			
6.	SOI LULC Map		1982	Scale: 1:50,000	Survey of India (SOI), India

Table 2.5 Details the historical datasets used

Data	**Spatial Resolution**	**Temporal Resolution**	**Source**	**Status**
DEM	Grid (30 m)	Fixed	SRTM/ ASTER/ ALOS World 3D-30m (AW3D30)/ Carto/ ALOS RTC	Free available, downloaded
Precipitation	Grid (0.25°)	Daily	IMD gridded data	Collected
	Point rainfall	Daily	WHRC-NIH	WHRC-NIH Observatory
	Point rainfall	Hourly	IMD / SKUAST Jammu	For 2014 and 2016 flood event at Chatha AMFU (Jammu) and Kawa (Udhampur)
Air temperature (max and Min)	Grid (0.25°)	Daily	IMD data	Collected
Soil type		Fixed	NBSSLUP/FAO	Collected
Land use	Grid (1 km)	Fixed	SoI/ Derived based on Landsat Image	Available/Prepared
Discharge		Annual maximum/10 daily/ daily	CWC/IFCD	Annual maximum/10 daily collected from CWC. Fresh request has been sent to provide event based hourly data for selected high flood events as daily data for selected month
Stage (Gauge)	Grid (500 m)	Annual maximum/10 daily/ daily	CWC/IFCD	Annual maximum/10 daily collected from CWC. Fresh request has been sent to provide event based hourly data for selected high flood events as daily data for selected month
Cross-section			JTFRP/ CWC/IFCD	To be collected. Request to provide data is sent.

2.4 Historical Floods in Tawi River Basin

The Tawi basin region is especially affected by hydrological disasters as it has a rather precipitous relief, witnesses heavy torrential rainstorms and frequent cloud bursts. Based on the monthly maximum observed records of 30 years from 1988 to 2017, discharges exceeding 1 lakh cusec seem to have occurred 16 times at the Jammu City gauging station. The most relevant flooding events occurred in the years of 1988, 1990, 1993, 1995, 1996, 1997, 2005, 2016 and 2014. Figure 2.4 illustrates the major flooding areas of the river basin considered in this study. Tables 2.6 details some of the major floods in the past. Similarly, Table 2.8 details the event-scale data procured / collected for the hydrologic and hydraulic modelling study. The hourly observed gauge and discharge data for the following past rainfall-runoff events are required for calibration and validation of the hydrologic and hydraulic models proposed for the flood inundation mapping in the Tawi River basin. Note that the events marked in bold fonts are most important events as the they are very high flood events.

Table 2.6 Some of the major historical floods experienced in the Tawi River basin

Rank	**Year**	**Date**	**Flood peak discharge (m^3/s)**	**Water stage (feet)**	**Flood volume (hm3)**	**Return Period (years)**	**Flood duration**
1	2014	06/09/2014	13552	33'0"	976	83	2-9th September, 2014
2	1988	25/09/1988	11403	30'0"	651	50	22-28 September, 1988
3	1996	22/08/1996	6507	22'0"	731	15	21-26 August, 1996
4	2005	07/07/2005	5768	20'6"	364	12	4-10 July, 2005
5	2016	07/08/2016	4955	19'0"	-	9	

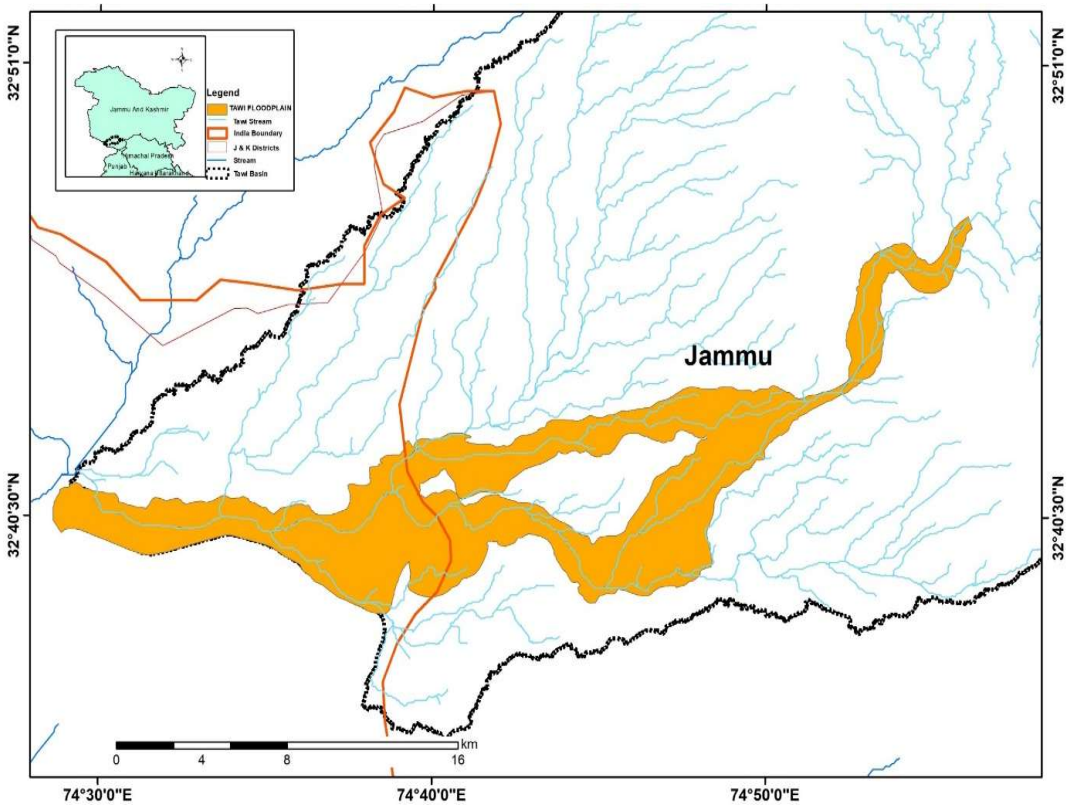

Figure 2.5 Major flood affected area of the Tawi River basin.

Table 2.7 Specific data procured for event-scale modelling of selected historical floods in the Tawi River basin

Sr. No.	**Year**	**Date**	**Flood/Rainfall event duration**	**Data required from CWC / IFCD (hourly stage and discharge data at Sidhara and Udhampur G&D site)**	**Other data required**
1	2019	19/08/2019	12-20 August, 2019	12-22 August, 2019	Rating curve (if available0, cross-section at each G&D site
2	2016	07/08/2016	5-8 August, 2016	1-10th August, 2016	-do-
3	2014	06/09/2014	2-9th September, 2014	1-10th September	-do-
4	2008	31/07/2008	29 July – 2	28 July – 4 Aug.	-do-

			Aug. 2008	2008	
5	2006	16/08/2006 and 16/09/2006	14-17 Aug. 2006 15-19 Aug. 2006	14-17 Aug. 2006 15-19 Aug. 2006	-do-
6	2005	07/07/2005	4-10 July, 2005	4-10 July, 2005	-do-
7	1997	28/08/1997	25-29 August, 1997	24-30 Aug., 1997	-do-
8	1996	22/08/1996	21-26 August, 1996	18-26 August, 1996	-do-
9	1995	05/09/1995	3-6 September, 1995	2-8 September, 1995	-do-
10	1993	11/07/1993	7-13 July, 1993	5-15 July, 1993	do-
11	1992	10/09/1992	7-12 September, 1993	5-15 September, 1993	-do-
12	1989	30/07/1989	27 July – 1 August, 1989	25 July – 2 August, 1989	do-
13	1988	25/09/1988	22-28 September, 1988	20-30 September, 1988	do-

3 LITERATURE REVIEW

3.1 General

It is essential to understand the characteristics of flood inundation for the Tawi River Basin under the climate change scenarios. With this study, we can know how much area will be inundated due to flood caused by rainfall event in the Tawi River catchment area. In addition to that, we need to know how fast or at what rate the flood plain areas are inundated due to that particular rainfall event, and how future rainfall extreme event due to climate change are going to impact the flood inundation extent in the Tawi river basin to answer these key questions, this study has been taken.

The rainfall and flow or discharge values needed to be translated into the water depth, velocity and the corresponding extent to understand its impact on the landscape, human society and their economic activities. For this purpose, we require the rainfall-runoff analysis with suitable hydrological and hydraulic modelling tools to achieve these objectives effectively and efficiently. Flood inundation mapping is an important tool for municipal and urban growth planning, emergency action plans, flood insurance rates and ecological studies. Mapping a floodplain requires a forecasting of the behavior of the stream in question for various recurrence interval storm events and the ability to translate the forecasted results into a plan-view extent of flooding.

The rainfall-runoff modelling is a well-recognized engineering tool which provide reliable estimates of stream flow from a catchment. This information is very essential to policy makers to chalk out appropriate water planning and management policy. There are range of methods available to estimate streamflow from catchments, using observed data wherever possible, or using empirical and statistical techniques to estimate river discharge, more commonly known as rainfall-runoff models (Vaze, 2012). All rainfall-runoff models are the simplified characterizations of the real-world system (Moradkhani, 2009). Runoff models helps to visualize the response of water systems due to changes in the land-use and meteorological events. Physical processes that convert rainfall to runoff is conceptualized with set of equations by employing various parameters that describes the catchment. Modelling surface runoff is challenging as the calculation involves complexities with many interconnected variables. However general model components include inputs, governing

equations, boundary conditions or parameters, model processes, and outputs. There are wide ranges of rainfall-runoff models currently used by researchers and practitioners, however their applications are highly dependent on the purposes for which the modelling is undertaken. As many of the rainfall-runoff models are used merely for research purposes for the purpose of understanding the hydrological processes that govern a real-world system, some are developed and employed as tools for simulation and prediction that in turn allows decision makers for proper planning and operation in context of flood risk management (Moradkhani, 2009). For instance, the real-time flood forecasting and warning, currently operational in many countries, employs the results of rainfall-runoff modelling. So far, these hydrological models also estimate flood frequencies, provide inputs for flood routing and inundation prediction. Often the end-results are utilized in the impact assessment of climate and land use change together with integrated watershed management.

After computation of catchment contribution as a flood into the river by rainfall-runoff modelling, the Flood inundation models are required to understand, assess and predict flood events and their impact in the areas. Recent years have shown systematic improvement in the capability of flood inundation modelling and mapping (Teng, 2017). The results from hydraulic models can be used in flood risk mapping, flood damage assessment, real time flood forecasting, flood related engineering, water resource planning, investigating flood plain erosion and sediment transport, floodplain ecology, river system hydrology (Teng, 2017). However accurate flood modelling at high spatio-temporal resolutions still remains a significant challenge in any hydrologic and hydraulic studies. This is mainly due to the complex and chaotic nature of flooding and uncertainty associated with the conceptualization of processes and the modelling parameters itself. Good inundation maps could help in designing the flood risk management strategies and their implementations. Preparedness activities and timely response can be undertaken if the forecast information comes with the level of impact of flood. Even for recovery and damage assessment, flood risk mapping plays a crucial role. So far flood inundation maps can be utilized in environmental and ecological assessments of the watersheds.

Hydrologic Modelling System (HEC-HMS) is an open-source computer software developed by U.S. Army Corps of Engineering´s Hydrologic Engineering Center that helps in simulating the hydrologic cycle (precipitation, evapotranspiration, infiltration, surface runoff and baseflow) of a catchment by describing it's physical and meteorological properties. In the present study id proposed to develop a physical based hydrological model with HEC-HMS software and simulate the effects of rainfall on surface runoff and flood discharges. Further

the study also aims to evaluate the performance of the models by doing a thorough sensitivity analysis. Further, it is proposed to develop a hydraulic model with HEC-RAS software to produce flood inundation maps for different flood scenarios under future climate change scenarios for the Tawi river basin.

3.2 HEC-HMS and HEC-RAS based modelling tool for flood inundation mapping

The Hydrologic Engineering Center's (HEC) Hydrologic Modeling System (HEC-HMS) and River Analysis System (HEC-RAS) software's developed by United State Army Corps of Engineers (USACE) are very popular due to its computational capabilities, friendly graphical user interface. The (HEC-HMS) is designed to simulate the complete hydrologic processes of dendritic watershed systems. The software includes many traditional hydrologic analysis procedures such as event infiltration, unit hydrographs, and hydrologic routing (USACE, 2021a). HEC-RAS is a computer program that models the hydraulics of water flow through natural rivers and other channels and useful for the management of the rivers (USACE, 2021b). The HEC-RAS software allows the user to perform one-dimensional steady flow, one and two-dimensional unsteady flow calculations etc using a common geometric data representation and common geometric and hydraulic computation routines (Traore et al., 2016). In this section, an attempt has made to review the application of these two models for flood inundation mapping.

Horritt and Bates (2002) have attempted to verify the 1D and 2D hydraulics models such as HEC-RAS, LISFLOOD-FP and TELEMAC-2D on a 60 km reach of the river Severn, UK. Synoptic views of flood extent from radar remote sensing satellites have been acquired for flood events in 1998 and 2000. Merwade et al. (2008) have argued that generally flood inundation extent maps are produced as a deterministic map without paying much attention to the variables responsible to introduce inherent uncertainties in its production such as topographic representation, precipitation, flow prediction, hydraulic models, techniques and their parameters, inundation mapping techniques and geospatial operations etc. In order to address some of the uncertainties, they have presented an idea of a probabilistic flood inundation map based on the integrated framework approach by connecting data, models, and uncertainty analysis techniques.

Chu et al., (2009) simulated the basins response to rainfall for a individual rainfall events (e.g., Peak, runoff volume, time to peak, detention). They used the event-based modeling approach of finer scale to study the basin characteristic and its response in details.

Thus, they derived model parameters and used it in studying the continuous hydrological phenomenon over a long-time scale of coarser time steps for both dry and wet period. HEC-HMS was used to simulate the rainfall-runoff process using the Soil conservation Service Curve Number and soil Moisture accounting methods. They concluded that model parameter derived from fine scale event hydrological modeling is very useful for improving coarse scale continuous modeling by providing more accurate and well – calibrated parameters.

Verma et al., (2010) compared HEC-HMS model and WEPP to find the best model in simulating the basins response to rainfall in the Upper Baitarani River basin of Eastern India. They modeled the daily monsoon streamflow of Six years (1999-2005) using corresponding daily rainfall data and other input data. The analysis showed that both the model under predicted the streamflow for the year 1999, 2002, 2004 and 2005 and over predicted for 2001 and 2003. HEC-HMS under predicts and WEPP over predicts 2002 streamflow. Different performance indices like root mean square error, Nash-Sutcliffe, percentage runoff volume deviation was calculated to find the best model representing the basin. Overall it was established that HEC-HMS model out performed WEPP model for simulating daily streamflow in the Upper Baitarani river Basin.

Oleyiblo et al., (2010) used HEC-HMS model to know its capabilities in runoff simulation in China. They presented a holistic application of HEC-HMS two catchments of China namely The Misai and Wan'an. Models' applicability, capability and suitability in chines region for flood forecasting was studied. The model was calibrated and validated with the observed historical streamflow data. The determination coefficients and coefficient of agreement for all the flood scenarios were above 0.9 and all the error in the peak flood discharge were all within the acceptable range.

Majidi et al., (2012) evaluated performance of the in the Abnama Watershed region of Iran. They used the model to quantify the discharge at the outlet of Abnama Watershed region based on the rate of precipitation received. Different conceptual methods like Green-Ampt, SCS Unit hydrograph and muskingum routing was used to compute infiltration, rainfall excess and channel routing respectively. After model was calibrated using the optimization model in the HEC-HMS and sensitive analysis was done it was found that the lag time parameter was the most sensitive. The model show good result in capturing the streamflow variation and was concluded that it can be used in Abnama Watershed with reasonable assumptions.

Halwatura et al., (2013) used HEC-HMS to find out the best method to calibrate the model among the three selected methods i.e., the Soil Conservation Service Curve number

loss method and the deficit constant loss method which include the Synder Unit hydrograph method and the Clark unit hydrograph method. The model was applied to Attanagalu Oya catchment which is in Sri Lanka. Twenty year daily rainfall data from five rain gauging stations scattered within the Attanagalu Oya catchment and monthly evaporation data for the same years for the agro-meteorological station Henarathgoda together with daily flow data at Dunamale from 2005 to 2010 were used in the study. The flows simulated from each methods were tested statistically employing the co- efficient of performance, the relative error and the residual method. The Snyder unit hydrograph method simulates flows more reliably than the Clark unit hydrograph method. As the loss method, the SCS Curve Number method does not perform well.

Asadi et al., (2013) applied HEC-HMS model for flood forecasting in Kabkian basin and Delibajak Sub-Basin in Iran. In this study, basins divided into a number of sub- basins where the hydrologic parameters may vary from one sub-basin to another. The SCS curve number method (Soil conservation Service, 1972) was considered for the Rainfall-runoff modelling and the model was carefully calibrated and verified in subbasin and basin using simultaneous historical observed data. The determination coefficients and coefficients of agreement for all the flood events were above 0.9, and the percent errors in peak flow and volume were all within the acceptable range. As well, the hydrologic parameters, curve number and initial abstraction were compared in these two basins.

Singh et al., (2015) used HEC-HMS model to simulate continuous river discharge in the Vamsadhara River Basin of India using Soil Moisture Accounting (SMA) Algorithm. The spatial domain of the catchment was discretised into smaller sub-basins to account for catchment heterogeneity in terms of topography, land use and soil. The model was calibrated for five years and validated for three years. The model statical and visual evaluation was conducted to determine the ability to simulate the streamflow in the Vamsadhara River Basin. The model showed Nash -Sutcliffe Efficiency of 0.7 which falls in very good range. Subsequently, statistical parameters were calculated. Overall, the SMA procedure in the HEC-HMS conceptual model performed satisfactorily and can be used for long-term runoff modeling in the Vamsadhara River Basin.

Sampath et al., (2015) performed continuous precipitation-discharge modelling using HEC-HMS for Deduru Oya riverbasin. The rainfall and discharge data in daily basis, with LULC and soil map the area research was utilized for the current research. The precipitation-excess was estimated using SMA method, while the discharge volume was computed using Clark UH model and recession model was utilized for base flow estimation. For the interval,

from October to December 1985 the calibration was done. For period October1984 to September 1985 and October1987 to September1989, the model validation was done. Hence, from the research, it is concluded that the HEC-HMS has enough potential for managing water in Deduru Oya river basin.

Azmat et al., (2017) compared the different loss and transform method available in HEC-HMS, for setting event based and continuous precipitation- discharge model for Jhelum river basin, India. The remotely sensed tropical rainfall measuring mission data was utilized for computing runoff. The value of curve number was identified using soil map and LULC of the study area. For period of 2000 to 2007 the calibration was done, while for period from 2007 to 2012 the model validation was done. The result concluded that the Clark Unit Hydrograph transform method works well with Green-Ampt loss method, for performing event-based simulation, while SMA works fine with Snyder UH, for continuous simulation in Jhelum `river basin.

Bhuiyan et al., (2017) studied the applicability of Soil moisture data in hydrological modeling using HEC-HMS derived from RADARSAT-2. The study was conducted study in the Sturgeon Creek watershed in Manitoba, Canada. In Manitoba the flooding in the winter season is influenced by the rainfall and the soil moisture condition. As a result, the soil moisture accounting (SMA) and the temperature index algorithms are employed in the simulation. Results from event and continuous simulations of HEC-HMS show that the model is suitable for flood forecasting in Manitoba. It also concluded that it is beneficial to use satellite data which will help in capturing peak flows in a snowmelt event. A sensitivity analysis of SMA parameters, such as soil storage, maximum infiltration, soil percolation, maximum canopy storage and tension storage, was performed and ranked to determine which parameters have a significant impact on the performance of the model. The results show that the soil moisture storage was the most sensitive parameter. The sensitivity analysis of initial soil moisture in a snowmelt event shows that cumulative flow and peak flow are highly influenced by the initial soil moisture setting of the model

Derdour et al., (2018) used HEC-HMS hydrological model for simulating runoff in the Ksour mountain's which can be categorized as semi-arid region in South West Algeria. In this study, the frequency storm is used for the meteorological model, the Soil Conservation Service – curve number (SCS-CN) is used to calculate the loss rate and Soil Conservation Service unit hydrograph method have been applied to simulate the runoff rate. The Nash–Sutcliffe efficiency coefficient was 0.95, indicates that the hydrological modeling results are satisfactory and accepted for simulation of rainfall-runoff.

Ma et al., (2018) used HEC-HMS in flood forecasting by calibrating and validating the model. The model was used in Huan river which is in the north of the Yangtze River in Hubei Province, at the southern foot of the Dabie Mountains, in Xiaogan City area in the North of Jianghan Plain. The net rainfall was calculated through the initial constant rate loss method. The surface runoff of the basin was calculated by the Snyder unit line model, and the basis was calculated by the exponential decay model. The river flow convergence was calculated by the Muskingum method. Based on the rainfall runoff data of 17 floods, three sets of Snyder unit lines were calculated according to the net rainfall intensity, and then three large, medium and small floods were employed to verify the flow process of the exit section of the basin. The results showed that: The determination coefficients and coefficients of agreement for all the flood events were above 0.92, and the relative errors in peak discharges were all within the acceptable range. It was concluded that accuracy of the model in the Huan River basin can be enhanced by synthesizing the Snyder unit line in the HEC-HMS model according to the net rain intensity.

Darji et al., (2019) used HEC-HMS model for capturing the precipitation runoff process for Machhu River basin in Gujarat. For this 40-year rainfall, data was taken in to consideration to estimate runoff and was corelated with the observed runoff data and the coefficient of determination value was found to be 0.89, which was in the acceptable range. Basin model was developed using the HEC-GEOHMS tool in Arc-GIS software. Subsequently, HEC-DSS application was utilized to analyze the result.

ShahiriParsa et al., (2016) used HEC-RAS and CCHE2D for flood plane zoning in Sungai Maka district in Kelantan state, Malaysia. The purpose of this study was to focus on the analysis of HEC-RAS and CCHE2D in order to assess and predict the flood depth and spatial extent of flood. This helped the decision- makers, especially the involved government's department, and developers make a proper plan for future development. The results show that the maximum difference between the 1D and 2D models is 6% in the meander's part of the river. They also concluded that most important hydraulic parameter is the roughness co-efficient, boundary condition influences the flow characteristics and accuracy of the river geometry improves the simulation results.

Traore et al., (2016) used HEC-RAS to understand the flow dynamics in the Kayanga River which originated from the Fouta Djallon Mountains in the Republic of Guinea. For each stream flow, HEC-RAS was used to calculate flow characteristics including: water surface profiles, energy grade line, water surface elevation, flow velocity, flow area, total surface area, volume, wetted perimeter, Froude number, top width, specific force, shear total,

power total, friction loss, head loss, conveyance total, and slope. Model was used to locate the high and low flows. The large and narrow section sectors have also been detected to estimate the floodplain. This study helped to provides an opportunity for stakeholders to identify important elements of irrigated agriculture for investment plans in this area.

Thol et al., (2016) analyzed possible flood scenarios using HEC-RAS in a 50 km long river reach located in Southeast Asia, Cambodia which is one of the top most disaster prone countries according to the National Committee for Disaster Management (NCDM) of Cambodia. A 50-km long of the Lower Mekong River in Cambodia was selected to delineate flood map from 2000 to 2013. A map of a ten-year return period flood was also established. The analysis is based mainly on the observed data of water level of 8 years, 18 river cross-sections and digital elevation model (30 m x 30 m). The output from the model including flood extent and flood depth from 2000 to 2013 (without 2009, 2010 and 2012) was spatially mapped for analysis. In addition, results of model calibration and validation show a quite good agreement with observed data. Shortly, HEC-RAS is a potential tool for the prediction of flood extent in Cambodia and the map of flood extent provides a useful information for a sustainable flood management. Afshari et al., (2018) also recommeded that as a low complex flood inundation mapping tool, it is which is very effective to apply at regional scale.

Costabile et al., (2020) tried to assess the potential and the capabilities of the 2-D HEC-RAS model in rainfall-runoff simulations at the basin scale, and compared the results obtained using both the options (fully dynamic equations and diffusion wave equations) to the simulations obtained by using a 2-D fully dynamic model i.e., Shallow Water Equation-Finite Volume Model (SWE-FVM) developed by the author. They used three performance measure criteria i.e., Hit Rate, False Alarm Ratio and Critical Success Index. Both models have been tested in a small basin in Northern Italy to analyze the differences in terms of discharge hydrographs and flooded areas. The analysis of flood extent, carried out for different pre-fixed water depth thresholds, highlights that, except for the smaller threshold, HEC-RAS has always overestimated the SWE-FVM flooded areas with variations approximately equal to 5–10% and 20–30% for the fine grid and coarse grid respectively. HEC-RAS and the SWE-FVM models describe the main channel in a similar way. These results provide practical indications for the water engineering community in the innovative research field related to the use of 2-D SWEs at the basin scale.

3.3 Concluding Remarks

So far, no published study did an in-depth assessment of the flood modelling capabilities of this new product. The purpose of this investigation is to: 1) assess the capacity of the AW3D30 DEM for flood modelling, and 2) compare its performance with regards to computed water levels and flood extent maps calculated using other freely available 30 m resolution DEMs for model setup (e.g., SRTM and ASTER). For this comparison, the reference to reality is given by the water levels and flood extent maps computed with the same numerical model but using a Light Detection And Ranging (LiDAR) based Digital Terrain Model (DTM) with 5 m of spatial resolution and re-sampled to 30m. The numerical model employed in this investigation is based on a damped partial inertia approximation of the Saint-Venant equations on a regular raster grid, which is forced with a simple and synthetic rainfall storm event. Numerical results using different elevation data in model setup are compared for two regions with contrasting topographic gradients. Results with regards to water depth and flood extent show that AW3D30 performs better than the SRTM DEM. Notably, in the case of mountainous regions, the results derived with the AW3D30 are comparable in skill to those obtained with a LiDAR-derived DSM, suggesting its suitability in the numerical reproduction of flood events. This encouraging performance paves the way to more accurate modelling for both data-scarce regions and global flood models.

Based on the reviews, the HEC-HMS and HEC-RAS model has wide spread use in India and other countries. Many engineers and hydrologist are familiar with it and understand how it works with various hydrological and hydraulic aspects. Both are public domain software's and easily available from USACE website. Further, the are various study which are applying numerous studies which are applying the HEC-HMS model to study the effect of climate change on the future flood peaks either using the event based or continuous model. However, some recent publication suggests that event-based modelling performs better than continuous simulation modelling in reproducing both total runoff hydrograph and direct runoff hydrograph (e.g. Hossain et al., 2019;). Considering the technical advantage as well as easy availability, wide spread application and better technical support from its developers, the HEC-HMS model (v 4.7.1) are selected for modelling of event based hourly flood hydrograph in present study. Further, many study suggest that the HEC-RAS is low complex flood inundation mapping tool which is widely used for flood inundation modelling in India and internationally. Therefore, the HEC-RAS software (version 6.1) is preferred to simulation flood inundation mapping in the Tawi river basin. Further, as reported by Guhathakurta et al.

(2011) extreme rainfall and flood risk are increasing significantly in the country except some parts of central India. However, research on evaluation of increased rainfall on the futuristic flood inundation and flood hazard mapping is still at its infancy state in India, particularly in western Himalayan region where Tawi river basin is existing may be due to scarcity of data.

4 METHODOLOGY

4.1 Assessment of Digital Elevation Models for Extraction of Drainage Morphometric Properties

To achieve the basic objective of the study to assess the DEMs based on the drainage morphometric properties of the Tawi river basin, several morphometric parameters (linear, areal and relief aspects) need to be calculated and interpreted. Standard procedure was followed to extract the stream network, slope, drainage density and basin from all five DEMs datasets in the GIS environment (Arc GIS 10.8). These extracted features are projected to the regional projection using UTM projection and WGS 84 datum (WGS_1984_UTM_Zone_43_N).

The extracted stream networks and basins from all five DEMs are used to calculate various drainage morphometric parameters (linear, areal and relief aspects) through a combination of geoprocessing tools available in Arc GIS and SAGA software. The calculated drainage morphometric parameters for each DEM are then compared with those of other data sources to assess the best-suited DEM. The details of the morphometric parameters compared and the methodologies adopted for the computation of these morphometric parameters are given in Table 4.1.

Table 4.1 Details of the drainage morphometric parameters and methodology adopted for their computations

Morphometric aspects	Parameters	Formulae	References
Linear aspect	Stream order (u)	Hierarchical rank	Strahler (1964)
	Stream numbers (Nu)	$Nu = N1 + N2 + N3 + \cdots Nn$	Strahler (1952)
	Bifurcation ratio (Rb)	$Rb = Nu/Nu + 1$	Schumm (1956)
	Weighted Mean bifurcation ratio (WMRb)	$\text{WMRb} = \sum (Rbu/(Rbu+1)) \times \frac{(Nu + (Nu+1))}{\sum N}$	Strahler (1952)
	Stream length (Lu)	$Lu = L1 + L2 + \cdots Ln$	Horton (1945)

	Mean stream length (Lum)	$Lum = Lu/Nu$	Horton (1945)
	Stream length ratio (R_l)	$Rl = Lu/Lu - 1$	Horton (1945)
Areal aspect	Basin area (A)	GIS software analysis	Schumm (1956)
	Basin Length (L)	GIS software analysis	Schumm (1956)
	Form factor (Ff)	$Ff = A/L^2$	Horton (1932)
	Drainage basin perimeter (P)	GIS software analysis	Schumm (1956)
	Circulatory ratio (Rc)	$Rc = 4\pi A/P^2$	Miller (1953)
	Elongation ratio (Re)	$Re = 2\sqrt{A/\pi}\,/L$	Schumm (1956)
	Drainage density (Dd)	$Dd = L/A$	Horton (1945)
	Constant of channel maintenance (CCM)	$CCM = 1/Dd$	Schumm (1956)
	Stream frequency (Fs)	$Fs = \sum_{i=1}^{u} Nu\,/A$	Horton (1945)
	Drainage Texture (Rt)	$Rt = Nu/P$	Horton (1945)
Relief aspect	Maximum elevation (Hmax)	GIS software analysis using DEM	
	Minimum elevation (Hmin)	GIS software analysis using DEM	
	Highest relief (R)	GIS software analysis using DEM	
	Lowest relief (r)	GIS software analysis using DEM	
	Relative relief (Rr)	$Rr = R - r$	Schumm (1956)
	Relief ratio (Rf)	$Rf = (Rr/L)/100$	Schumm (1956)
	Dissection index (Di)	$Di = Rr/R$	Schumm (1956)
	Ruggedness index (Ri)	$Ri = Dd * Rr/1000$	Schumm (1956)
	Hypsometric Integral (HI)	HI = (Elevmean -Elevmin)/ (Elevmax - Elevmin)	Strahler (1952)

4.2 Rainfall-runoff and hydrodynamic modelling for flood severity assessment

Flood hazard maps for the Tawi River flooding events for current climate and future low, medium and high climate scenarios under 21st century climate change was carried out using the well-known hydrodynamic hydraulic models. Mainly three softwares are used for this research project: ArcGIS, HEC-HMS and HEC-RAS. HEC-HMS is used for hydrologic modelling of rainfall-runoff transformation process, and HEC-RAS is used for hydraulic modelling to assess the possible flood risk under flow extremes. Subsequently, ArcGIS is used as a platform for generating some primary GIS layers required for in HEC-HMS and HEC-RAS models as an input. Previous versions of HEC-HMS (Prior to HEC-HMS version 4.4 and HEC-RAS models were required preparation of physical (basin and meteorological) models and geometric model of river using interfacing hydrological extensions HEC-GeoHMS and HECGeoRAS in the ArcGIS software, respectively. However, recent versions of the HEC-HMS (e.g. HEC-HMS 4.7.1 used in this study) incorporates GIS menu in the main software package, therefore it eliminates a need to use the HEC-GeoHMS in ArcGIS. GIS tools included in the HEC-HMS 4.7.1 and later versions allows modelers to delineate elements, define a discretization, compute subbasin and reach characteristics, and estimate model parameters (USACE, 2021a). Similarly, HEC-RAS Mapper included in the HEC-RAS (Version 6.0 onward) assist user to create, redefine and visualize the combination of geometric data (terrain, river networks, cross-section locations, cross section parameters, 2D meshes etc.) and analyse simulation results (water surface depths, velocities etc.) (USACE, 2020). The methodology combines the time series perturbation of rainfall, impact simulations on catchment/sub-catchment rainfall-runoff flows by means of HEC-HMS model, simulation of synthetic hydrographs in full hydrodynamic river model (i.e. HEC-RAS) and GIS-based inundation mapping. The schematic overview of the overall methodology followed is presented in Figure 4.1.

The following sub-sections provides information regarding the theoretical and mathematical background involved behind the software describing the data processing and modelling procedures.

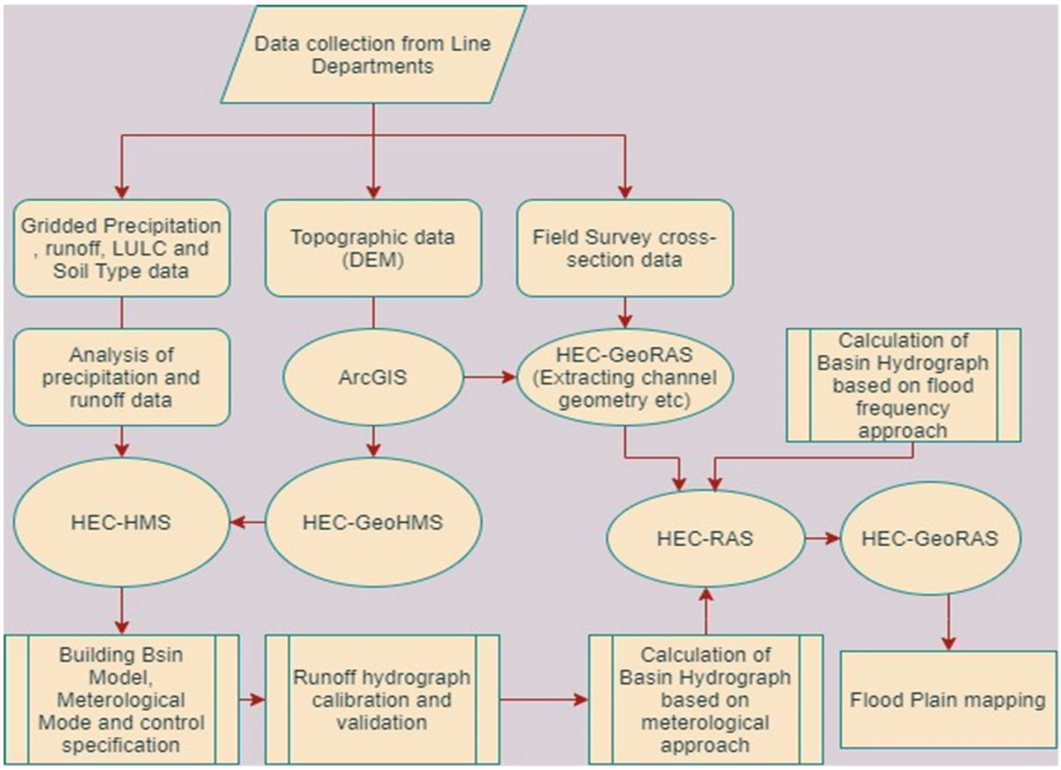

Figure 4.1 Schematic of hydrologic and hydrodynamic modelling for flood inundation mapping of the Tawi River basin.

4.2.1 Rainfall Runoff Model: HEC-HMS

For the impact analysis on rivers and riverine hydrology, a well-known hydrologic rainfall-runoff model such as the HEC-HMS was applied. Hydrologic Modelling System (HEC-HMS) is semi distributed conceptual and open-source computer software developed by U.S. Army Corps of Engineering´s Hydrologic Engineering Center that helps in simulating the hydrologic cycle (precipitation, evapotranspiration, infiltration, surface runoff and baseflow) of a catchment by describing it's physical and meteorological properties. A simple schematic representation of runoff process replicated in HEC-HMS. Wide options of mathematical models for all the hydrological components that conceptually represent watershed behaviour are incorporated in this program. The program uses separate model to represent each component of the runoff process like model to compute runoff volume, model of direct runoff/baseflow/ channel flow as well as alternative models to account for the cumulative losses for e.g.: Initial and constant loss model. Then, it computes runoff volume by subtracting losses (infiltration, storage, interception, evaporation etc.) from precipitation. HEC-HMS 4.7.1 was used during this project (USACE, 2021a).

4.2.1.1 Components of HEC-HMS model

Different components included in the HEC-HMS are listed below.

Basin Models: The physical basin area with hydrologic elements (subbasins, junctions, reach, reservoirs) and drainage network of the catchment are included in basin models. The river basin model (with various sub-basins) in HEC-HMS was created and visualized using GIS menu option. Using GIS menu, the information and features of the physical and hydrological parameters of the sub-basin can also be obtained. Sub-basins in the basin model are connected to meteorological models.

Meteorological Models: Information regarding meteorological components such as temperature, precipitation evapotranspiration, sunshine, humidity, snowmelt is defined in meteorological model. HEC-HMS provides variety of options to define each meteorological element.

Control Specification: Starting date and time, ending date and time and computational time step for the simulation are defines in control specification.

Timeseries Data: Real time series data for all the meteorological elements defined in meteorological model are fed in this part. Apart from above mentioned meteorological element, discharge data can also be supplied for calibration and simulation of the developed model. It can be supplied to the software manually or in the form of HECDSS, the Hydrologic Engineering Center Data Storage System.

Paired Data: Meteorological data in tabular/graphical form are supplied as paired data.

Terrain Data: Each terrain data component stores a single continuous digital elevation model (DEM) and can be linked to multiple basin models.

4.2.1.2 Rainfall-Runoff Transformation

In HEC-HMS, the hydrological procedure of changing rainfall into runoff has been represented by four processes: loss, transform, baseflow and channel routing. These processes are described in following section:

Loss method

This model computes the runoff volume of the catchment by calculating losses through interception/canopy storages, surface/depression storage, infiltration/soil storages, evaporation, transpiration and then subtracting it to the excess precipitation at each time step. HEC-HMS provides five options for calculating the losses. In this project, Simple canopy method is used to represent the interception/ canopy storages over the subbasins. The simple canopy method represents the plant canopy which intercept all precipitation until the canopy storage is filled. The precipitation above the canopy storage directly allotted to surface and surface runoff processes. The surface and depression storage losses over sub-basins were accounted using Simple Surface method. The simple surface method is the represents of the soil surface and account for the all surface and depression storage loss. The water from surface storage infiltrate into the ground. In order to account for the infiltration and soil storages, Initial and Constant loss method was used. This method assumes single hypothetical soil layer to account for the changes in the soil moisture. Although it is simple method, it is widely used for the river basin with limited surface information. This method is generally preferred for the simulation of the single rainfall-runoff event. The concept behind the development of this method is that the maximum potential rate of precipitation loss (f_p) is constant and unchanged during the simulation of the rainfall-runoff event. Therefore, when the precipitation rate (i) less than f_p , then no runoff will occur.

Transform method

Transform methods is an approach for computing direct runoff at the outlet of watershed area from the excess precipitation falling over it and this is done based on principles of Clack unit hydrograph. In 1945, C. O. Clark proposed original Clark Unit hydrograph transform method. This method represents the two critical processes in the transformation of catchment excess rainfall into runoff component: (1) translation or movement of excess rainfall from its origin to watershed outlet using time-area method (i.e time-area histogram and time of concentration of runoff), and (2) reduction or attenuation of excess discharge thorough storage in the basin using linear routing method (i.e. concept of storage coefficient R).

During rainfall-runoff event, temporary storage of water on the surfaces, in the soil and in channel plays important role in the transformation of the excess precipitation into the direct runoff. Therefore, Clack unit Hydrograph model use following continuity equation (Clark, 1945).

$$\frac{dS}{dt} = I_t - O_t \tag{3.1}$$

where dS/dt = time rate of change of water in the storage at time t, I_t = average inflow to the storage at time t, and O_t = average outflow from the storage at time t.

Using the linear reservoir concept, the relation between storage and outflow at time t can be given as

$$S_t = RO_t \tag{3.2}$$

Solving this equation (3.2) using finite difference approximation yields

$$O_t = C_A I_t + C_B O_t \tag{3.3}$$

where C_A and C_B = runoff coefficients which are given as

$$C_A = \frac{\Delta t}{R + 0.5\Delta t}$$
$$C_B = 1 - C_A \tag{3.4}$$

Finally, the average outflow at time t is given by

$$\bar{O}_t = \frac{O_{t-1} + O_t}{2} \tag{3.5}$$

The Clark model which is based liner reservoir concept considers that the storage reservoir is located at the catchment outlet. Beside this lumped storage model, the Clark model consider the time of concentration, that is time required by water to move from farthest point to the catchment outlet. Therefore, the time-area histogram concept is employed through unit hydrograph theory by solving equation 3.5 recursively.

The application of Clark unit hydrograph method requires the estimation of two parameters namely the properties of time-area histogram and the storage coefficient. In the linear routing model, the routing properties are defined implicitly by the time-area histogram. Thus, the HEC-HMS model by default incorporate time-area curve for the Clark unit hydrograph transform model as many studies suggests that time-area relationship is adequate to represent temporal distribution adequately for the most of catchments. The default time-area relationship used in HEC-HMS (USACE, 2021a) is given as follows.

$$\frac{A_t}{A} = \begin{cases} 1.414\left(\frac{t}{t_c}\right)^{1.5} & for\ t \le \frac{t_c}{2} \\ 1 - 1.414\left(1 - \frac{t}{t_c}\right)^{1.5} & for\ t \ge \frac{t_c}{2} \end{cases} \quad (3.6)$$

where A_t= cumulative catchment area contributing at time t, A = total catchment area, t_c = time of concentration of the catchment.

The application of the equation (3.6) requires the estimation of the parameter t_c. This parameter can be estimated by calibration or using standard area specific equation Kerbey-Kirpich equation, velocity method, drainage area-method and other suitable method. Another parameter of the Clark unit hydrograph method, the storage coefficient R for reservoir routing is estimated based on the calibration but also can be estimated based on the results of the past studies in the identical catchment area (Clark, 1945). It should be, although the R has unit of time, it has physical meaning as an index of watershed storage effect.

Base-flow Method

Subsurface flow in the catchment is illustrated by baseflow in HMS. Baseflow comprises of interflow and flow in groundwater aquifer. In this study, recession model has been used for baseflow computation. The Master recession curve technique has been used to divided the flow component into three flow segment viz. rapid flow, intermittent flow and low flow components based on the flow duration curve (FDC).

Routing Method

Flood routing is a technique of determining the flow hydrograph at the downstream point of catchment with sound information regarding hydrograph at its upstream. It is an approach to estimate how the magnitude and celerity of a flood wave varies than that at the inflow point as it moves along the catchment. Flood routing along the catchment is a function of basin characteristics such as slope and length of channel, channel roughness, channel shape, downstream control and initial flow condition (Rahman et al., 2017). The hydrologic modelling is based on continuity equation while hydraulic modelling is based on combination of continuity and momentum equation which is known as Saint-Venant equations. In this study, Muskingum-Cunge method has been used for river routing because of its high accuracy over other methods.

Muskingum-Cunge routing method is based on simplification of convective diffusion equation which is combination of continuity equation and momentum equation. The equations are as follows:

The Continuity equation

$$\frac{\partial A}{\partial t} + \frac{\partial Q}{\partial x} = qL \tag{3.7}$$

The diffusion form of momentum equation

$$S_f = S_o - \frac{\partial y}{\partial x} \tag{3.8}$$

The convective diffusion equation

$$\frac{\partial Q}{\partial t} + c\frac{\partial Q}{\partial x} = \mu\frac{\partial 2Q}{\partial x2} + cq_L \tag{3.9}$$

where, q_L= lateral flow, c = Celerity of wave and μ = Hydraulic diffusivity.

The outflow at is given by following equation:

$$O_t = C_1 Q_t^{x+1} + C_2 Q_t^x + C_3 Q_{t-1}^x + C_4(q_L \Delta x) \tag{3.9}$$

The routing coefficients are given as follows

$$\begin{aligned} C_1 &= \frac{\frac{\Delta t}{K} - 2X}{\frac{\Delta t}{K} + 2(1-X)}, \\ C_2 &= \frac{\frac{\Delta t}{K} + 2X}{\frac{\Delta t}{K} + 2(1-X)}, \\ C_3 &= \frac{2(1-X) - \frac{\Delta t}{K}}{\frac{\Delta t}{K} + 2(1-X)} \\ C_4 &= \frac{2\frac{\Delta t}{K}}{\frac{\Delta t}{K} + 2(1-X)} \end{aligned} \tag{3.10}$$

The parameters K and X are calculated as:

$$K = \frac{\Delta x}{c} \; and \; X = \frac{1}{2}\left(1 - \frac{Q}{BS_o\Delta x}\right) \tag{3.11}$$

where, Δt and Δx are time and distance steps for computation.

X will approach 0 for channels with mild slopes and overbank flow while for steeper streams with well-defined channels X approach 0.5. (USACE, 2000).

Q = reference flow from inflow hydrograph = x Am (3.12)

The exponent m has major effect on the calculation of travel time of the hydrograph through a reach which can be calculated using Manning's Equation. Further, the equation for X and K shows that they dependency on channel parameters and Manning's coefficient which makes this method more reliable for flood routing. (Merkel, 2002).

4.2.1.3 Set-up of the HEC-HMS model for the Tawi Basin

The suitable component models in HEC-HMS package were selected and step-wise calibration and validation methodology were followed to develop suitable hydrological model for future climate impact assessment. Figure 4.2 details the step-by-step procedure followed to set up the HEC-HMS for the Tawi River basin. Figure 4.3 illustrates the schematic of HEC-HMS set up for the Tawi River basin along with the delineated sub-basins (Table 4.3).

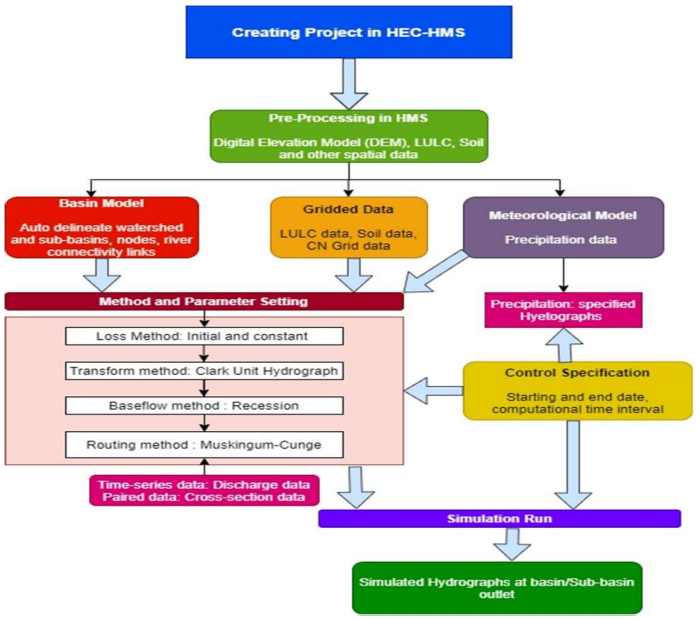

Figure 4.2 Step-by-step procedure followed for setting up of the HEC-HMS model for the Tawi River basin.

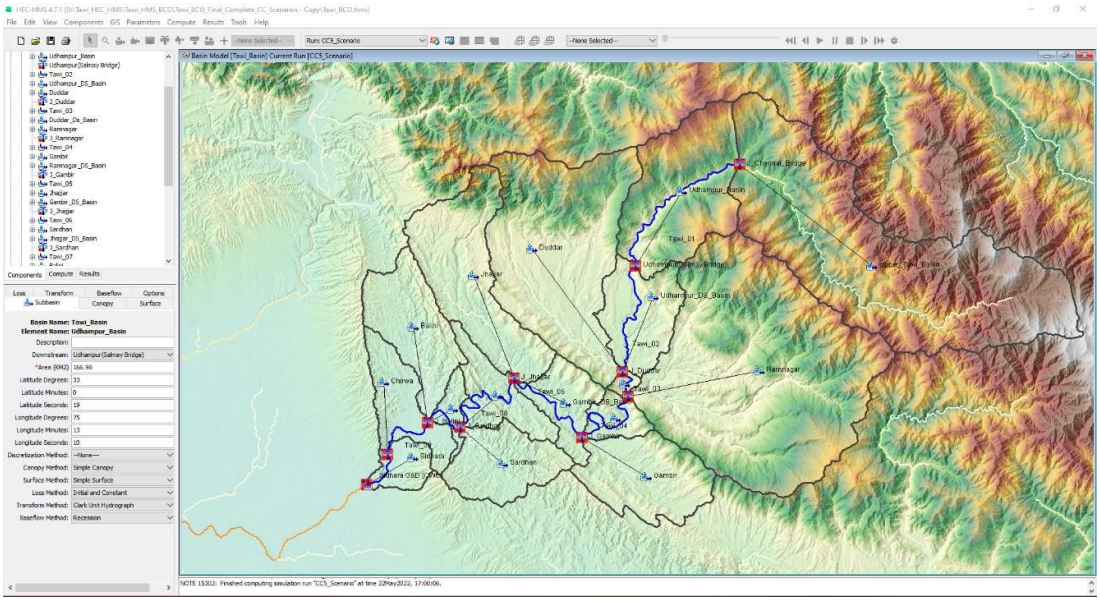

Figure 4.3 Schematic of HEC-HMS set up for the Tawi River basin upto Jammu (Bikram Chowk) Gauge site along with the delineated sub-basins.

Table 4.2 Delineated sub-basins of the Tawi River basin for HEC-HMS modelling.

S. No.	Sub Basin	Area (km^2)	Longitude Degrees	Latitude Degrees
1	Upper_Tawi_Basin	466.75	75.45	32.95
2	Udhampur_Basin	166.98	75.22	33.01
3	Udhampur_DS_Basin	81.64	75.17	32.89
4	Duddar	275.51	75.08	32.95
5	Duddar_Ds_Basin	5.9334	75.15	32.82
6	Ramnagar	486.57	75.31	32.83
7	Gambir	104.8	75.18	32.73
8	Ramnagar_DS_Basin	26.91	75.14	32.78
9	Jhajjar	156.48	74.98	32.92
10	Gambir_DS_Basin	51.626	75.09	32.8
11	Sardhan	80.09	75.01	32.74
12	Jhajjar_DS_Basin	58.664	75.01	32.81
13	Balini	97.767	74.91	32.87
14	Sardhan_DS_Basin	17.083	74.96	32.79
15	Chirwa	64.853	74.9	32.8
16	Sidhara	28.165	74.9	32.74
	Total	2169.82		

4.2.2 Hydraulic Model: HEC-RAS

HEC-RAS is a tool developed for analysing hydraulics of river system developed by U.S. Army Corps of Engineering´s Hydrologic Engineering Center. It consists of graphical user interface, data storage and management capabilities as well as reporting facilities. The main input of HEC- RAS for performing hydraulic analysis are geometric data and flow data. Basic geometric data consists of physical feature of river i.e. channel length, banks, flood banks and cross-sections of the river while additional geometric data defining bridge and culverts, levee alignment, blocked structures, inline structures and storage area can also be incorporated in the software. HEC-RAS has capability of performing one-dimensional and two-dimensional hydraulic calculations. Based on the purpose of the study, HEC-RAS provides different options for performing river analysis which are one-dimensional steady flow for water surface profile computation, one and two-dimensional unsteady flow simulation, quasi unsteady flow for sediment transport computation and water quality analysis (Brunner, 2016).

In this study, one dimensional (1-D) steady flow analysis has been performed for the Lower Tawi river basin (Downstream of the Sidhara G&D site) and the result has been used to generate flood inundation area. 1-D steady flow analysis is useful for calculating water surface profile. In this analysis, the flow is assumed to be gradually varying along its length. It can calculate the water surface profile for subcritical, supercritical and mixed flow condition. Governing equation for calculation of water surface profile is energy equation which is written as follows (Brunner, 2016):

$$Z_2 + Y_2 + \frac{a_2 {V_2}^2}{2g} = Z_1 + Y_1 + \frac{a_1 {V_1}^2}{2g} + h_e \tag{3.13}$$

where Z_1 and Z_2 = elevation of bottom of the channel at cross-section 1 and 2, Y_1 and Y_2 = depth of water at cross-section 1 and 2, V_1 and V_2 = velocity of water at cross-section 1 and 2, α_1 and α_2 = velocity weighing factors, g = acceleration due to gravity, and h_e = energy head loss.

Water surface profile between any two cross sections is calculated by solving the energy equation (3.13) in an iterative way. This process is called as standard step method. The calculation proceeds upstream if the flow is subcritical and downstream if the flow is

supercritical (French, 1985). For the computation of water surface, each cross-section of river is divided into left overbank, main channel and right over bank and the energy is calculated for each section. The final energy of the channel is the mean of the energy calculated for all three sections (Brunner, 2016). The head loss in the equation (3.13) comprises of loss due to friction and contraction/expansion. The friction loss is given by Manning's equation which is given below:

$$h_f = LS_f \tag{3.14}$$

Where S_f = representative friction slope (slope of energy grade line) = Q/K , Q = Flow in the channel length, K = conveyance factor = $1.486\,AR^{2/3}$, n= Manning's roughness coefficient, A = Area of the channel, R = hydraulic radius which is calculated as area per wetted perimeter, L = distance weighted reach length which is given as follow

$$L = \frac{L_{lob}Q_{lob} + L_{ch}Q_{ch} + L_{rob}Q_{rob}}{Q_{lob} + Q_{ch} + Q_{rob}} \tag{3.15}$$

where L_{lob}, L_{ch}, L_{rob} = reach length in left overbank, main channel and right overbank respectively, and Q_{lob}, Q_{ch}, Q_{rob}= average mean flow between sections for left overbank, main channel and right over bank respectively.

The contraction/expansion loss is calculated as:

$$h_{ce} = C\left|\frac{a_2{V_2}^2}{2g} - \frac{a_1{V_1}^2}{2g}\right| \tag{3.16}$$

where C = Coefficient of contraction/expansion.

Combining friction loss and loss due to contraction/expansion, the total energy loss equation is given below:

$$h_e = LS_f + C\left|\frac{a_2{V_2}^2}{2g} - \frac{a_1{V_1}^2}{2g}\right| \tag{3.17}$$

Velocity weighing factor, α is calculated as

$$\alpha = \frac{Q_1{V_1}^2 + Q_2{V_2}^2}{(Q_1 + Q_2)V^2} \tag{3.18}$$

4.2.3 Setting-up of HEC-RAS model in HEC-RAS Mapper

The HEC-RAS version 6.1 model developed by United State Army Corps of Engineers Hydrologic Engineering Centre (USACE, 2021b) with 1D steady state hydraulic model capable to computes cross-section average water surface elevation and flood depth and steady state velocity at discrete cross-sections by solving energy equations presented in above section 4.2.2. The HEC-RAS software is designed to perform 1D and 2D hydraulic calculations for a flow network of natural rivers or channels. The main capabilities of HEC-RAS are: 1. User Interface – user can interact through this graphical user interface (GUI). The GUI provides functions such as file management, data entry and editing, hydraulic analysis, tabulation and graphical display of input and output data, inundation mapping and animation of flood water, reporting facilities and help, 2. Hydraulic Analysis Components – Steady Flow Water Surface Profiles, 1D and 2D Unsteady flow simulation etc, 3. Data Storage and Management, 4. Graphic and Reporting and 6. RAS Mapper – has capability to create, redefine and visualize the combination of geometric data (terrain, river networks, cross-section locations, cross section parameters, 2D meshes etc.) and analyse simulation results (water surface depths, velocities etc.) (USACE, 2020).

In the present study, the HEC-RAS model has been set-up for Lower Tawi river basin (downstream of the Sidhara G&D site in HEC-RAS 6.1. The Copernicus DEM GLO-30 dataset (https://spacedata.copernicus.eu/web/cscda/home) has been used in the HEC-RAS Mapper (USACE, 2020) to generate various inputs require by HEC-RAS in order to perform various calculations. In this analysis the Lower Tawi basin (downstream of the Sidhara G&D site) is divided into four sections: 1. Upper Tawi – river section from Sidhara G&D site to split of the Tawi river before fourth tawi bridge 2. Nikki Tawi 3. Wadi Tawi and 4. Lower Tawi as shown in Figure 4.4. The geometric data (terrain, river networks, cross-section locations, junctions and hydraulic structures etc) crted in the HEC-RAS mapper is shown in Figure 4.5. The total river length of 76.22 Km is divided into 405 cross-sections approximately at every 100 m interval as shown in Figure 4.5. In the vicinity of the Jammu city, there are mainly four bridge structures are existing on the Lower Tawi river are 1. Katara Byepass Bridge 2. New Gujjar Nagar Bridge 3. Bikram chowk bridge and 4. Fourth Tawi bridge which are considered in this analysis. Tawi- Barrage is an inline structure on Wadi and Nikki Tawi is also incorporated into the analysis. The Tawi barrage inline structure exists in between Bikram chowk bridge and the fourth Tawi bridge as shown in Figure 4.5. The river profile showing elevation at defined four sections of the Lower Tawi river are graphically shown in Figure 4.6. Further, the existing slope variations in these four river sections of the Lower Tawi are presented in Table 4.3. based on the slope of river and land use cover, the data of the Manning's roughness coefficient for each created cross-section including right and lift bank will be allotted in HEC-RAS mapper.

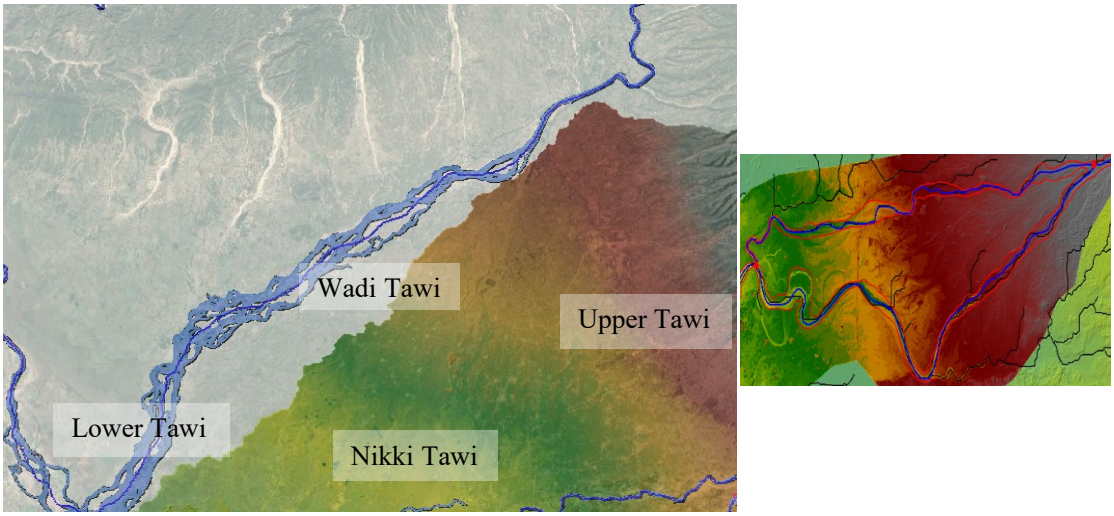

Figure 4.4 River sections of Lower Tawi basin (downstream of the Sidhara G&D site) used for the HEC-RAS schematic.

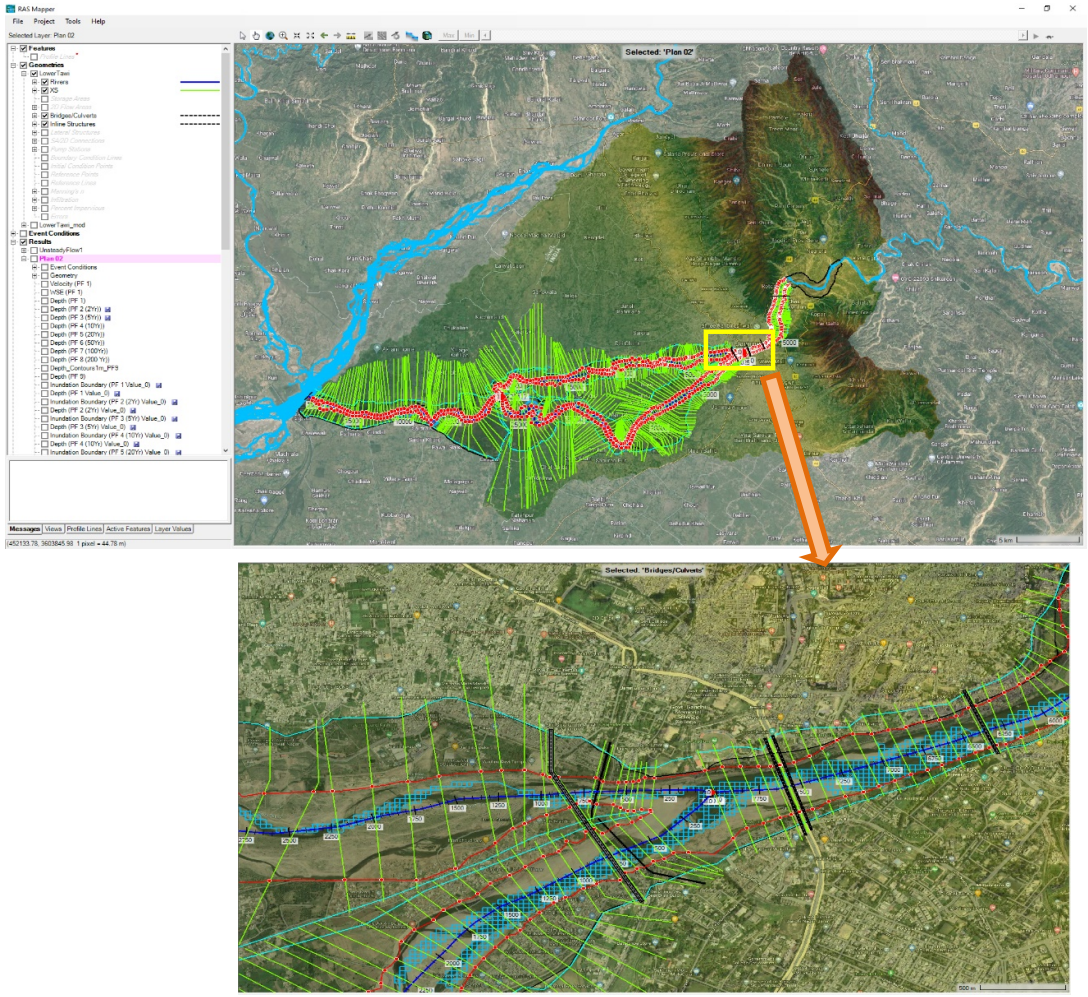

Figure 4.5 Geometric data created in HEC-RAS mapper for the Lower Tawi River basin downstream of the Sidhara G&D site.

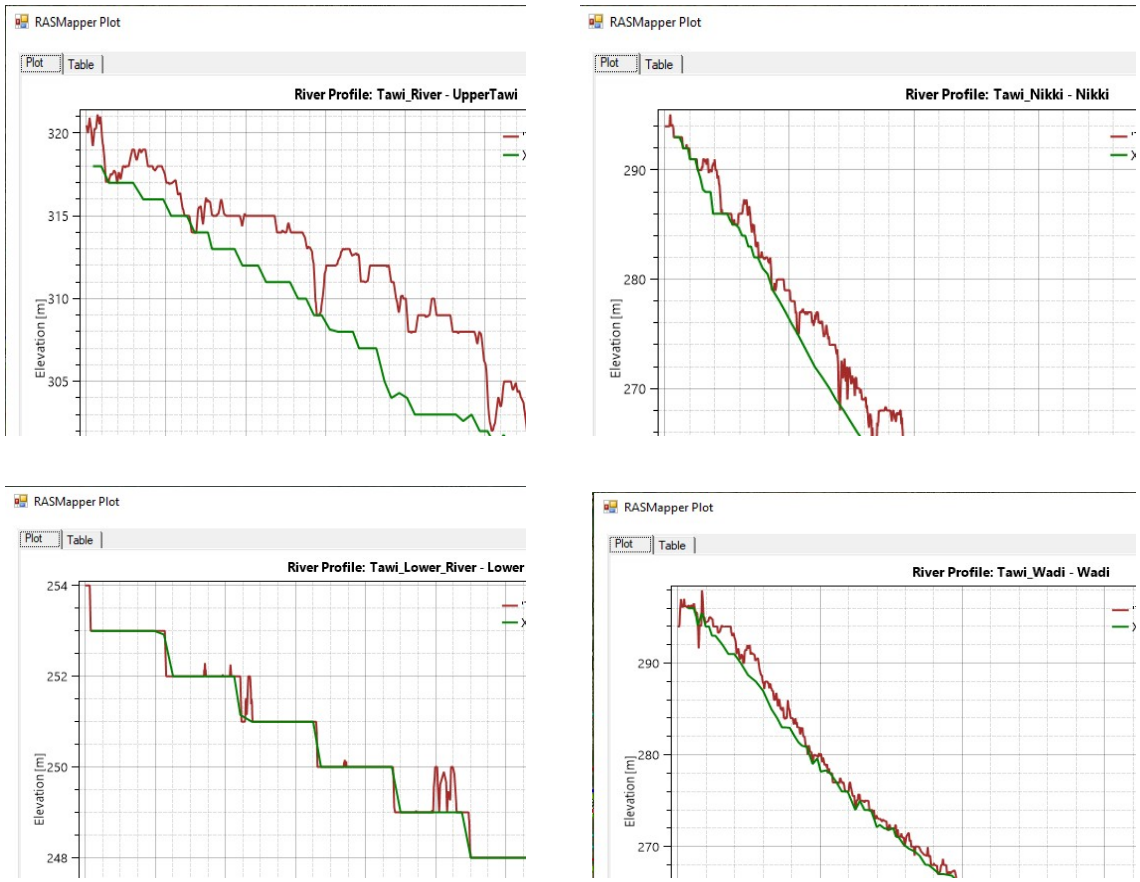

Figure 4.6 Geometric data created in HEC-RAS mapper for the Tawi River basin downstream of the Sidhara G&D site.

Table 4.2 Details of the slope variation among the four river sections in the Lower Tawi basin.

S. N.	River section	Total length (km)	Slope (in %) for entire river section	River Section Distance (m)	Elevation, (m), AMSL	Slope (in %)
1	Upper Tawi	8.025	0.30	0	318	0.30
				8025.43	294	
2	Nikki Tawi	27.28	0.15	0	294	0.36
				8859.51	262	
				8859.51	262	0.04
				27279.76	254	
3	Wadi Tawi	23.21	0.02	0	294	0.23
				17026.65	254.19	
				17026.65	254.19	0.0001
				232114.5	254	
4	Lower Tawi	17.7	0.05	0	254	0.05
				17786.06	245	

After the preparation of geometric data in the HEC-RAS mapper the model is imported in the main HEC-RAS software window. In HEC-RAS, all the geometric data of rivers, cross sections, bridges/culverts and inline structures created based on the input DEM will be imported. Check the data of cross sections imported from HEC-RAS mapper in the HEC-RAS through geometry editor. The cross section generated based on the Copernicus DEM with 30 m resolution is verified with the available observed cross-section data at few cross sections between upstream of the Katra bridge to downstream of the fourth Tawi bridge collected from Jammu development Authority (JDA), Jammu. The comparison of cross-sections extracted from DEM data (see Figure 4.7) with observed data suggest that the extracted cross-section data from Dem is reasonably accurate. Further, the data of bridges/culverts and inline structure needed to be assigned for each respective hydraulic structure in HEC-RAS through geometry editor. The geometry data for New Gujjar Nagar Bridge entered in the geometry editor is shown in Fig. 4.8.

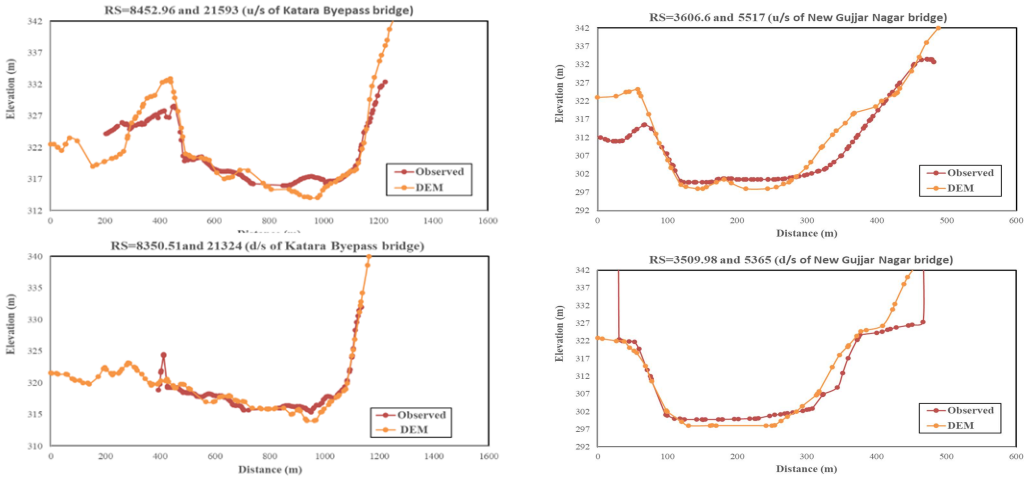

Figure 4.7 Comparison of the cross-section data extracted from DEM and observed cross-section data at some selected locations.

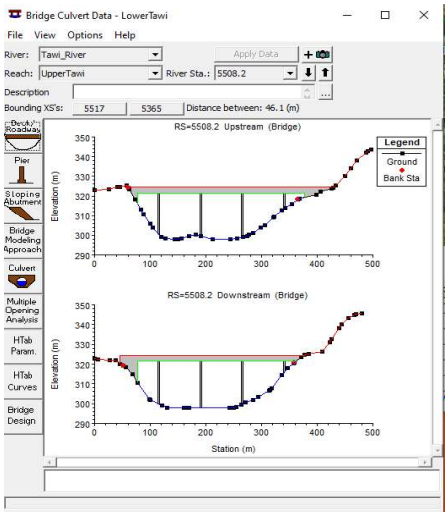

Figure 4.8 Comparison of the cross-section data extracted from DEM and observed cross-section data at some selected locations.

After all the required data id provided and checked in the HEC-RAS, the steady state flow data file is required to be generated. The observed flood timeseries data or simulated output of HEC-HMS can provided in the as upstream boundary conditions for the HEC-RAS model. If all the input data and computation criteria requirements are fulfilled the HEC-RAS provides the results based on the input data. The HEC-RAS model required to be calibrated with observed data at downstream gauge site (if available) or the simulated flood inundation extent or depth may be calibrated using the satellite data for that particular flood event or using other secondary food depth data at known locations in the flood prone area.

4.2.4 Flood frequency analysis

In order to provide protection against devasting flood, the planning and construction of flood defence is always carried out based on the flood frequency analysis (FFA). FFA is a technique commonly used by hydrologists to predict the magnitude of extreme river flow (commonly called as design flood) by relating it to their frequency of occurrence through the application of probability distribution function. In other words, FFA is an estimation of how often a certain amount of flow is reoccurring that's is estimation of the design flood quantiles. Such estimation is pre-requisite for carrying out hydraulic computation of river and developing flood inundation map. Estimation of design flood is needed for flood plains management, planning and design of hydraulic structures, flood insurance studies etc. Among the various method applied for the design flood estimation, the most commonly used method is the at-site FFA (Cunnane, 1987; Bhat et al., 2019; Sahoo and Ghosh 2021). Gumbel was first researcher to provide statistical flood frequency curve. At-site FFA method needs an observed annual maximum or peak flood flow data at river gauging stations for longer period as its main input to calculate statistical information such as mean, standard deviation and skewness. The analysis is done by fitting a probability model to the sample of annual extreme flood values recorded over a long period of time, for a catchment (Schendel and Thongwichian, 2017). The model parameters established can then be used to predict the extreme events of large recurrence interval (Pegram and Perak, 2004). It may noted that, the at-site FFA method is based on the assumption that used flood data are space and time independent, identically distributed, and uninfluenced by natural or man-made changes in the hydrological system (Rao and Hamed, 2000). Many types of distribution functions and goodness-of-fit tests exist, all with their own properties and drawbacks (Bomers et al., 2019; Rao and Hamed, 2000). In India, standard statistical procedures (e.g. suggested in CWC flood report for Subzone-7) was followed for the flood frequency analysis (at-site) based on the

assumption of stationary; that is, the extreme flood statistics do not change in time, and hence past observations can be considered as representative of future observations and thus used to estimate design flood events.

As mentioned earlier, the Gumbel was first researcher to propose distribution known as Gumbel's Distribution. It is a statistical method commonly used for predicting extreme hydrological events such as floods (Haan, 1977). According to Gumbel, the probability (P) of occurrence of any extreme event is given by the following equation:

$$P(x_0 \geq x) = 1 - e^{-e^y} \tag{3.1}$$

where y is a dimensionless variable given by

$$y = \frac{1.285(x - \overline{x})}{\sigma_x + 0.577} \tag{3.2}$$

where, $\bar{x}$ = mean and σ_x = standard deviation of the variate x.
Rearranging the above equation (3.2), the equation for fitting the Gumbel distribution to observed series of flood flows at different return periods T is given as

$$x_T = \bar{x} + K\sigma_x \tag{3.3}$$

Where

$$K = \frac{y_T - 0.577}{1.2825} \text{ and } y_T = -\left[\ln \ln \frac{T}{T-1}\right] \tag{3.4}$$

Recurrence interval T is calculated as $T = \frac{1}{P}$ (Subramanya, 2008).

Similarly, there are number of the flood frequency distribution functions are developed. Particularly, the present study, attempts to use the Flood Frequency Distribution (FFD 2.1) (Tarik Benkaci, 2021) MATLAB code for flood analysis, estimate flood quantile for different return periods and Flood frequency relations. The probability distributions used in the present study are as follows:

1. Normal Distribution
2. Racine-Normal Distribution
3. Log Normal Distribution (2p)
4. LogNormal (3p) Distribution
5. Gumbel Distribution
6. General Extreme Values Distribution (GEV)
7. Gamma Distribution (2p)

8. Log Pearson 3 Distribution
9. Goodrich Distribution
10. Weibull Distribution (2p)

The overview of these used probability density functions (PDF) for selection of above FFA distributions are presented in Table 3.2.

In FFD 2.1, the parameters of some of the above distribution can be estimated with (1) Method of Moment (MOM) or (2) L-Moment. FFD 2.1 provides five options to choose probability plot position namely: (1) Hazen method (2) Weibull method (3) Cunane method (4) Chegodayev method and (5) Grigortan method. In indian condition, the Weibll method is widely prefered method, therefore, present study also utilize Weibull method as probability plot position method. Based on the selected probability distributions and probability plotting position, FFD 2.1 provide the results as a probability plot. It is usual practice in FFA of hydrologic data is to fit several probability distributions to flood flow data at any given river gauging station and to make final selection of best fitting theoretical probaility distributions based on several criteria. Uusally, the selection of the best fitting distribution is made based on (1) visual insepction of probability plot, and/ or (2) goodness-of-fit-criteria. There are three in-built goodness-of-fit-criteria available in FFD 2.1: (1) Kolmogorov–Smirnov (KS) (2) Chi-squared, and (3) Anderson–Darling (AD) tests which are employed at significance level 0.05.

Table 4.3 Overview of probability density function (pdfs) for selection of FFA distribution functions (Adapted from Rao and Hamed, 2000 and Tarik Benkaci, 2021)

Distribution	Probability density function	Range	Parameter in terms of sample moments
Normal	$f(x) = \frac{1}{\sigma\sqrt{2\pi}} exp\left[-\frac{(x-\mu)^2}{2\sigma^2}\right]$	$-\infty < x < \infty$	$\mu = \bar{x}$ (μ *and* $\bar{x} = m$ean of observed data) $\sigma = S_x$ (σ *and* S_x = Standard deviation of observed data)
Racine-Normal	$f(x) = \frac{1}{\sigma\sqrt{2\pi}} exp\left[-\frac{(x-\mu)^2}{2\sigma^2}\right]$	$-\infty < x < \infty$	$\mu = \frac{x-\bar{x}}{S_x}$ $\sigma = S_x$ $x = \sqrt{x}$
Log Normal (2p)	$f(x) = \frac{1}{x\sigma_y\sqrt{2\pi}} \exp\left[-\frac{(y-\mu_y)^2}{2\sigma_y^2}\right]$ where $y = \ln x$	$x > 0$	$\mu_y = \bar{y}$ $x\sigma_y = S_y$
LogNormal (3p)	$f(x) = \frac{1}{(x-x_0)\sigma_y\sqrt{2\pi}} \exp\left[-\frac{((y-\ln x_0)-\mu_y)^2}{2\sigma_y^2}\right]$ where $y = \ln x$	$x > 0$ $0 \le x_0 < x$ $-\infty < \mu_y < \infty$	$\mu_y = \bar{y}$ $\sigma_y = S_y$

Gumbel (EV I)	$f(x) = \frac{1}{\alpha} exp\left[-\frac{x-u}{\alpha} - exp\left(\frac{x-u}{\alpha}\right)\right]$	$-\infty < x < \infty$	$\alpha = 0.78 S_x$ $u = \bar{x} - 0.45 S_x$
General Extreme Values (GEV)	$f_{\xi,\mu,\sigma}(x) = \frac{1}{\sigma}\left(1 + \xi\frac{x-\mu}{\sigma}\right)^{-1-1/\xi} exp\left(-\left(1 + \xi\frac{x-\mu}{\sigma}\right)^{-1/\xi}\right)$ for $\xi \neq 0$ $f_{0,\mu,\sigma}(x) = \frac{1}{\sigma}\, e^{-(x-\mu)/\alpha} \exp\left(-e^{e^{-(x-\mu)/\alpha}}\right)$ for $\xi = 0$	$x \geq 0$	$\kappa = 7.8590c + 2.9554c^2$ $in\ which\ c = \frac{2}{3+\tau_3} - \frac{\ln 2}{\ln 3}$ $\alpha = \frac{\lambda_2 \kappa}{(1-2^{-\kappa})\Gamma(1+\kappa)}$ $\xi = \lambda_1 - \alpha\{1 - \Gamma(1+\kappa)\}/\kappa$
Gamma (2p)	$f(x) = \frac{1}{\beta\Gamma(\alpha)}\left(\frac{x}{\beta}\right)^{\alpha-1} e^{-x/\beta}$	$x \geq 0$	$\alpha = \frac{\bar{x}^2}{S_x^2} = \frac{1}{C_v^2}$, $\beta = \frac{S_x^2}{\bar{x}}$ $c = \bar{y} - \alpha\beta$
Log Pearson 3	$f(x) = \frac{1}{x\beta\Gamma(\alpha)}\left(\frac{y-c}{\beta}\right)^{\alpha-1} e^{-(y-c)/\beta}$	$y = lnx \geq c$	$\alpha = \frac{4}{C_{S_y}^2}$, $\beta = \frac{S_y C_{S_y}}{2}$ $c = \bar{y} - \alpha\beta$
Goodrich	$F(x) = 1 - Exp\left[-a(x-b)^{1/n}\right]$	$b \leq x \leq +\infty$	
Weibull	$f(t) = \frac{\beta t^{\beta-1}}{\eta^\beta} e^{-\left(\frac{t}{\eta}\right)^\beta}$		$\beta = 1$

The null-hypothesis can be accepted or rejected if the observed test surpasses the critical value for constant sigficance level. The statistical analysis of the flood series at particular gauging site may not be "true" parameters of distribution of flood population at that site (so called parent population). Therefore, uncertainty araised in the flood estimates from statistical analysis is taken care by measure of uncertainty of a quantile estimate xp (flood with probability of exceedance equal to p). The standard error SE[xp], which is equal to the square root of variance of quantile estimate, var[xp]. Accordingly in FFD 2.1, the results of quantiles are estimated with lower and upper bounds 95% (Except Goodrich distribution). The Quantile-Quantile plot (QQ-plot) is displayed with correlation coefficient R, Root Mean Squared Error (RMSE) between quantile and observed data for various return periods 2, 5 10, 20, 50 100 and 500 years.

4.2.5 Future floods under changing Climate

Under the global warming, the assumption of stationarity might not be applicable, and more advanced statistical methods are required that explicitly accounts for the non-stationarity of extreme flood characteristics. Therefore, the projections of future climatic conditions (i.e., non-stationary conditions) based on available Global Climate Models (GCM) and Regional Climate Model (RCM) under different future emission scenarios, also known as the representative concentration pathways (RCPs) was used to assess its impact on the flood frequency analysis due to changing extreme precipitation quantiles under changing climate. The climate change scenarios based on CMIP5 GCM and RCM (e.g. Corrected Coordinated regional Climate Downscaling Experiment (CORDEX)) and methods for statistical downscaling and bias correction (e.g. Quantile perturbation) were used to analyze the changes in extreme precipitation statistics. Figure 4.4 details the methodology for modelling the impact of climate change on flood inundation using climate perturbation method and hydrological modelling. Similarly, Figure 4.5 details the processing of future climate data for inundation maps preparation. Based on the estimated perturbation factors during the retrospective period, the meteorological forcing for the scenario run are determine that are subsequently used as input to the hydrodynamic modelling framework to assess the climate change impact. The output is finally processed in the GIS for developing scenarios-based future inundation maps for the study area.

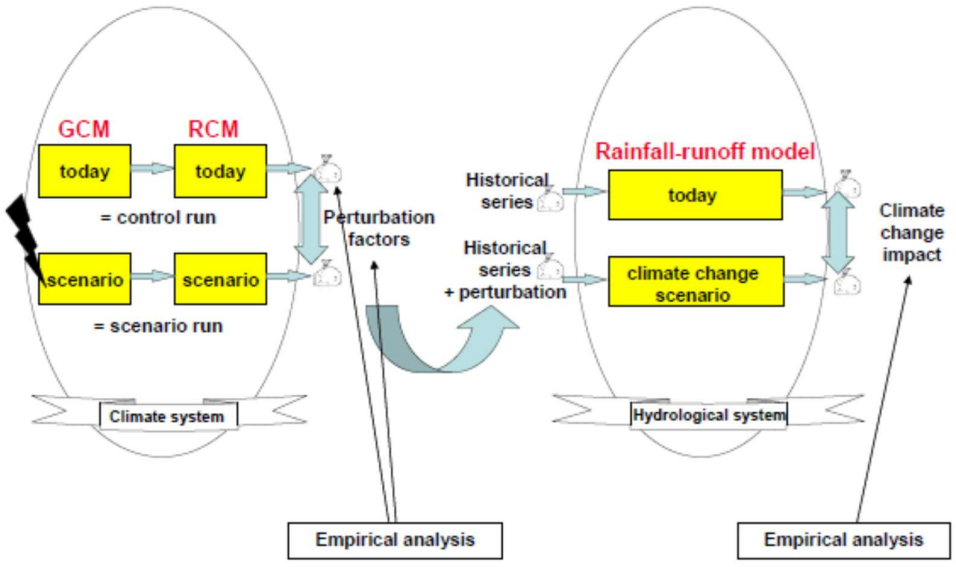

Figure 4.9 Overview of the method proposed for modelling the impact of climate change on flood inundation using climate perturbation method and hydrological modelling.

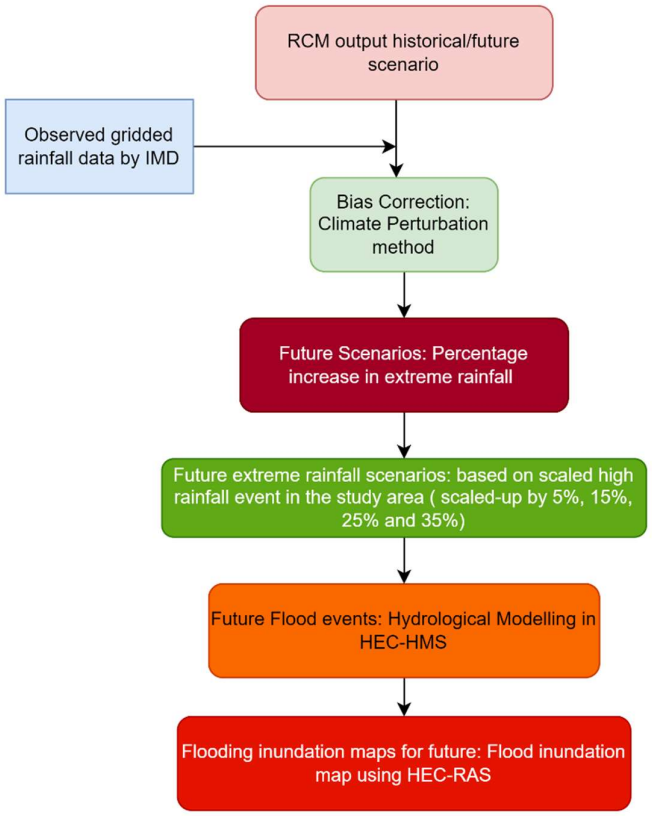

Figure 4.10 Methodology followed to prepare flood inundation maps for different climate change scenarios.

4.2.5 Model performance evaluation

The hydrological models' statistical performance indicators are computed to see how closely the values simulated by the HEC-HMS model match those with the observed high flood event data. There are numerous studies which have proposed performance criterion for evaluation of hydrological models' simulation capabilities. The model performance evaluation criterion used in this study were Nash-Sutcliffe Efficiency (NSE), Percentage Biased Error in observed and simulated data (PBIAS), Coefficient of determination (R^2), Error in peak discharge (E_p) and Error in time to peak discharge (E_{pt}).

Nash-Sutcliffe Efficiency (NSE):

The NSE is expressed by the normalized statistic difference in total variance and residual variance of observed and simulated flow data (Nash and Sutcliffe, 1970). Its value range from - ∞ to 1.0, with 1 being the best performance of the model which means the observed data is perfectly match with simulated data. General performance ratings for each of the performance indices recommended by Moriasi et al. (2007) if 0.75 < NSE ≤ 1.00 (Very good), 0.65 < NSE ≤ 0.75 (good), 0.50 < NSE ≤ 0.65 (satisfactory), NSE ≤ 0.50 (unsatisfactory).

$$\text{NSE (Maximize)} = 1 - \frac{\sum_{i=1}^{n}(Q_o - Q_s)_i^2}{\sum_{i=1}^{n}\left(Q_{o,i} - \overline{Q}_s\right)^2} \tag{3.5}$$

Where Q_o is observed discharge, Q_S is simulated discharge.

Coefficient of determination (R^2)

The coefficient of determination or coefficient of multiple determination is a statistical measure of how well calibrated data resembles the best-fit observed data. It has a value ranging from 0 to 1, with a greater value indicating a better model. General performance ratings for each of the performance indices recommended by Moriasi et al. (2007) if 0.75 < R^2 ≤ 1.00 (Very good), 0.65 < R^2 ≤ 0.75 (good), 0.50 < R^2 ≤ 0.65 (satisfactory), R^2 ≤ 0.50 (unsatisfactory).

$$R^2(\text{Maximize}) = \frac{\text{Variance of the model}}{\text{Total variance}} = 1 - \frac{SS_{res}}{SS_{tot}} = \frac{\sum_{i=1}^{n}\left(Q_{o,i} - Q_{s,i}\right)^2}{\sum_{i=1}^{n}\left(Q_{o,i} - \overline{Q}_o\right)^2} \tag{3.6}$$

Percentage Biased Error in observed and simulated data (PBIAS)

It is the percentage biased error in observed and simulated data (Gupta et al.,1999). For best performing model, PBIAS is closer to zero. The lower the value, the better the model's performance, whereas a positive value implies underestimation of the model performance and a negative value shows overestimation of the model performance (Gupta et al.,1999). It is given as a percentage. General performance ratings for each of the performance indices recommended by Moriasi et al. (2007) if PBIAS < ± 10 (Very good), ± 10 < PBIAS < ± 15 (good), ± 15 < PBIAS < ± 25 (satisfactory), PBIAS > ± 25 (unsatisfactory).

$$\text{PBIAS (Minimize)} = \left[\frac{\sum_{i=1}^{n}(Q_o - Q_s)}{\sum_{i=1}^{n} Q_o} * 100\right] \tag{3.6}$$

Error in peak flow (or stage) in percentages or absolute value (Ep):

$$E_p = \frac{Q_{op} - Q_{sp}}{Q_{op}} \tag{3.7}$$

Q_{op} is the observed peak value, Q_{sp} is the simulated peak value. The value closer to 0 shows the perfect prediction.

Error in peak flow time (or stage) in hours (Ep):

$$E_{pt} = Q_{opt} - Q_{spt} \tag{3.8}$$

Q_{opt} is time to peak observed value, Q_{sp} is time to peak simulated value. The value closer to 0 shows the perfect prediction.

5 RESULTS AND DISCUSSIONS

5.1 General

This section presenting the results on evaluation of the various open source DEMs to select best suitable DEM for the hydrological and hydraulic modelling study, Set-up of HEC-HMS and HEC-RAS model for the Tawi river basin, flood frequency analysis, climate change scenarios in the Tawi river basin using NEX-GDDP GCM and CORDEX-South Asia RCM data. Finally, the flood risk maps are generated for the Tawi River basin using design flood hydrograph from flood frequency analysis and developed in HEC-HMS for various climate change scenarios are presented and discussed.

5.2 Evaluation of DEMs

Nowadays, there are various DEM data are available with coarse to finer resolution with various accuracy to particular location. In case of flood inundation mapping study, an accurate and with fine resolution data is always preferred. In this connection it is at most necessary to check available DEM data with possible high resolution to conduct the hydrologic or hydraulic modelling study. Therefore, the analysis of the various available open DEM data is carried out for the Tawi river basin.

5.2.1 Comparison of the Stream network and sub-watersheds

The stream drainage pattern in any watershed is a representation of spatial structure and attributes of geography and hydrology of that particular basin. In a hydrological environment, drainage pattern mainly depends on composite factors such as spatial pattern and hydrological features formulated by the surface runoff phenomenon occurring in that particular watershed. Therefore, the representation of the stream network is an important aspect of any hydrological modelling study. In the present study, the drainage networks extracted from all these DEMs have also compared with drainage networks on the Land Use Land Cover map by SoI (Scale: 1:50 k) and on google earth map and shown in Fig. 5.1 Based on the visual interpretation of the results shown in Fig 5.1, it can be seen that almost every stream network extracted from each DEM dataset follows an identical drainage pattern

particularly upstream of the Jammu. As it can be noted that the elevation of the Tawi river basin upstream of the Sidhra gauging station at Jammu is ranging between approximately 294 to 4331 m. However, the stream network pattern extracted by using different DEM datasets downstream of the Jammu gauging site is significantly different. Among the five stream networks extracted from the selected different DEMs, the stream network extracted from the AW3D30 DSM is closely matched with those by the SoI LULC map and google earth topographic map used as a standard. Further, the stream network extracted from Carto DEM was very close to those by AW3D30 DEM. However, ASTER, SRTM and ALOS PALSAR-RTC DEMs were failed to represent the stream network in the Tawi River basin downstream of the Jammu gauging site.

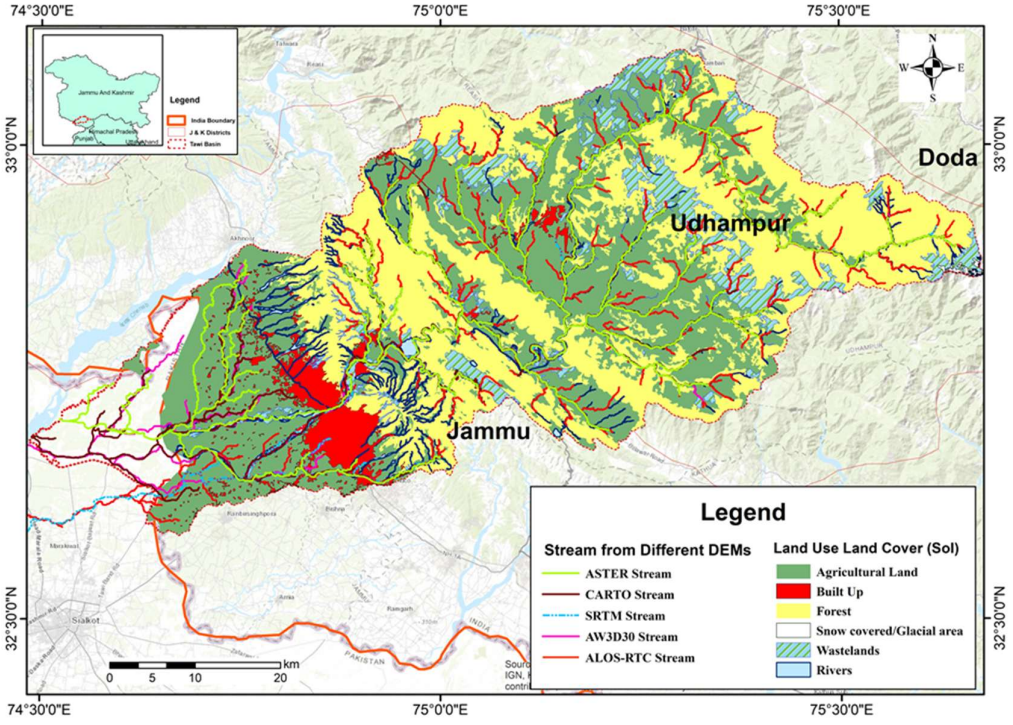

Figure 5.1 Drainage networks extracted from all five DEMs and overlaid on the LULC map by SoI.

As mentioned earlier there are major nine tributaries (nallahs) namely Balini, Chirwa, Duddar, Gambir, Jhajjar, Ramnagar, Sardhan, Balole and Sohagni that joins the main Tawi stream to form the drainage network of the river Tawi. Out of these nine tributaries, seven tributaries except Balole and Sohagni are drains into the main Tawi river located in the upstream catchment area from Sidhra gauging station at Jammu. Based on the discussion in the previous section, geomorphological properties of the Tawi river basin were analyzed

separately for sub-watershed upstream and downstream of the Sidhra gauging site at Jammu and hence the complete Tawi river basin is subdivided into 14 sub-watersheds. The extracted drainage networks, sub-watershed extracted from all the five DEM datasets along with elevation overlaid on the google earth map are shown in Fig. 5.1. The comparison of the sub-watersheds areas derived from different DEMs are shown in Fig. 5.2.

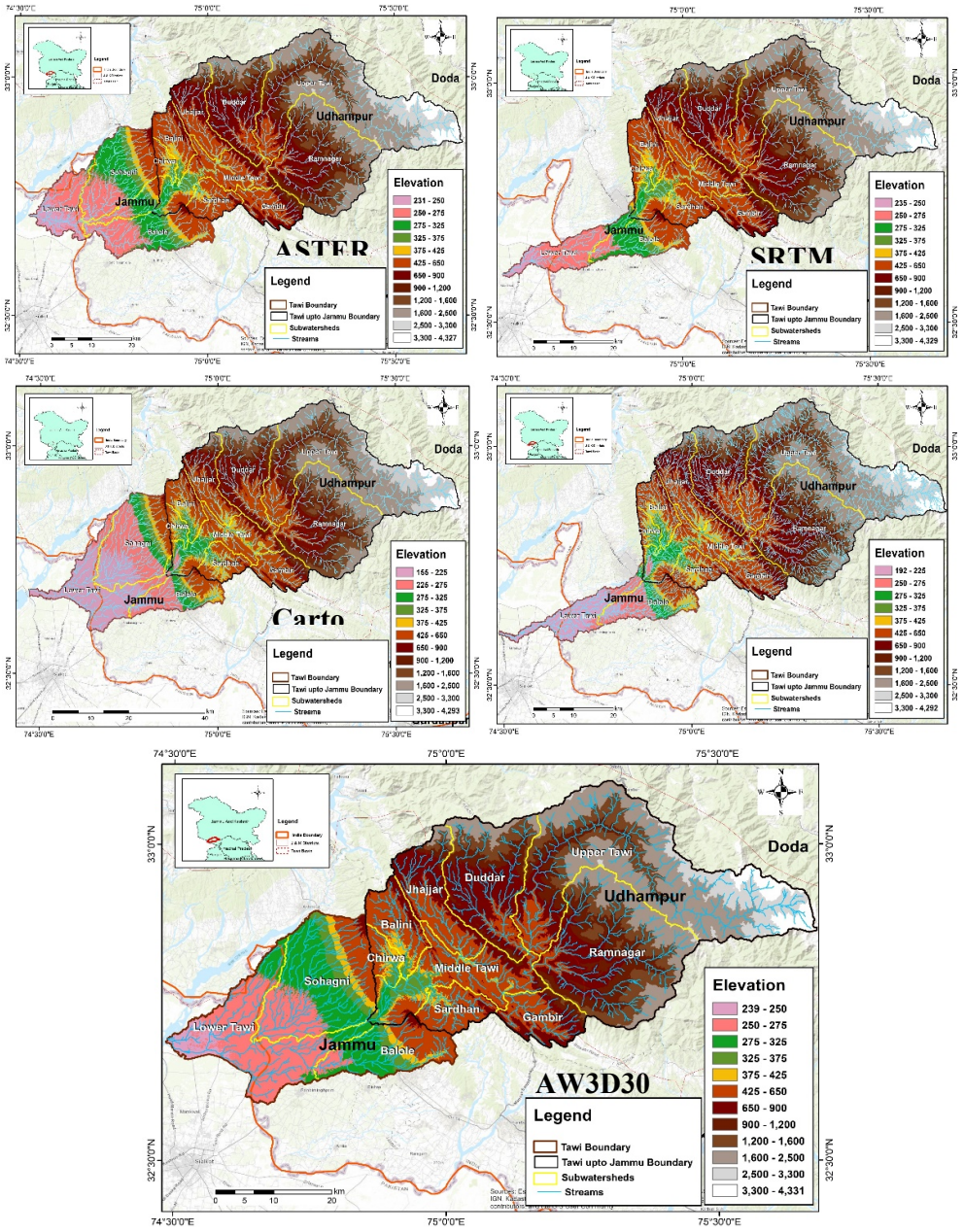

Figure 5.2 Drainage networks and sub-watersheds extracted from all the five DEM datasets along with elevation overlaid on the google earth map.

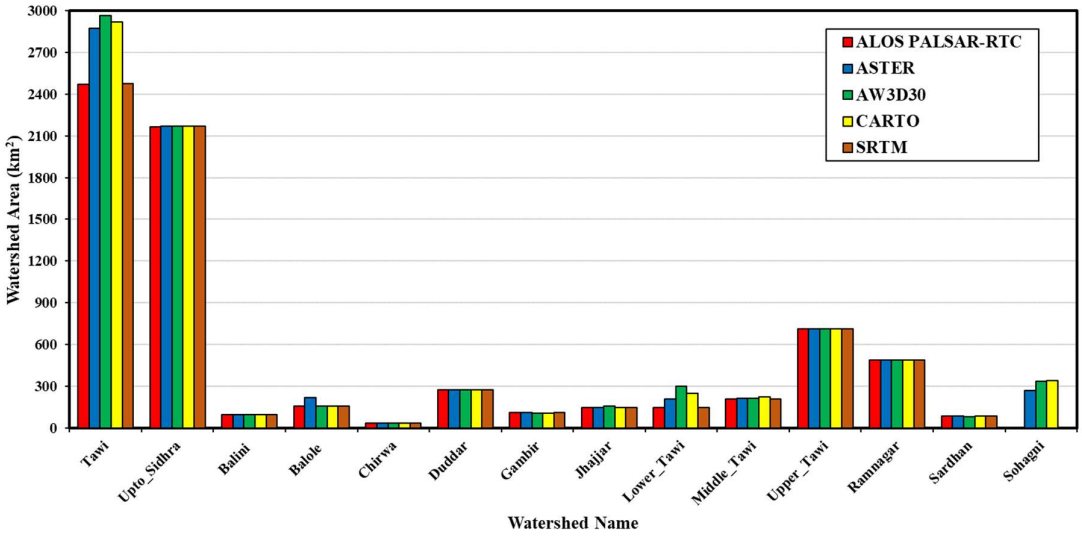

Figure 5.3 Comparison of sub-watershed areas computed by different DEMs.

From the sub-watershed areas shown in Fig. 5.3, it can be inferred that the sub-watershed area extracted from selected five DEMs upstream of the Sidhra gauging site at Jammu are nearly the same. However, as there is a very large difference in the sub-watersheds area below the Sidhara gauging site. This conclusion can also be verified from the results shown in Fig. 5.2. Further, from the results shown in Fig. 5.2, it can be seen that the Sohagni sub-watershed is extracted from AW3D30, Carto and ASTER DEMs. SRTM and ALSO PALSAR-RTC DEMs do not able to extract the Sohagni sub-watershed as these DEMs failed to represent the Tawi river stream accurately in the downstream reach.

5.2.2 Comparison of the drainage morphometric properties

Several morphometric parameters (linear, areal and relief aspects) from all five selected DEM datasets were calculated in order to facilitate inter-comparison to choose the best DEM dataset. Linear aspect parameters computed were stream order, stream numbers, bifurcation ratio, weighted mean bifurcation ratio, stream length, mean stream length and stream length ratio. The areal aspect parameters computed were basin area, basin length, form factor, drainage basin perimeter, circularity ratio, elongation ratio, drainage density, constant of channel maintenance, stream frequency and texture ratio. The relief aspect parameters computed were maximum elevation, minimum elevation, highest relief, lowest relief, relative relief, relief ratio, dissection index and ruggedness index. These different morphometric properties of the Tawi river basin derived from selected five DEMs are shown in Table 3. Referring to Table 3, it can be seen that all the DEMs with a spatial resolution of the 30 m

(AW3D30, SRTM, ASTER and CartoDEM) gave 6th as higher-order stream except ALOS PALSAR-RTC DEM which gave 7th as a higher-order stream. It is very interesting to see that the stream numbers and stream lengths derived from AW3D30, CartoDEM and ASTER DEMs were approximately the same as the watershed delineated with these DEMs were also approximately similar. Although, the stream numbers and stream lengths derived from SRTM were lower as compared to the former three DEMs as the SRTM DEM failed to accurately delineate the Tawi river watershed in the lower reaches. The highest stream numbers and stream lengths were derived from ALOS-PALSAR-RTC DEM which means that the finer the resolution, the more stream counts will be derived from DEM. The bifurcation ratio for the highest order stream as well as the weighted mean bifurcation ratio for all the DEMs was significantly different. It can be noted that the bifurcation ratio is considered as an important morphometric parameter as it denotes the water carrying capacity and related flood potentiality of any basin. Further, the mean stream length and stream length ratio derived from the AW3D30, SRTM, CartoDEM and ASTER DEMs were nearly close to each other. However, these values derived from ALOS PALSAR DEM are significantly lower.

The areal aspects seen from Table 5.1 reveals that the basin area derived from AW3D30 and CartoDEM were nearly the same which shows the highest basin area estimates. Although, the basin area derived from SRTM and ALSO PALSAR-RTC DEMs was approximately the same but significantly lower than those from the other three DEMs due to inaccurate delineation of the watershed area by these DEMs (see Fig. 5.2). Further, the basin length in kilometers derived from all five DEMs was approximately the same. The form factor values derived from all the DEMs are ranging between 0.183 to 0.239 with ASTER and AW3D30 DEMs shows higher values. These value of form factors suggest that the Tawi river catchment is elongated. Although the values of the other areal aspect parameters derived from AW3D30, CartoDEM, ASTER and SRTM are approximately very close to each other, the values derived from ASTER and CartoDEM are closer to AW3D30 DEM. The drainage density, stream frequency and drainage texture parameters derived from the ALOS PALSAR-RTC DEM are significantly higher than those from the other four DEMs. Referring to Table 5.1, the AW3D30 DEM shows higher values maximum as well as minimum elevation followed by SRTM, ASTER, ALOS PALSAR and CARTO DEMs, respectively. Interestingly the elevation values given by the AW3D30, ASTER and SRTM DEM are very close. The values of the highest relief, relative relief, relief ratio, dissection index and ruggedness index derived from Aw3d30 and SRTM DEMs are very close as compared to

other DEMs. These results show that the DEM quality play important role in the extraction of the morphometric parameters.

Table 5.1 Drainage Morphometric properties of the Tawi river basin derived from selected five DEMs.

Morphometric parameters	ALOS PALSAR-RTC DEM	ASTER DEM	AW3D30 DEM	CARTO DEM	SRTM DEM
Linear aspect					
Stream order (u)	7	6	6	6	6
Stream numbers (Nu)	7997	1861	1929	1861	1596
Bifurcation ratio (Rb)	0.24	0.26	0.17	0.41	0.09
Weighted Mean bifurcation ratio (WMRb)	3.09	3.57	4.13	2.64	6.88
Stream length (Lu)	4291.79	2580.66	2705.01	2636.41	2173.44
Mean stream length (Lum)	0.56	1.39	1.44	1.64	1.64
Stream length ratio (Rl)	0.73	0.98	0.80	0.85	0.87
Areal aspect					
Basin area (A)	2471.62	2870.21	2964.08	2919.02	2482.54
Basin length (L)	115.75	109.54	113.17	115.10	116.21
Form Factor (Ff)	0.184	0.239	0.231	0.220	0.183
Drainage basin perimeter (P)	489.7	468.72	465.4	481.01	487.08
Circulatory ratio (Rc)	0.129	0.164	0.172	0.1586	0.131
Elongation ratio (Re)	1.35	1.36	1.30	1.32	1.33
Drainage density (Dd)	1.736	0.899	0.912	0.903	0.875
Constant of channel maintenance (CCM)	0.576	1.112	1.096	1.107	1.142
Stream frequency (Fs)	3.23	0.648	0.650	0.637	0.642
Drainage texture (Rt)	5.608	0.582	0.593	0.575	0.562
Relief aspect					
Maximum elevation (Hmax)	4292	4327	4331	4293	4329
Minimum elevation (Hmin)	192	231	239	155	235
Highest relief (R)	978	826.38	1000.33	761.46	1017.56
Lowest relief (r)	2.052	4.283	1.918	0.700	3.115
Relative relief (Rr)	975.9	822.1	998.4	760.7	1014.4
Relief ratio (Rf)	0.0084	0.0075	0.0088	0.0066	0.0087
Dissection index (Di)	0.998	0.994	0.998	0.999	0.999
Ruggedness index (Ri)	1.695	0.739	0.911	0.688	0.888

5.2.3 Comparison based on the hypsometric analysis

Topographical characteristics have a high influence on the hydrologic response of the drainage basin. The hypsometric tool developed by Strahler (1952) is popularly used in the field of hydrology. The hypsometric curve and Hypsometric Integral (HI) values which are considered important indicators of the watershed conditions are commonly employed to analyze the topography of the basin (Ritter, 2002). Technically, hypsometry is related to the measurement of the heights. Hypsometric analysis (area-altitude analysis) provides an understanding of the stage of the development of the watershed. The hypsometric curve, which is essentially a graphical representation of the watershed area and elevation, is essentially a normalized cumulative frequency distribution of the elevation (Strahler, 1952). The hypsometric analysis is commonly used to understand the erosion status as well as the runoff potential of the watershed. The shape of the hypsometric curve is an important indicator in the determination of the role of topography in streamflow generation. According to Niyazi et al (2019), the hypsometric curve shape is the best parameter to select the suitable DEM for studying the hydrologic behavior of the river basin.

The hypsometric integral is the area beneath the curve which relates the percentage of the total relief to the cumulative percentage area. The HI index can be estimated using the elevation-relief ratio method (see Table 3.1) proposed by Pike and Wilson (1971). Theoretically, HI values range between 0 - 1. The HI index is important in identifying either tectonic or erosive forces which are predominant in the determination of the drainage basin shape (Gopinath et al. 2014; Girish et al., 2016). Further, due to its dimensionless nature, it is more effective in comparing the catchments and thus accuracy of the DEMs irrespective of their scale.

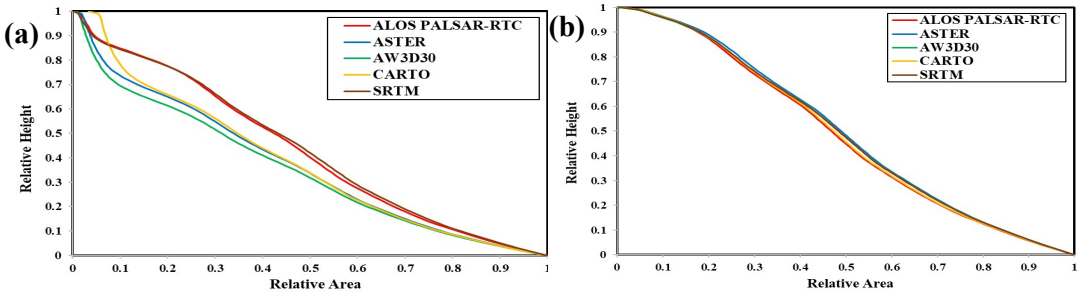

Figure 5.4 Hypsometric curves derived from five selected DEMs of the Tawi river basin (a) up to its confluence with Chenab River, and (b) up to Sidhra gauging site, Jammu.

Fig. 5.4a, b shows the results of the hypsometric curves of the Tawi river basin up to its confluence with Chenab River and up to Sidhra gauging site, Jammu, respectively. From Fig. 5.4a, it can be seen that the hypsometric curves derived from AW3D30, ASTER and CartoDEM were significantly different from those by SRTM and ALOS PALSAR-RTC DEMs. However, interestingly, there is no much noticeable difference between the hypsometric curves derived from all the five DEMs (Fig 5.4b) of the Tawi river basin upstream of the Sidhra gauging site. It can be observed from the shape of these hypsometric curves that the drainage system of the Tawi river basin is in the younger stage of geomorphometric development.

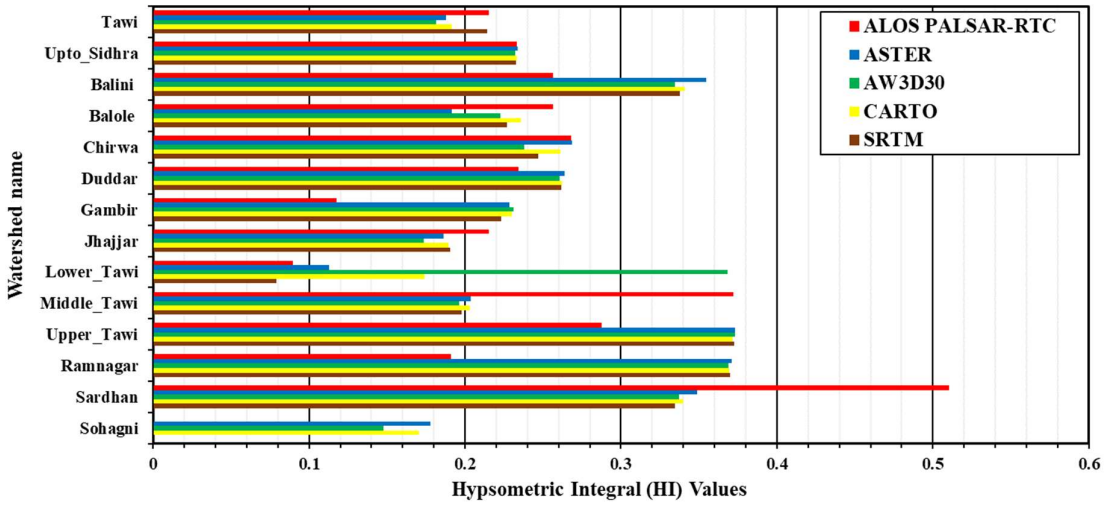

Figure 5.5 Hypsometric integral (HI) values of all the14 sub-watersheds derived from five selected DEMs of the Tawi river basin up to its confluence with Chenab river.

Fig. 5.5 shows the hypsometric integral values of the 14 sub-watersheds of the Tawi River basin derived from the selected five DEM datasets. From Fig. 5.5, it can be seen that the HI values derived from the SRTM and ALOS PALSAR-RTC DEMs of the whole Tawi basin were slightly higher as compared to those from other DEMs. However, the HI values of the Tawi basin up to the Sidhra gauging site were approximately the same. These results are confirming the results of hypsometric curves shown in Fig. 5.4. In the case of the lower Tawi sub-watershed, the HI values derived from AW3D30 DEM are significantly higher as compared to those given by the other DEMs. These results for the lower Tawi sub-watershed are important because in these lower reaches of the Tawi river only AW3D30 DEM following the stream as on the google earth map and considered to be accurate. Particularly, the HI values derived from four DEMs except for ALOS-PALSAR-RTC of the sub-

watersheds laying upstream of the Sidhara gauging site were very close to each other. From these hypsometric integral (HI) analyses, it can be seen that Ramnagar, Sardhan, Upper Tawi, Balini and lower Tawi sub-watersheds are in the late mature stage of erosion (0<HI<0.4). The remaining sub-watersheds are in the old stage of the erosion (0<HI<0.3), representing a more incisive fluvial process.

5.3 Setting-up HEC-HMS model for Tawi Basin

In this section the HEC-HMS model set-up for the Tawi river basin and results during calibration and validation are discussed.

5.3.1 Daily Rainfall disaggregation

Burian and Durrans (2002) have argued that the accurate hydrologic simulation of small catchment require the rainfall timeseries with fine resolution. Many studies have reported that the when the catchment response time is shorter as compared to the total duration of the rainfall excess, the direct runoff observed at the catchment outlet is influenced by rainfall depth and the intensity distribution ((Ball,1994; Woolhiser and Goodrich, 1988; Hjelmfelt, 1981). However, Ball (1994) found that the temporal pattern of rainfall excess had a minimum influence when the catchment response time is higher i.e if the hydrograph has fully developed. Thus, for short duration storms, coarse temporal pattern results in the underestimation of the runoff due to smoothing of the high rainfall intensities. Therefore, hhourly or sub-hourly rainfall depths are probably the most important data input for the simulation of flood hydrograph at outlet of catchment characterized by flash flood. Tawi basin is also subjected to flash floods due to its topographic and climatological setting. Therefore, disaggregation of daily rainfall into hourly rainfall is necessary, in order to simulate high rainfall-runoff event.

Usually, the density of rain gauges station hourly rainfall depth measurement is low, therefore the disaggregation of daily rainfall or transfer of information from the nearby station is commonly preferred. When the daily rainfall measuring stations are far away from the hourly rainfall measuring station (i.e., satellite rain gauge station), then the disaggregation of the daily rainfall can be carried out using “Uniform Disaggregation method” by simply dividing the daily total by 24. However, Gutierrez-Magness and McCuen (2004) have shown that the uniform disaggregation method is not an accurate predictor, because most of the smaller storms have durations much less than 24 hrs and also shows rainfall during zero rainfall hours. Therefore, Gutierrez-Magness and McCuen (2004) have proposed “Bivariate

Satellite Ratio Disaggregation method". This method is useful when the daily rainfall depths have been recorded at the rain gauge stations in the watershed, hourly proportion from the hourly satellite rain gauge stations within or outside watershed can be used to distribute the measured daily rainfall depth into hourly depths. Therefore, the measured hourly rainfall depths ($X_{i,j,m}$) at the satellite stations X are used to proportion daily rainfall depths measured within watershed ($Y_{j,m}$) using the proportion of the daily rainfall ($X_{j,m}$) at X by using following equation

$$Y_{i,j,m} = \left(\frac{X_{i,j,m}}{X_{j,m}}\right) Y_{j,m} \tag{5.1}$$

where $X_{i,j,m}$= measured hourly rainfall depth at the satellite Gauge X for hour i, day j, and year m; and $Y_{i,j,m}$ = predicted hourly rainfall value for daily rainfall depth rain gauge station Y. In this analysis, the values of $Y_{j,m}$ are obtained by summations of the measured values of $Y_{i,j,m}$ for any j and m by following equation

$$\hat{Y}_{j,m} = \sum_{i=1}^{24} Y_{i,j,m} \tag{5.2}$$

In India the 24 hr rainfall for any day j is measured between 8:30 AM (IST) on day $j-1$ to 8:30 AM (IST) on day j.

Accordingly, the disaggregation of daily rainfall depth at IMD grids covering the Tawi catchment river basin up to Jammu (Bikram Chowk) has been carried out. The locations of the daily rainfall depth measuring IMD grids (considered as rain gauge stations) and hourly rainfall measuring rain gauge station such as Chatha and Kawa (i.e. satellite rain gauge stations) are shown in Figure 5.6.

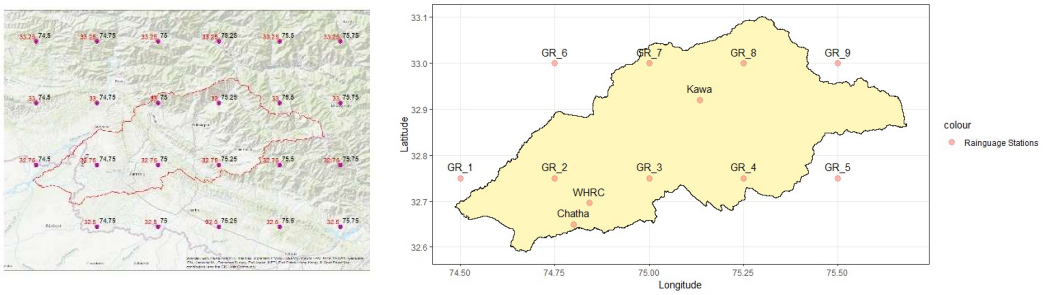

Figure 5.6 Locations of rain gauge stations considered in this study.

For calibration and validation of HEC-HMS model, the high flood event of 1-10 September, 2014 and 1-10 August, 2016 are considered, respectively. The daily rainfall depth

values at various IMD grid points along with observed daily rainfall depth at in-house WHRC-NIH observatory covering the Tawi catchment are shown in Figure 5.7 and 5.8 for 2014 and 2016 flood event, respectively. The results presented in Figure shows that the gridded rainfall equally good as compared to observed data. Similarly, the daily rainfall depth at these grid point verified with those records presented in Ray et al. (2015).

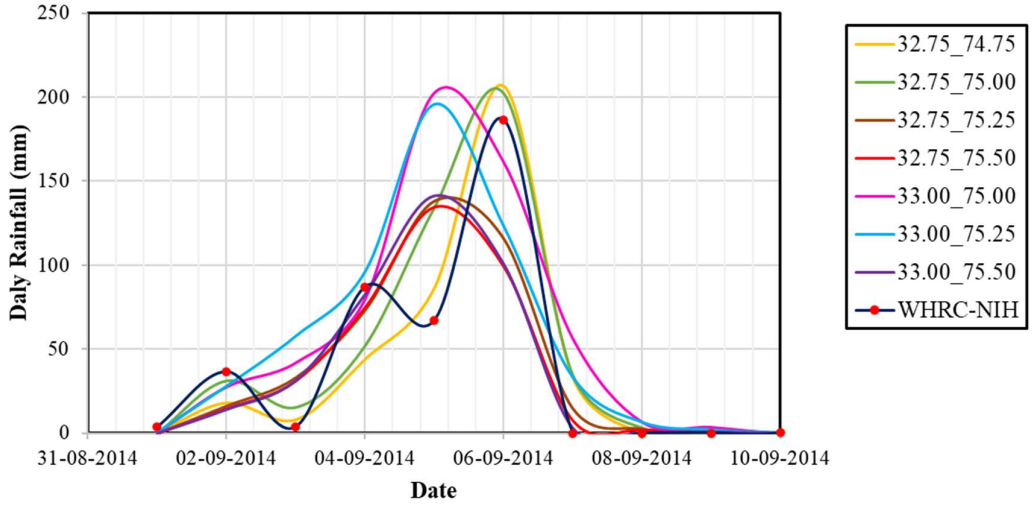

Figure 5.7 Daily rainfall depth at various locations during 3-6 September, 2014 in the Tawi River basin.

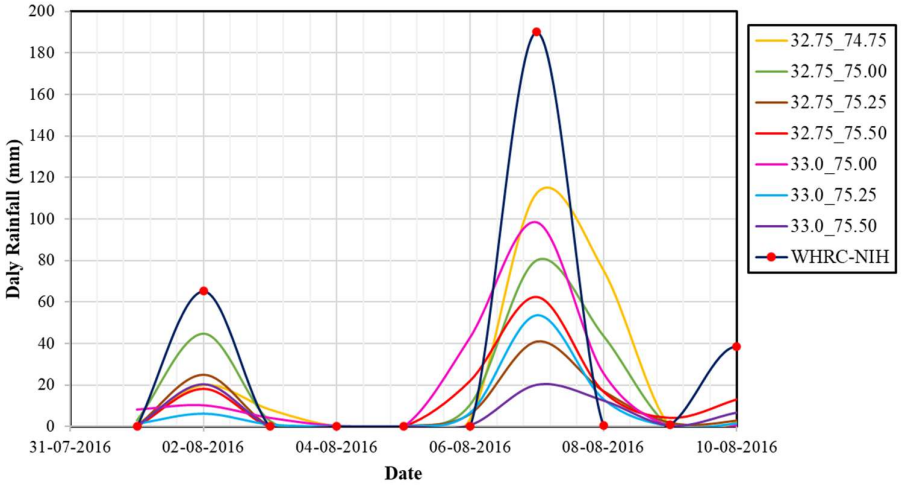

Figure 5.8 Daily rainfall depth at various locations during 1-10 August, 2016 in the Tawi River basin.

Similarly, the hourly Global Satellite Mapping of Precipitation (GSMaP v6 and v7) (https://sharaku.eorc.jaxa.jp/GSMaP/) rainfall data resampled at the observed hourly rainfall depth at Chatha and Kawa stations are shown in Figure 5.9 and Figure 5.10, respectively for 2014 and 2016 flood event. Note that, in case of August 2016 event the hourly rainfall data at

only Chatha, Jammu is available. However, looking at GSMaP hourly data, the hourly time series at Kawa, Udhampur is assumed as same as Chatha, Jammu but delayed by one hour. From these Figures 5.9 and 5.10, it can be revealed that the (GSMaP v6 and v7) product capable to produce the temporal pattern of the rainfall reasonably well but they tend to significantly underestimate during high intensity rainfall event. Therefore, the Bivariate Satellite Ratio Disaggregation method is employed in the present investigation to disaggregate daily rainfall depth at IMD grid points into the hourly rainfall depth using Chatha, Jammu and Kawa, Udhampur as a satellite rain gauge station.

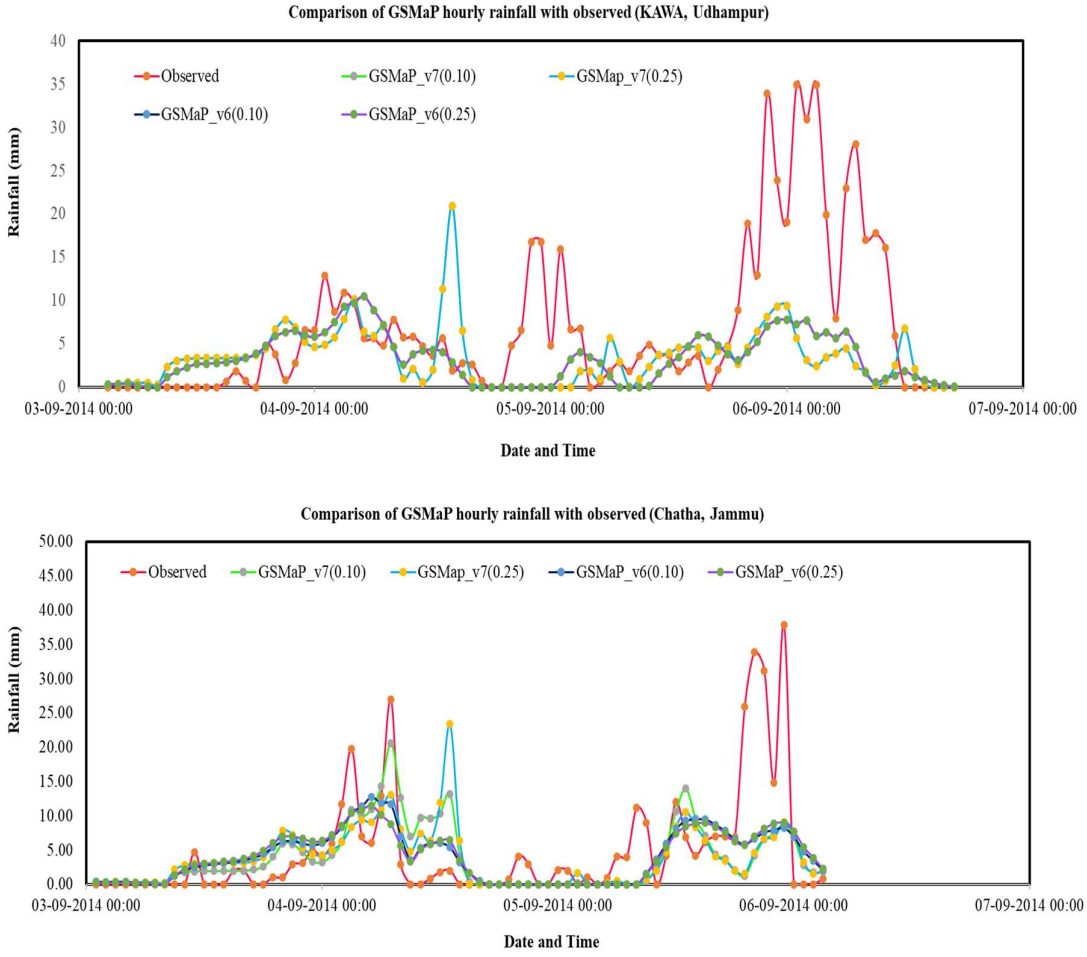

Figure 5.9 Hourly rainfall depth at Chatha-AFMU (Jammu) AND Kawa (Udhampur) rain gauge station (Satellite stations) during 3-6 September, 2014 in the Tawi River basin.

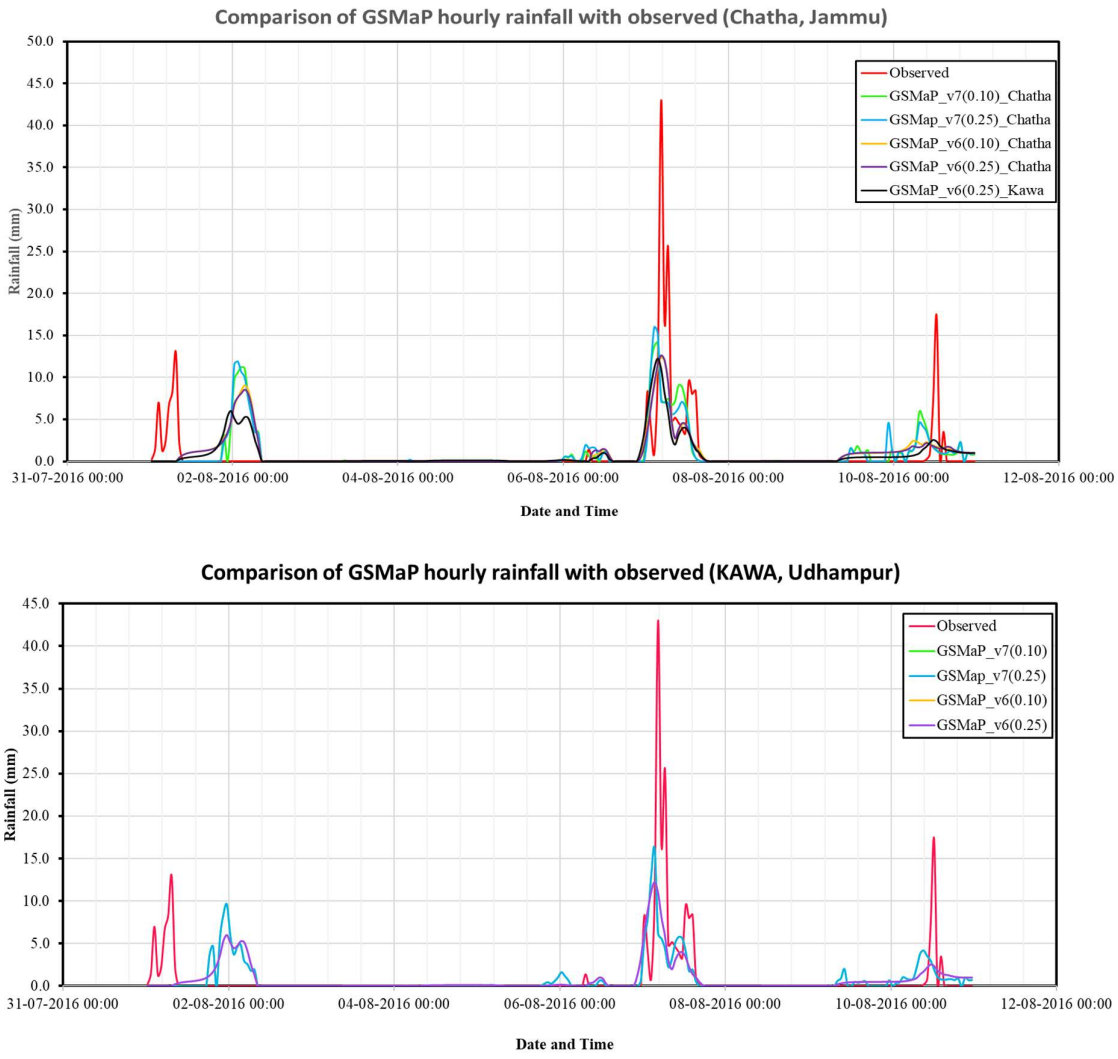

Figure 5.10 Hourly rainfall depth at Chatha-AFMU (Jammu) AND Kawa (Udhampur) rain gauge station (Satellite stations) during 1-10 August, 2016 in the Tawi River basin.

The disaggregated hourly rainfall depth at IMD grid points along with hourly rainfall depth measuring stations Chatha, Jammu and Kawa, Udhampur are shown in Figure 5.11. The disaggregated hourly rainfall depth timeseries data at the IMD grid points and Chatha, Jammu and Kawa, Udhampur rain gauge stations are converted it into the subbasin-wise average rainfall (see Figure 4.3) using the Thiessen polygon method in the FORTRAN programming. The obtained results of subbasin-wise hourly rainfall depth are presented in Figure 5.12. From analysis of Figures 5.11 and 5.12, the observed 24 hr maximum rainfall intensity at Chatha, Jammu and Kawa, Udhampur hourly rain gauge stations were 37.90 mm/hr (during 10:00 to 11:00 PM on the 5th September 2014) and 35 mm/hr (during 01:00 to 03:00 AM on the 6th September 2014), respectively. The predicted rainfall intensity at

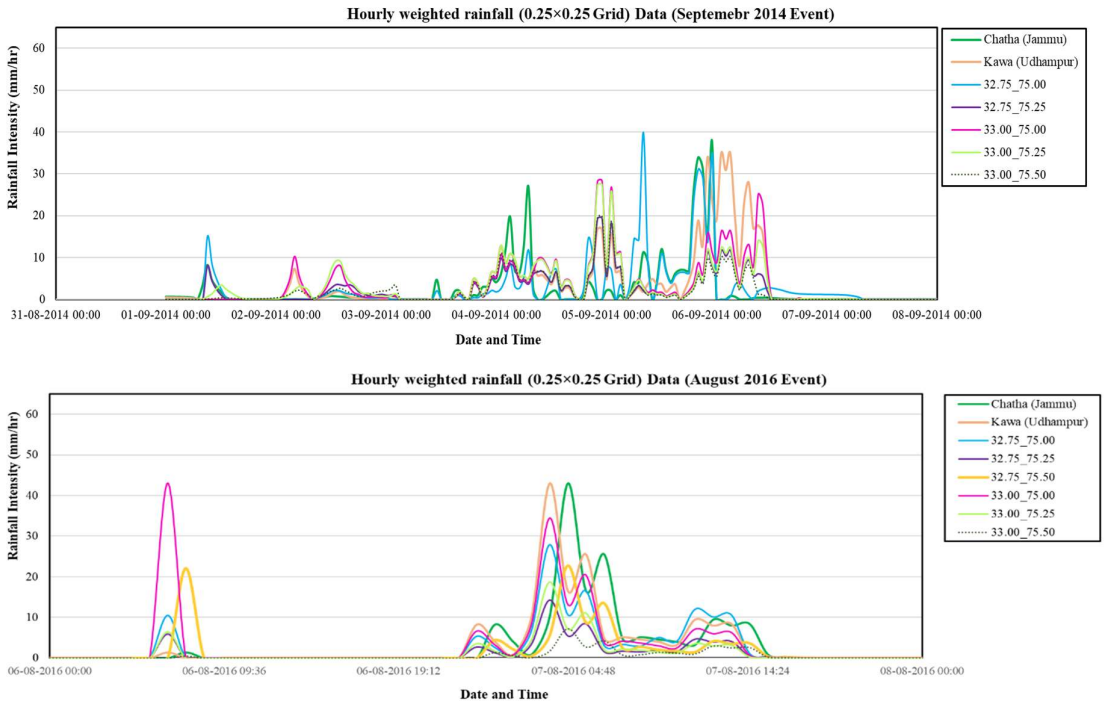

Figure 5.11 The disaggregated hourly rainfall depth at IMD grid points along with hourly rainfall depth measuring stations Chatha, Jammu and Kawa, Udhampur for 2014 and 2016 flood event.

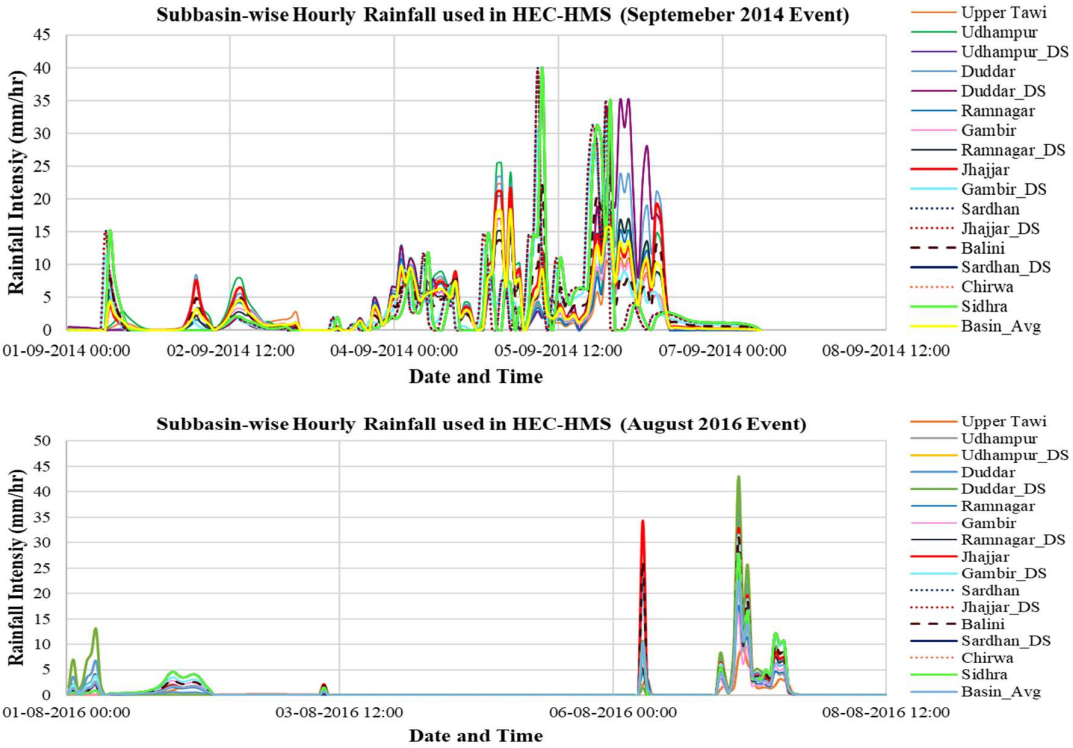

Figure 5.12 Subbasin-wise hourly rainfall for HEC-HMS mode for Tawi basin up to Jammu (Bikram Chowk) for 2014 and 2016 flood event.

Sidhara and Udhampur subbasins were 39.97 mm/hr (during 10:00 to 11:00 PM on the 5th September 2014) and 35 mm/hr (during 01:00 to 03:00 AM on the 6th September 2014), respectively. Therefore, it can be concluded that the application of Bivariate Satellite Ratio Disaggregation method to transform daily rainfall depths at IMD grid points to hourly rainfall depths and conversion of these disaggregated hourly rainfall into subbasin average rainfall provides reasonably well hourly rainfall depths timeseries by maintaining the rainfall intensities IMD grid points as well as for the subbasins considered for the HEC-HMS model set-up.

5.3.2 Calibration and validation of event-based HEC-HMS model

Event-based hydrologic models are frequently applied to assess flood and estimate design flood. In these events based hydrologic models, the loss values are required to relate with antecedent conditions in the catchment. The loss values are key parameter in any hydrological based model which are generally obtained by matching the model output with the observed or derived streamflow information. In this study, event-based HEC-HMS model is calibrated using the high flood event from 1-10 September, 2014. The HEC-HMS model has been set-up up to the Jammu (Bikram Chowk) gauging station (see Figure 4.3). the subbasin-wise hourly disaggregated rainfall depths data (as generated in above section 5.31) were forced into the meteorological module of HEC-HMS model. The Curve number (CN) grids also generated for the Tawi River basin and shown in Figure 5.13. The CN range varied between 58-98. Note that the major locations in the western part belongs to low CN range; whereas, the middle and northern part has very high CN indicating high runoff generation potential.

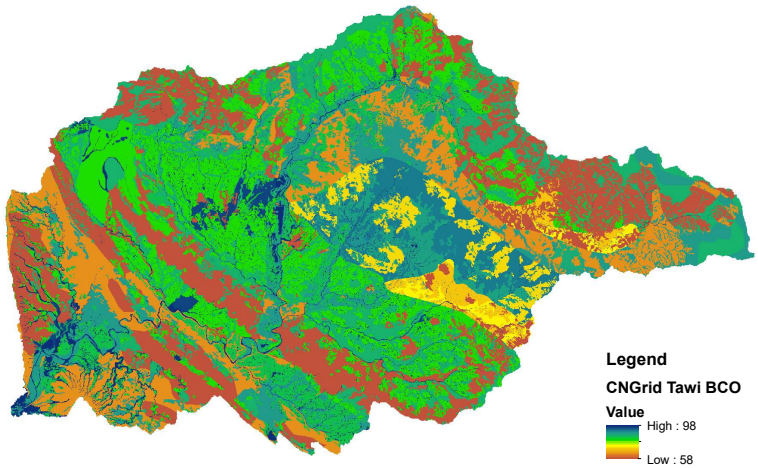

Figure 5.13 Curve number grids generated for estimation of the runoff from different sub-basins of the Tawi river basin.

The stand procedure and methods are followed to calibrate the HEC-HMS model parameters of four processes: loss, transform, baseflow and channel routing. To consider losses the Simple Canopy method (to account canopy losses), the Simple Surface method (to account surface/depression storage losses) and Initial and Constant loss (to account infiltration and soil storages losses) have been used. The calibrated maximum storage parameters of the Simple Canopy method for the various subbasins were varying between 5 – 10 mm. The calibrated maximum storage parameters of the Simple Canopy method for the various subbasins were varying between 5 – 20 mm. The initial loss rate and constant loss rate parameters required in the Simple Surface method were varying between 100 – 550 mm and 0.1 – 0.15, respectively. The initial loss rate and constant loss rate parameters required in the Simple Surface method were varying between 100 – 550 mm and 0.1 – 0.15, respectively. The transform method used is Clark Unit hydrograph transform method whereas recession method is used to account for baseflow contribution The storage coefficient and time of concentration parameters of the Clark Unit hydrograph transform method for the various subbasins were varying between 0.03 – 0.18 (hr) and 0.09 – 0.54 (hr), respectively. In order to estimate calibrated parameters of the baseflow recession model, the master recession flow technique was used. The results of this technique are presented in Figure 5.13. From the observed flood discharge at Sidhara (Jammu) gauging station, the derived flow duration curve is presented as Fig. 5.14a. Similarly, the master recession curve fitted is presented in Fig. 5.14b. To prepare the direct runoff hydrograph, the event-scale baseflow contribution to the streamflow was estimated by baseflow separation technique (Fig. 5.14c). The resulting master recession curve was found out to be: $Q(t) = 16637 \times e^{-3.959}$. Accordingly, the calibrated initial discharge and recession constant parameters of the baseflow Recession method for the various subbasins were varying between 0.87 – 7.96 (m^3/s) and 0.1 (for all), respectively.

Finally, the Muskingum-Cunge method was used to route the flow in the river channel. As shown in Figure 5.15, the cross-sections were generated using AW3D30 DEM at the identified three locations at upper end, middle and lower end of the longitudinal river profile of each subbasin and used to compute average cross-section for river reach. As shown in Figure 5.15, the highest drop was observed for the reach 1 due to the steep terrain that causes faster removal of flood water and may result in attaining the peak faster. Typical cross sections at some selected reaches are presented in Fig. 5.16. The data of these cross-section for each river reach in the HEC-HMS model is supplied as 8-point in the paired data module

(cross-sections). The range of the calibrated Manning's roughness coefficient for all the considered subbasin were 0.04 -0.12. the higher roughness values in upper reaches were found. Another parameter index celerity is varying between 6.5 to 9.5.

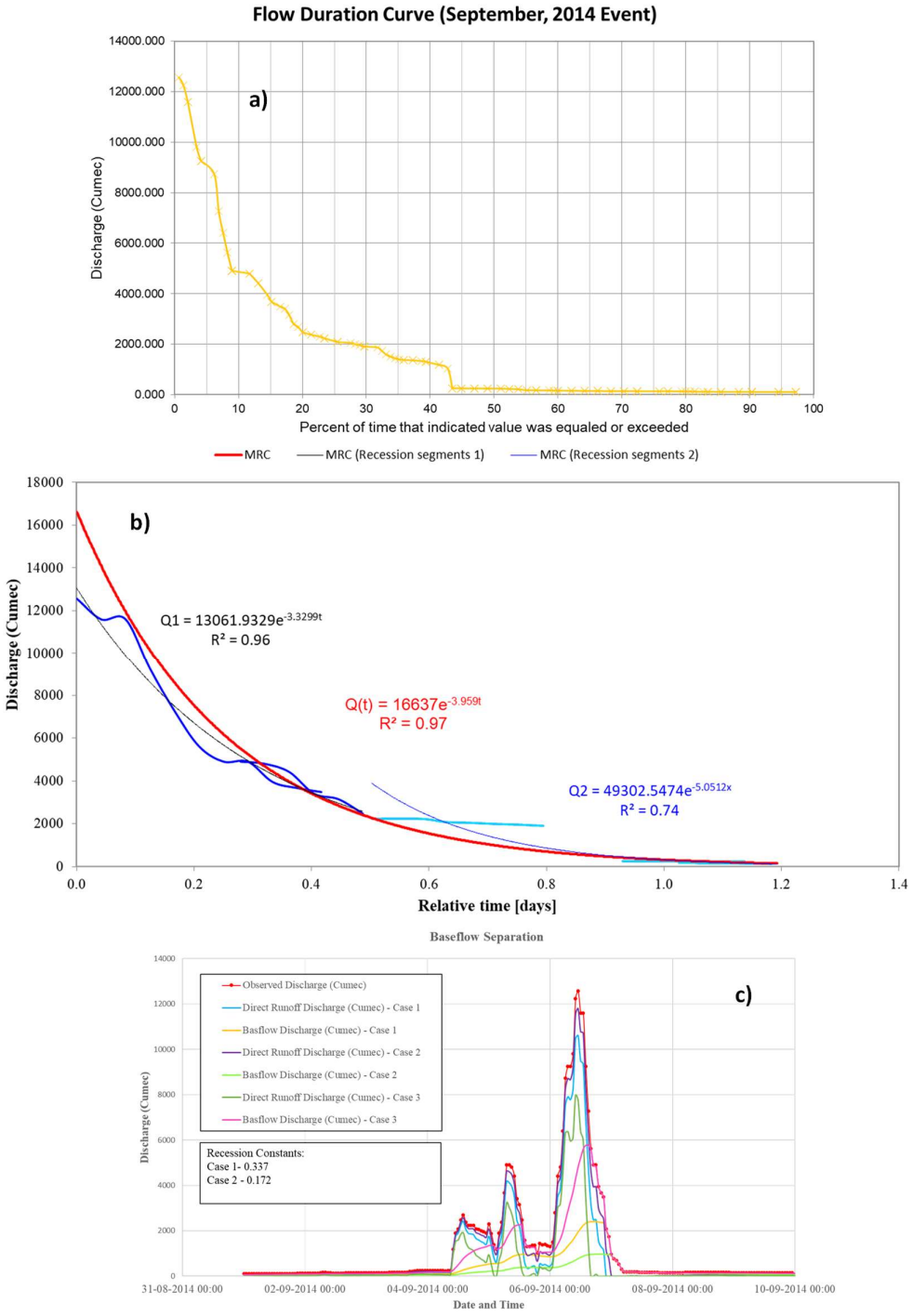

Figure 5.14 (a) Flow duration curve (FDC) for the event of 1-6 Sep. 2014, (b) Recession curve analysis for the event, and (c) baseflow separation for generation off the event-scale direct runoff hydrograph.

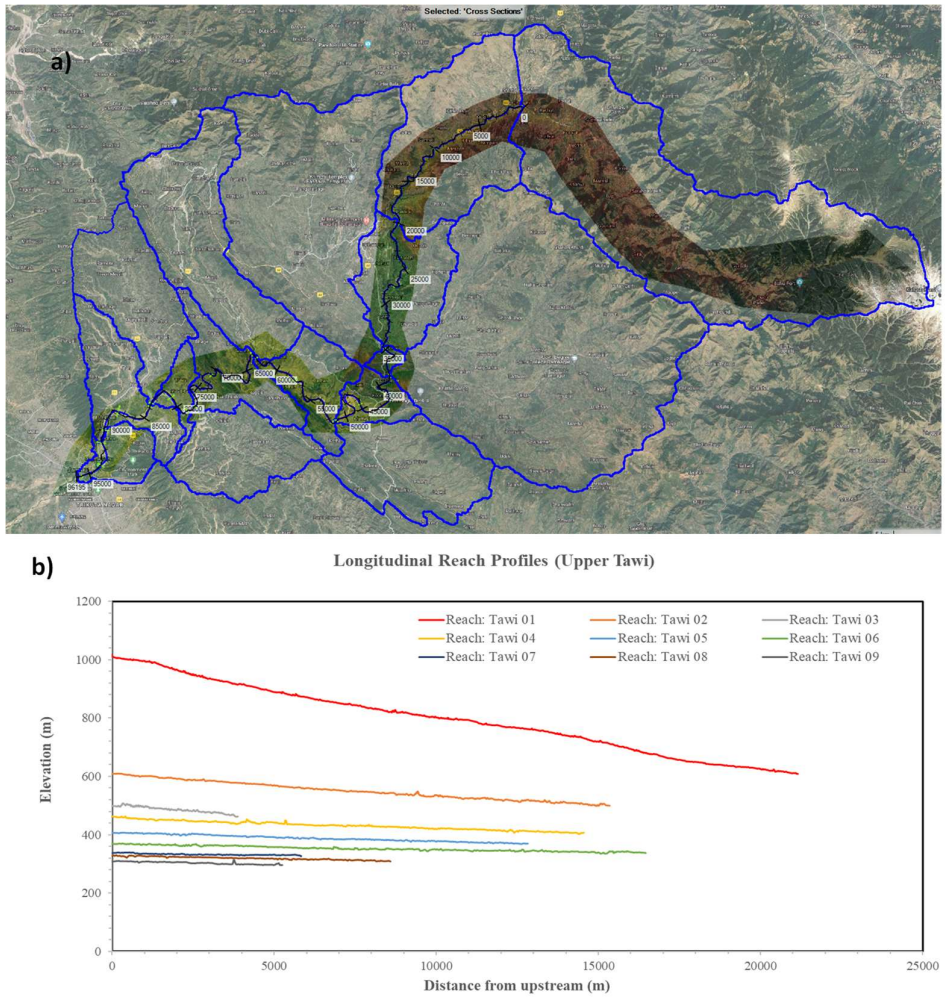

Figure 5.15 (a) Delineation of sub-basins, and (b) longitudinal profiles for setting up Muskingum-Cunge model.

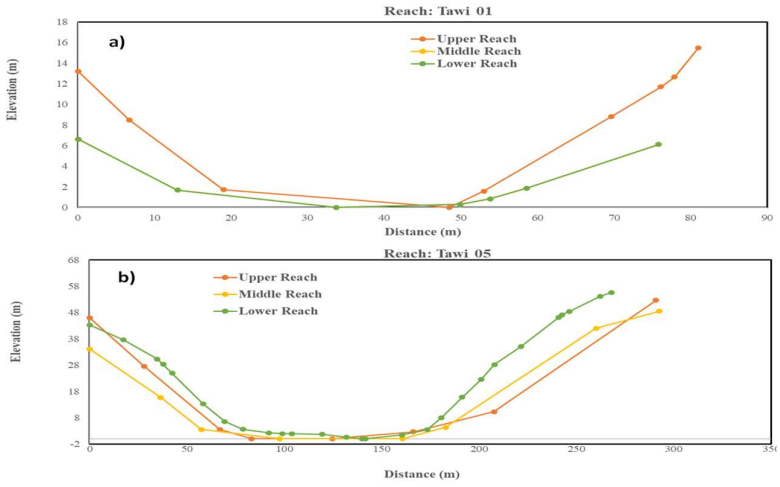

Figure 5.16 Extracted cross-section at some selected reaches of the Tawi River basin for flood routing in HEC-HMS model.

The HEC-HMS model run was successful during its calibration and validation using the 1-10 September 2014 and 1-10 August 2016 high flood event with 10-minute time step. The results of the observed and simulated discharge and stage hydrographs using the HEC-HMS model during calibration and validation period are presented in Figures 5.17 – 5.22. During the calibration and validation, the performance of the HEC-HMS model for the Tawi basin was evaluated using various performance criteria such as Nash-Sutcliffe Efficiency (NSE), Percentage Biased Error in observed and simulated data (PBIAS), Coefficient of determination (R^2), Error in peak discharge (E_p) and Error in time to peak discharge (E_{pt}) and results are presented in Table 5.2.

The visualization of observed and simulated hydrographs in Figures 5.17 – 5.22 suggest that there is some kind of error in observation have been also occurred. However, the calibrated HEC-HMS model shows a very good and acceptable hydrograph shape and also responding very well to the rainfall occurrence in the Tawi river basin catchment. Referring to Table 5.2, during calibration using September 2014 flood event, the observed and computed peak discharges were 3724 m^3/s & 3214.7 m^3/s (with E_p= 15.8% & E_{pt}= -1.0 hr, NSE = 0.63, R^2 = 0.65, RMSE = 0.61 and PBIAS = 11.47%), 12569 m^3/s & 12201 m^3/s (E_p= 3.9% & E_{pt}= -0.16%, NSE = 0.79, R^2 = 0.86, RMSE = 0.47 and PBIAS = 36.48%), and 13552.4 m^3/s and 12232 m^3/s (E_p= 10.8%, E_{pt}= -0.83 hr, NSE = 0.82, R^2 = 0.87, RMSE = 0.42 and PBIAS = 28.55%), respectively at Udhampur (Salmay Bridge), Sidhara (Jammu) and Jammu (Bikram Chowk) gauging stations. Similarly, the observed and computed peak stages during calibration using September 2014 flood event were 9 m & 8.6 m (E_p= 4.7% & E_{pt}= -1.0 hr, NSE = 0.61, R^2 = 0.72, RMSE = 0.6 and PBIAS = 25.46%), 8.85 m & 8.9 m (E_p= -0.6%, E_{pt}= 0.16 hr, NSE = 0.57, R^2 = 0.75, RMSE = 0.7 and PBIAS = 10.37%), and 10.08 m & 10.1 m (E_p= -0.2%, E_{pt}= -0.83 hr, NSE = 0.81, R^2 = 0.87, RMSE = 0.4 and PBIAS = 13.14%) respectively at Udhampur (Salmay Bridge), Sidhara (Jammu) and Jammu (Bikram Chowk) gauging stations. These results suggest that the performance of the HEC-HMS model in prediction of the discharge hydrograph is slightly higher efficient than those for production of stage hydrographs at considered gauging stations in the Tawi river basin. The performance of discharge and stage hydrograph simulation higher at Jammu (Bikram Chowk) and Sidhara (Jammu) gauging stations than those at Udhampur station because the rating curve at Jammu (Bikram Chowk) and Sidhara (Jammu) is verified using the results of 1D hydrodynamic HEC-RAC model results. According to Moriasi et al. (2007),

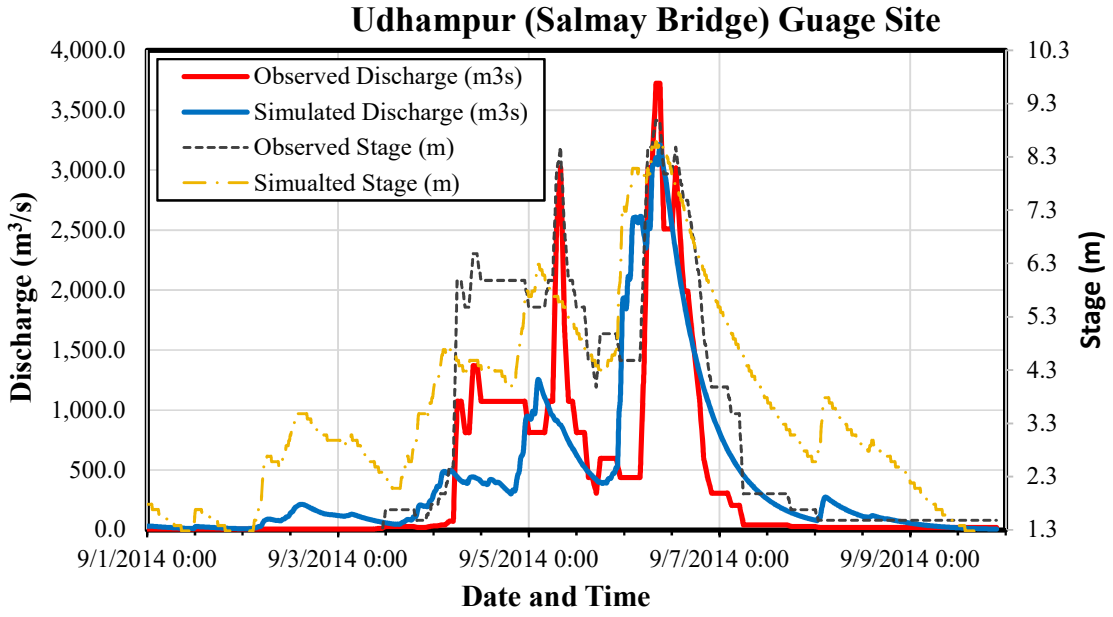

Figure 5.17 Observed and simulated discharge and stage hydrographs using the HEC-HMS model (calibration using September 2014 high flood event) at Udhampur (Salmay Bridge) gauging station on the Tawi River basin.

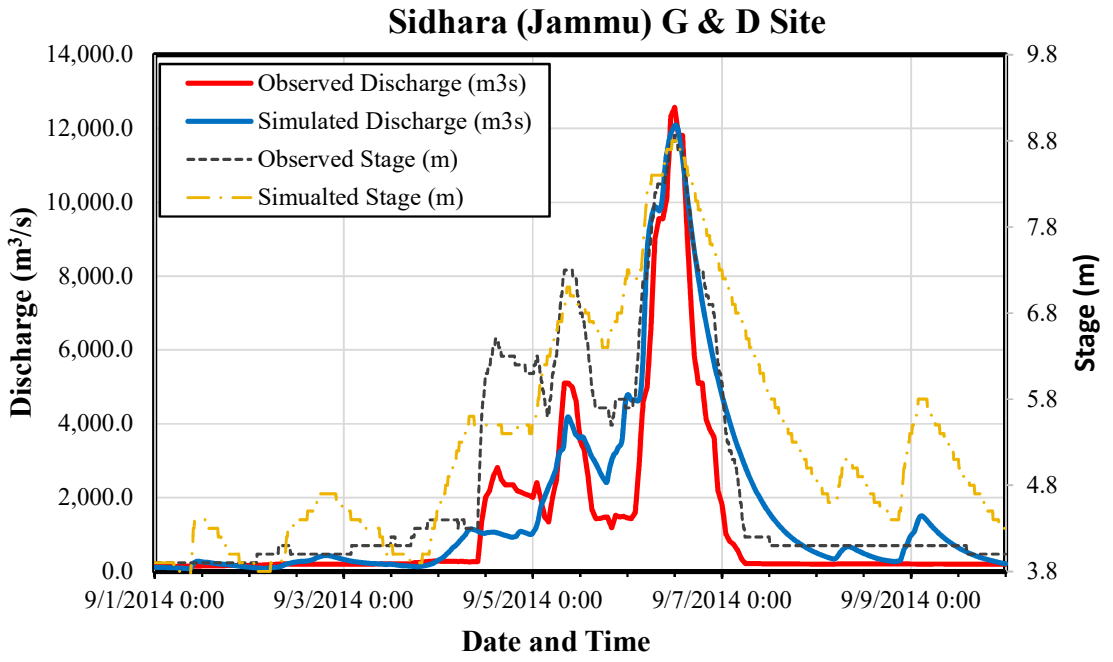

Figure 5.18 Observed and simulated discharge and stage hydrographs using the HEC-HMS model (calibration using September 2014 high flood event) at Sidhara (Jammu) gauging station on the Tawi River basin.

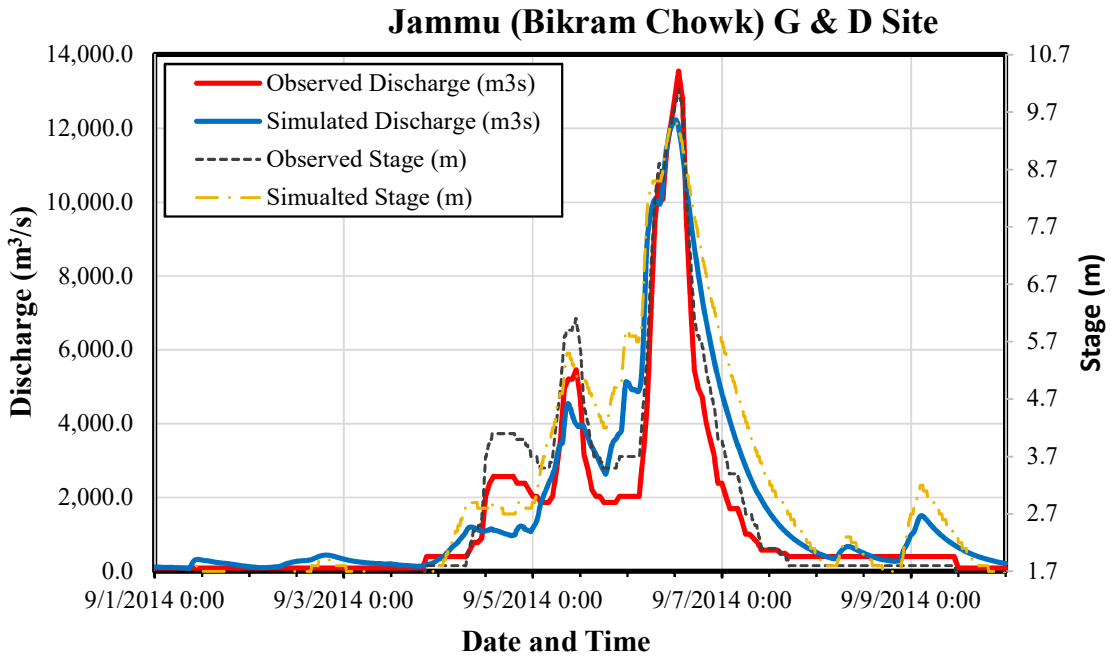

Figure 5.19 Observed and simulated discharge and stage hydrographs using the HEC-HMS model (calibration using September 2014 high flood event) at Jammu (Bikram Chowk) gauging station on the Tawi River basin.

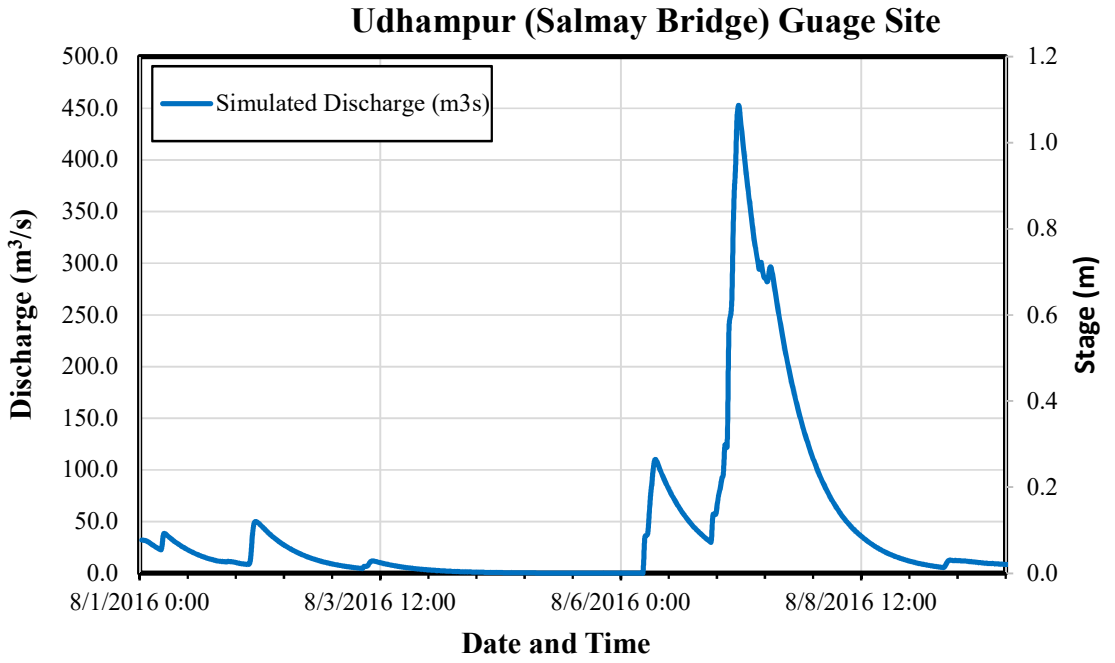

Figure 5.20 Simulated discharge hydrograph using the HEC-HMS model (validation using August 2016 high flood event) at Udhampur (Salmay Bridge) gauging station on the Tawi River basin.

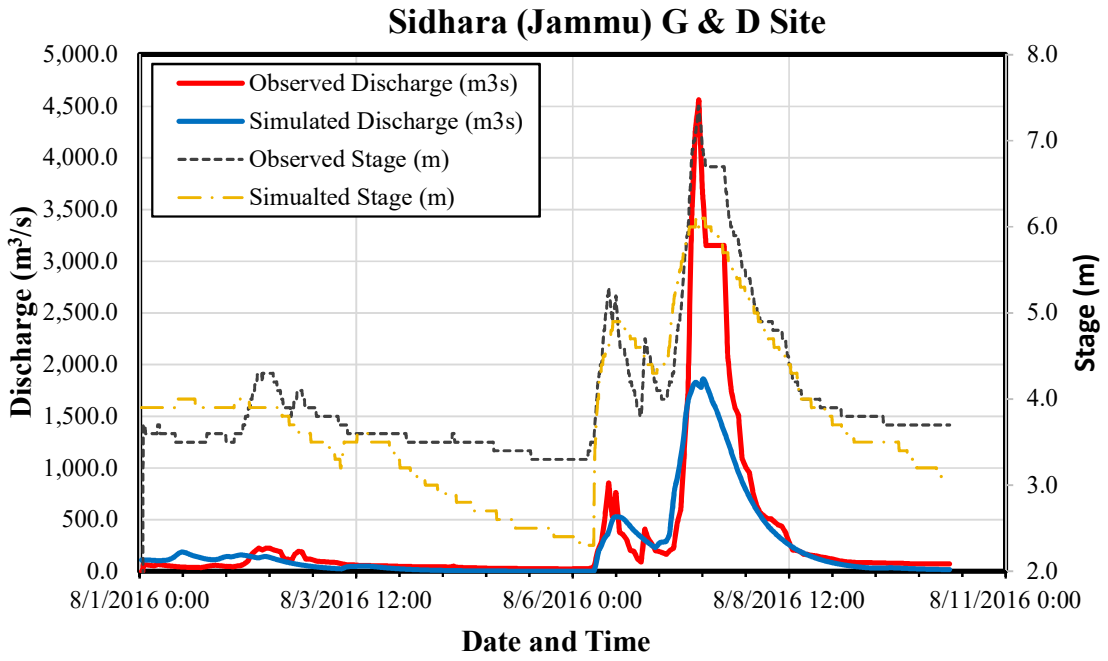

Figure 5.21 Observed and simulated discharge and stage hydrographs using the HEC-HMS model (validation using August 2016 high flood event) at Sidhara (Jammu) gauging station on the Tawi River basin.

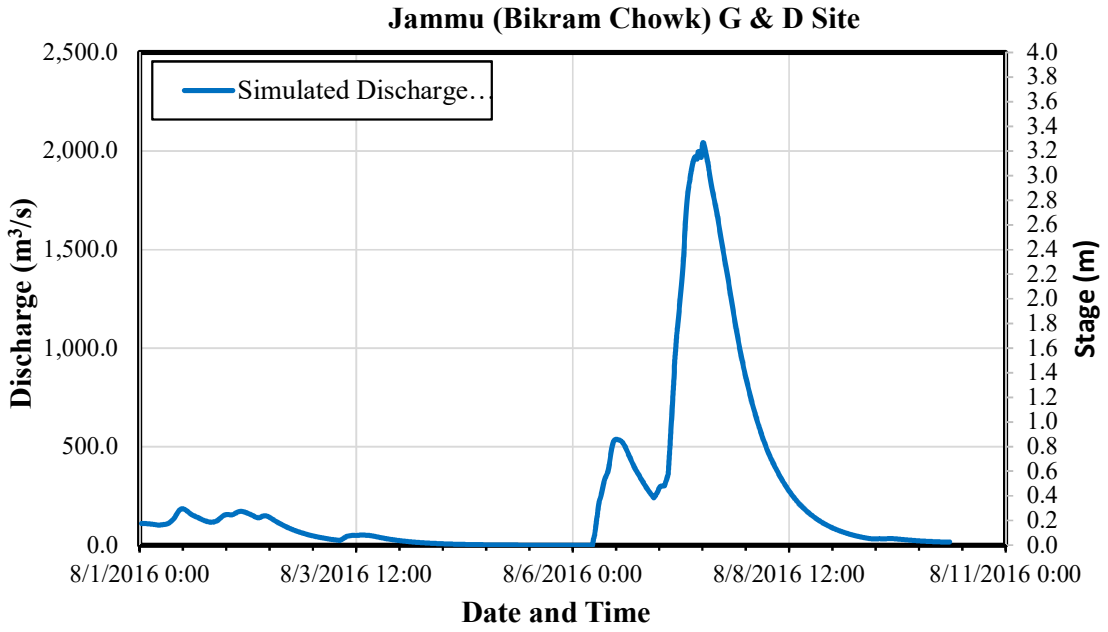

Figure 5.22 Simulated discharge hydrograph using the HEC-HMS model (under validation process using August 2016 high flood event) at Jammu (Bikram Chowk) gauging station on the Tawi River basin.

Table 5.2 Summary of calibration and validation results of the HEC-HMS model for the Tawi River basin.

	Observed	Simulated	Error in Peak Discharge (%)	Error in Time to Peak Discharge (hr)	NSE	R^2	RMSE Stddev	Percentage Bias (%)
Calibration (1-10 September 2014 Flood Event)								
Udhampur (Salmay Bridge) G & D Site								
Discharge (m^3s)	3724	3214.7	15.8	(-1.00)	0.63	0.65	0.61	11.47
Stage (m)	9	8.6	4.7	(-1.00)	0.61	0.72	0.6	25.46
Sidhara (Jammu) G&D Site								
Discharge (m^3s)	12569	12101	3.9	0.16	0.79	0.86	0.47	36.48
Stage (m)	8.85	8.9	-0.6	0.16	0.57	0.75	0.7	10.37
Jammu (Bikram Chowk) G&D Site								
Discharge (m^3s)	13552.4	12232.5	10.8	(-0.83)	0.82	0.87	0.42	28.55
Stage (m)	10.08	10.1	-0.2	(-0.83)	0.81	0.87	0.40	13.14
Validation (1-10 August 2016 Flood Event)								
Udhampur (Salmay Bridge) G & D Site								
Discharge (m^3s)		452.8						
Sidhara (Jammu) G&D Site								
Discharge (m^3s)	4559.7	1860.8	145.0	(-1.1)	0.70	0.88	0.5	(-30.86)
Stage (m)	7.4	6.1	21.3	(-1.1)	0.63	0.77	0.6	(-6.62)
Jammu (Bikram Chowk) G&D Site								
Discharge (m^3s)		2042						

based on the presented various performance evaluation criteria, the performance of HEC-HMS model for Tawi river basin up to Jammu (Bikram Chowk) gauging station is considered as very good at Jammu (Bikram Chowk) and Sidhara (Jammu) gauging stations for simulation of discharge and stage hydrograph. However, the performance of the HEC-HMS model to simulate discharge and stage hydrograph at Udhampur (Salmay Bridge gauging station is considered as good model performance.

Similarly, the performance evaluation criteria during validation using August 2016 flood event (see Table 7.2) are suggesting that the observed and computed peak discharges were 4559.7 m^3/s & 1860.8 m^3/s (with E_p= 145% & E_{pt}= -1.1 hr, NSE = 0.70, R^2 = 0.88, RMSE = 0.5 and PBIAS = 30.86%) at Sidhara (Jammu) gauging station. Similarly, the observed and computed peak stages during validation were 7.4 m & 6.1 m (E_p= 21.3% & E_{pt}= -1.1 hr, NSE = 0.63, R^2 = 0.77, RMSE = 0.6 and PBIAS = -6.62%) at Sidhara (Jammu) gauging station. Although the magnitude extreme flood during September 2014 flood is 2.76 times higher than the peak discharge during August 2016, the HEC-HMS model is performed very well as can be seen from Figure 5.21. Further, according to Moriasi et al. (2007) recommendations, the HEC-HMS model performance is considered good to very good during validation process. Based on these results it can be concluded that the results of the calibrated HEC-HMS model for the Tawi River basin up to Jammu (Bikram Chowk) can be confidently used for flood inundation mapping under climate change.

5.4 HEC-RAS Model Setup for Flood Inundation Mapping

The methodology presented in section 4.2.3 is used to set-up 1D steady state HEC-RAS (version 6.1) model based on the solution of energy equation for the lower Tawi basin downstream of the Sidhara (Jammu) gauging station for generation of flood inundation maps. In case of steady state HEC-RAS model only extreme peak discharge value as an upstream boundary condition required to provided. Further, in order to decide on Manning's roughness coefficient to be used in river channel, the 1D unsteady state model was set-up from Sidhara (Jammu) to the 200 m from the downstream of Wadi and Nikki Tawi. The observed flood hydrograph at Sidhara (Jammu) for September 2014 event was provided as an input to the unsteady state HEC-RAS model. After calibrating this 1D unsteady state model, the optimum Manning's roughness coefficient found was 0.022 in the main river channel. The Manning's roughness is used as primary Manning's roughness coefficient to calibrate and validate 1D steady state HEC-RAS model for the Lower Tawi basin. Further, the predicted Discharge-

stage (Q-h) relationships by 1D steady state HEC-RAS model are used to update the observed rating curve at Sidhara (Jammu) and Jammu (Bikram Chowk) gauging stations as shown in Figure 5.23. There was a close match between the simulated and the observed rating curve depicting the efficacy of the model for use in flood inundation mapping.

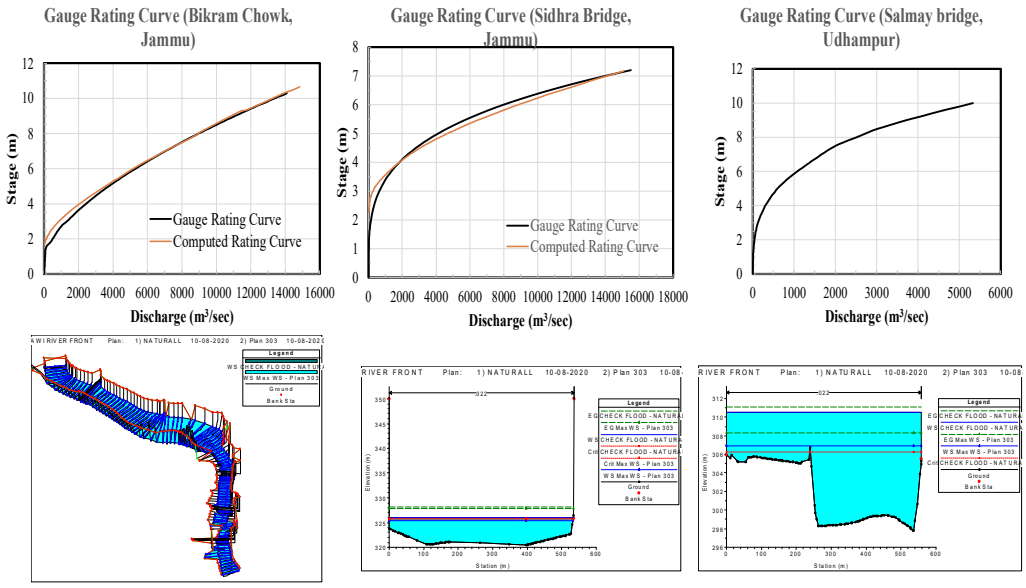

Figure 5.23 Comparison of observed and predicted Q-h rating curve for different gauging stations in Tawi River basin.

The resulting flood inundation map of the event of Sep-2014 by HEC-RAS model for lower Tawi basin is presented in Figure 5.23. It can be inferred that the mid reach of the river was mostly affected with a flood water depth of about 8 m with a great lateral extent. Similarly, the average flooding depth was 3-4 m for most part of the mid-reach of the river with substantial lateral extent. Further, the flood inundation extent obtained with HEC-RAS model (Figure 5.24) is compared with Pre and post Landsat 8 images dated 25 August 2014 and 10 September 2014 for lower Tawi (Figure 5.25). By visual inspection of Figures 5.24 and 5.25, it can be inferred that although there is significant cloud cover over inundated area in the study area, but results of HEC-RAS model seem to closely match with the flood inundation shown on the Landsat 8 imagery.

Further, the validation of the flood inundation map for the lower Tawi is carried out using the photographs during flood event at selected location and are shown in Figure 5.26. From Figure 5.26, it can be inferred that the area near the split of Tawi into Nikki Tawi and

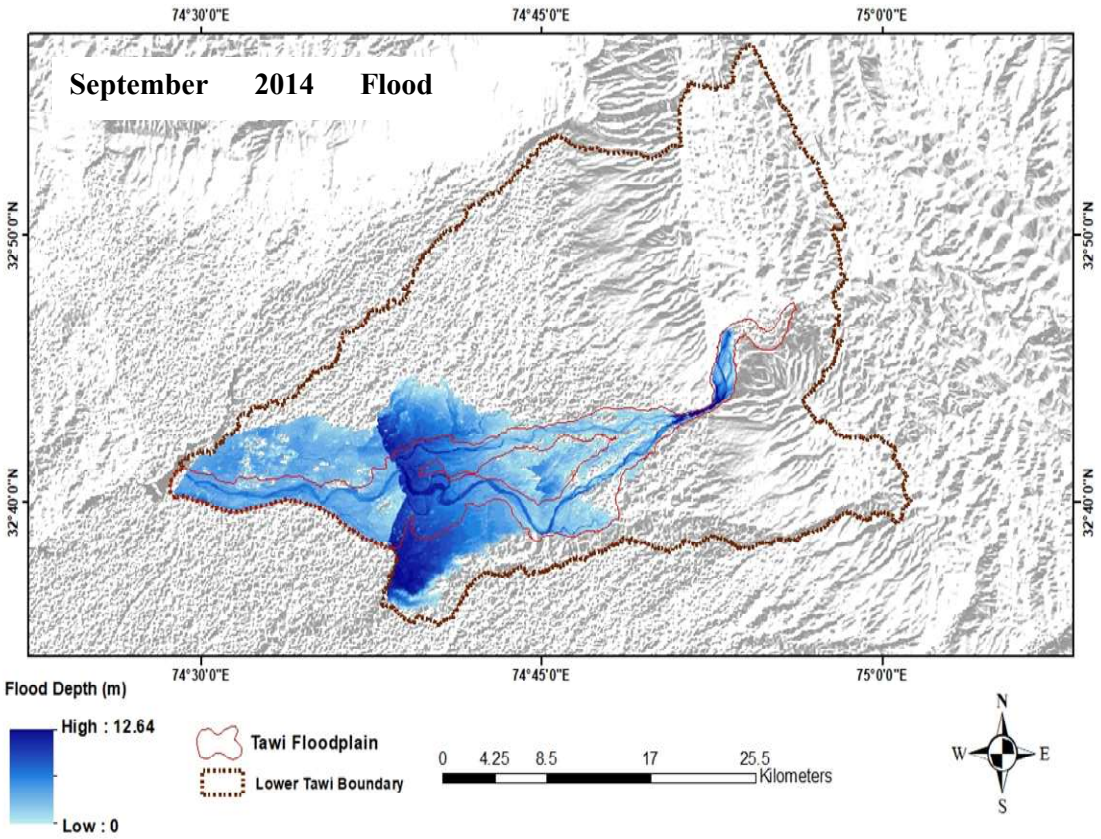

Figure 5.24 Flood inundation map by the 1D steady state HEC-HMS model using peak discharge of September 2014 high flood event at Sidhara (Jammu) gauging station on the Tawi River basin.

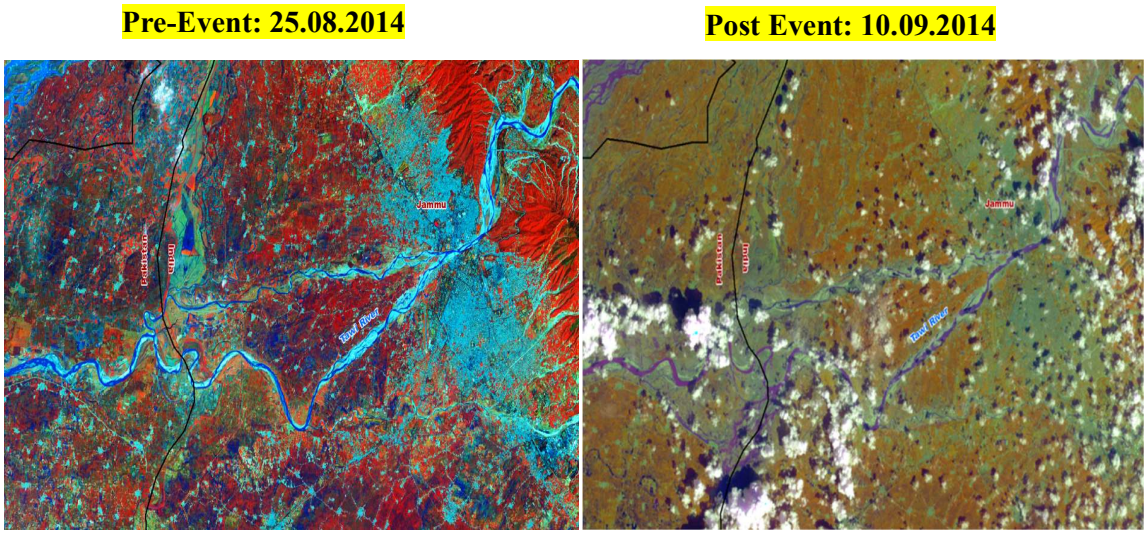

Figure 5.25 Pre and post September 2014 Landsat 8 imagery showing flood inundation the lower Tawi River basin.

Wadi is washed away, the HEC-RAC model shows the similar flood inundated pattern at this location. Further, photograph from the campus of Sher-e-Kashmir University of Agricultural Sciences and Technology of Jammu (SKUAST-Jammu) was available. The close observation of this photograph SKUAST-Jammu (see Figure 5.26) shows that the flood inundation depth at the campus is around 35 cm (as seen from the height of flood at the wheel of vehicle (car), probably with 45 cm diameter wheel). The flood inundation depth observed from HEC-RAS model at university campus is around 44 to 60 cm. Therefore, it can be said that the HEC-RAS model reasonable predicting the flood inundating depth in the lower Tawi basin.

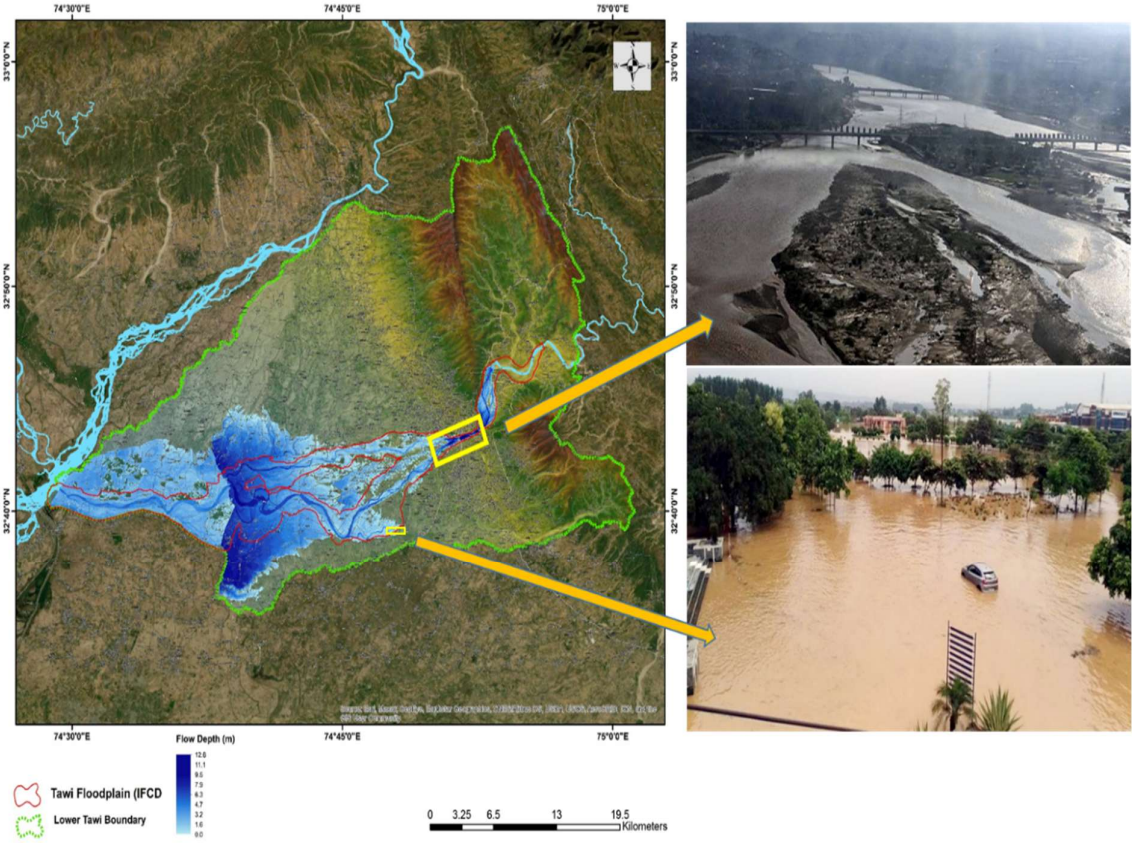

Figure 5.26 Validation of flood inundation map for 6th September 2014 event by HEC-RAS model with field photographs at selected locations for the lower Tawi River basin. [Source: Photos are from intermate].

Further, the scientific validation of flood inundation map by HEC-RAS model is carried out by comparing with Linear Imaging Self-Scanning Sensor 3- LISS-III and Linear Imaging Self-Scanning Sensor 4- LISS-IV by Indian Space Research Organization (ISRO), India. LISS III is a remote sensing satellite camera from ISRO, India (https://bhuvan-app3.nrsc.gov.in/data/download/index.php?c=s&s=L3). The LISS – III camera provides

multispectral data in 4 bands. The spatial resolution for visible (two bands) and near infrared (one band) is 23.5 meters with a ground swath of 141 kms. The fourth band (short wave infrared band) has a spatial resolution of 70.5 meters with a ground swath of 148 kms. The repetitively of LISS–III is 24 days. The LISS-IV is a high resolution multi-spectral sensor operating in three spectral bands (B2 0.52 - 0.59, B3 0.62 - 0.68, B4 0.77 - 0.86). LISS-IV provides a ground resolution of 5.8 m (at nadir) and can be operated in either of two modes: In Multispectral mode (Mx) LISS-IV covers a swath of 23 km. (selectable out of 70 km. total swath) in three bands, while in mono mode (Mono) the full swath of 70 km. The repetitively of LISS–IV is 5 days. The LISS-III images available for 7th September 2014 immediately after high flood event on 6th September 2014 for part of the lower Tawi basin. The LISS-IV image is available for 9th September, 2014 for part of the lower Tawi basin. The results of validation of the flood inundation extent simulated using HEC-RAS model and LISS-III (dated 7th September 2014) and LISS-IV Validation of the flood inundation extent simulated using HEC-RAS model and LISS-IV image (dated 9th September 2014) images are shown in the Figure 5.27 and 5.28.

Referring to results from Figure 5.27, it can be seen that the flood extent estimated by HEC-RAS matching reasonably well with those from LISS-III image with former showing overpredicting of flood extent as compared latter. Similar conclusion drawn from the Figure 5.27 where HEC-RAS extracted flood extent slightly higher than the LISS-IV image. The computation of flood extent area as shown in Figure 5.27(b) and 5.28(b) along with respective area computed for HEC-RAS flood inundation extent area are shown in Table 5.3.

From results in Table 5.3 the error in the flood extent area by HEC-RAS model for the part of lower Tawi basin is -9.17 % and -4.08 % as compared to the those by LISS-III and LISS-IV imagery. The total flood inundated area computed in the lower Tawi basin based on the HEC-RAS simulated flood inundation map is about 22251.4 hectors (Ha) out of which 12096 Ha (120.96 km^2) in India.

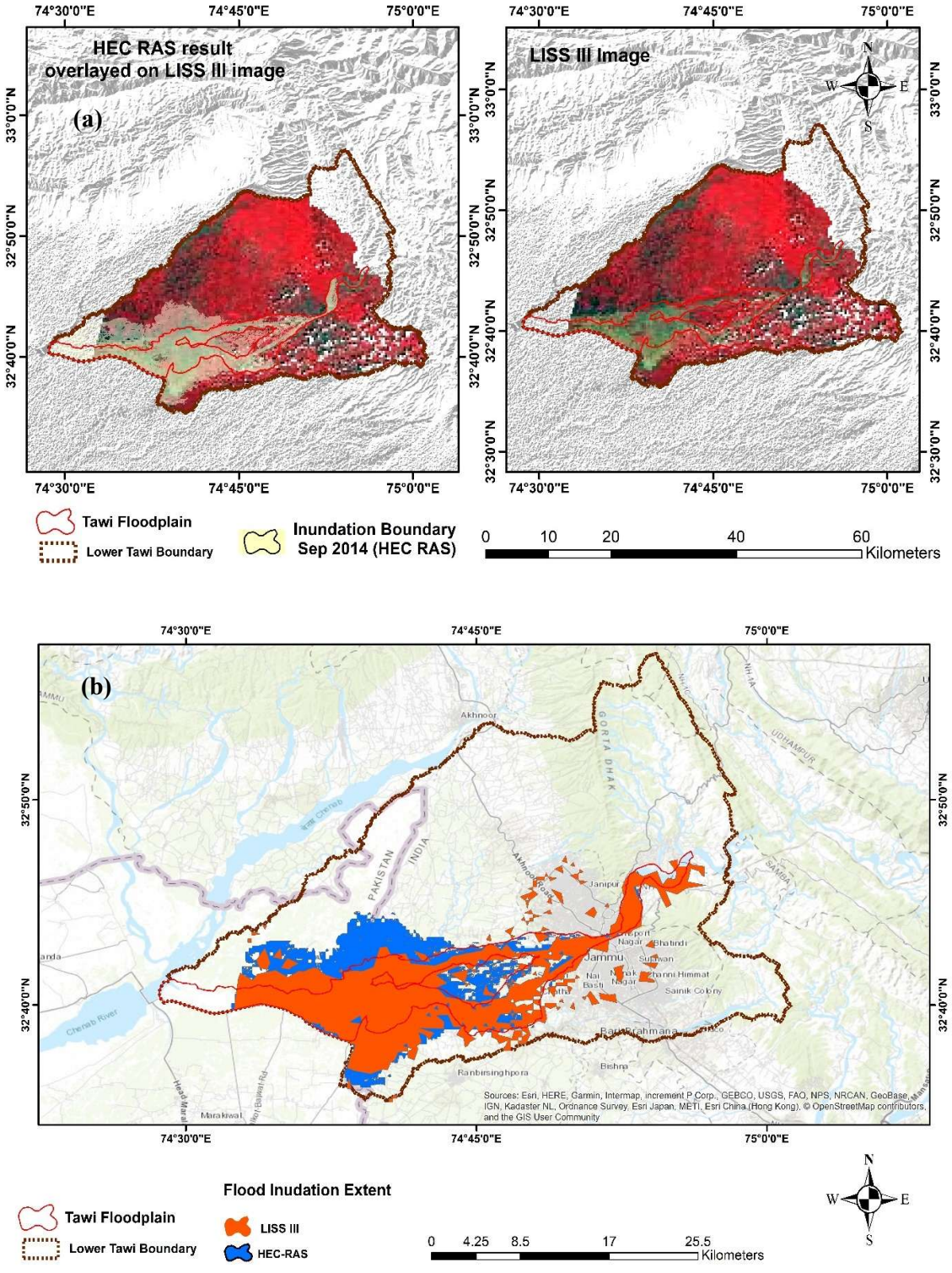

Figure 5.27 Validation of the flood inundation extent simulated using HEC-RAS model and LISS-III image (dated 7th September 2014) (a) HEC-RAS simulated flood extent overlaid on the LISS-III imagery, and (b) comparison of the flood extent extracted from LISS-III and HEC-RAS.

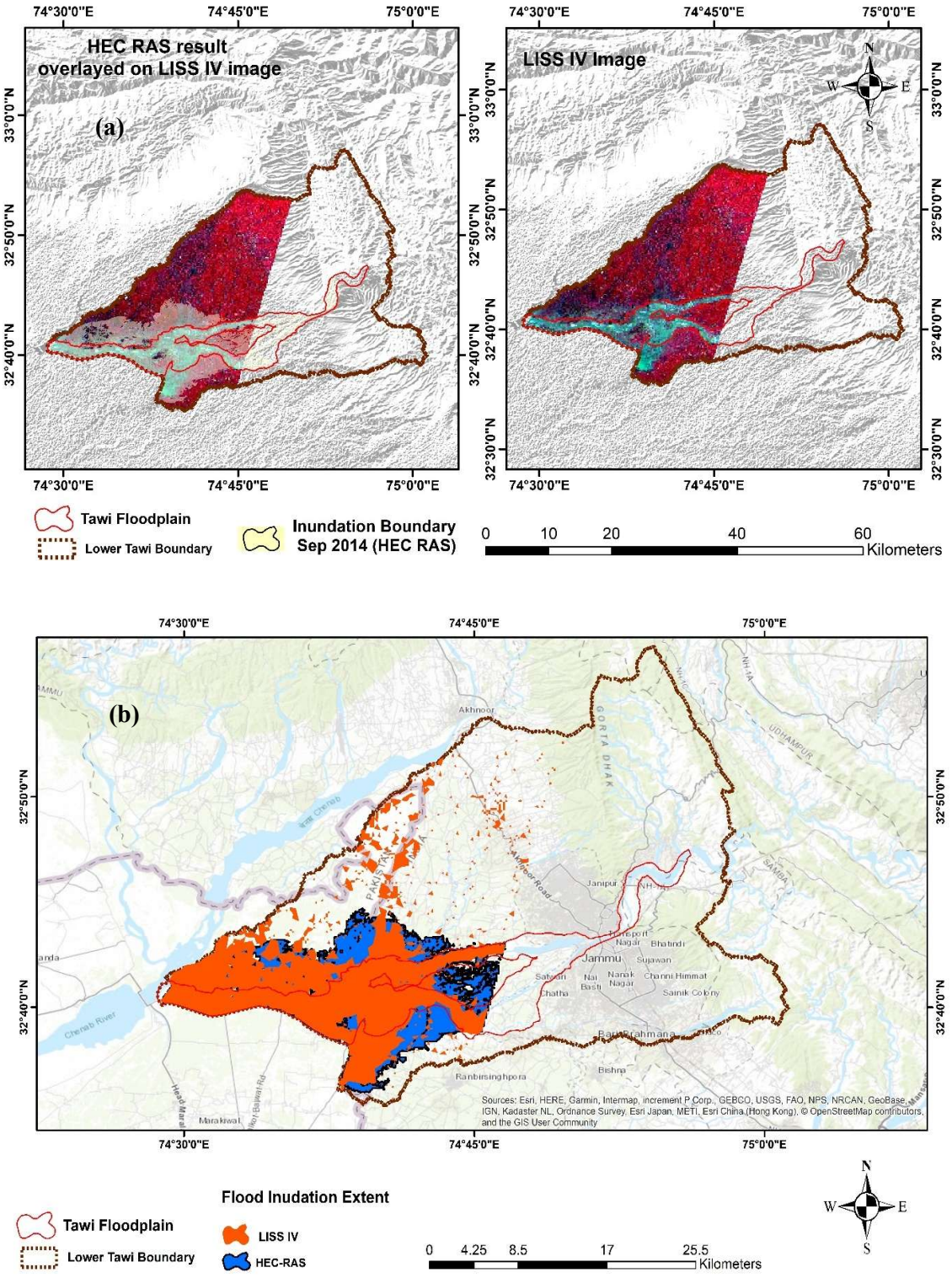

Figure 5.28 Validation of the flood inundation extent simulated using HEC-RAS model and LISS-IV image (dated 9th September 2014) (a) HEC-RAS simulated flood extent overlaid on the LISS-III imagery, and (b) comparison of the flood extent extracted from LISS-III and HEC-RAS.

Table 5.3 Flood extent area of LISS-III, LISS-IV and corresponding HEC-RAS for part of lower Tawi basin.

Satellite Imagery with Date	Flood inundated Area ($km^{2)}$		
	LISS Imagery	HEC-RAS	Error
LISS III (9^{th} September 2014)	175.56	191.67	-9.17
LISS IV (9^{th} September 2014)	179.07	186.37	-4.08

5.5 DESIGN FLOOD ESTIMATION

A purpose of FFA is to predict the magnitude of extreme floods (called as design flood) by relating it to their frequency of occurrence through the application of probability distribution functions (See section 4.2.4). These design flood values are important for planning and design of flood defence against devasting floods. For more precise estimation of extreme flood quantile for various returned periods, it is the prerequisite that the long and continuous historic annual peak flood records should be available with good data quality. In the present study, historic flood records at three G&D sites namely Jammu (Bikram chowk) maintained by IFCD (for period 1977 -2019), Sidhara (Jammu) maintained by CWC (for period 1977 -2019), and Udhampur (Salmay Bridge) maintained by IFCD (for period 1997 -2018) have been used. The annual maximum peak flow data at these G&D sites are presented in Figure 5.29. The details of the annual maximum discharge values at various G&D site are presented in Table 5.4.

Table 5.4 The details of the annual maximum discharge values at various G&D site on Tawi River

G&D site	Mean	Variance	Stand Deviation (SD)	Maximum Discharge (m^3/s)	Minimum Discharge (m^3/s)	Median	Coefficient of variation	Coefficient of Skewness	Coefficient of Kurtosis	Drainage area 9sq. Km)
Udhampur (Bikram Chowk)	1285.9	1619270.3	1272.5	4498	42	994	0.99	1.88	2.7	633-73
Sidhara (Jammu)	2357.4	6355436.8	2521	12569	320	1411.5	1.07	2.54	6.89	2141.65
Jammu (Bikram Chowk)	3657	7335842.9	2708.5	13552	756	2758	0.74	2.45	6.76	2169.82

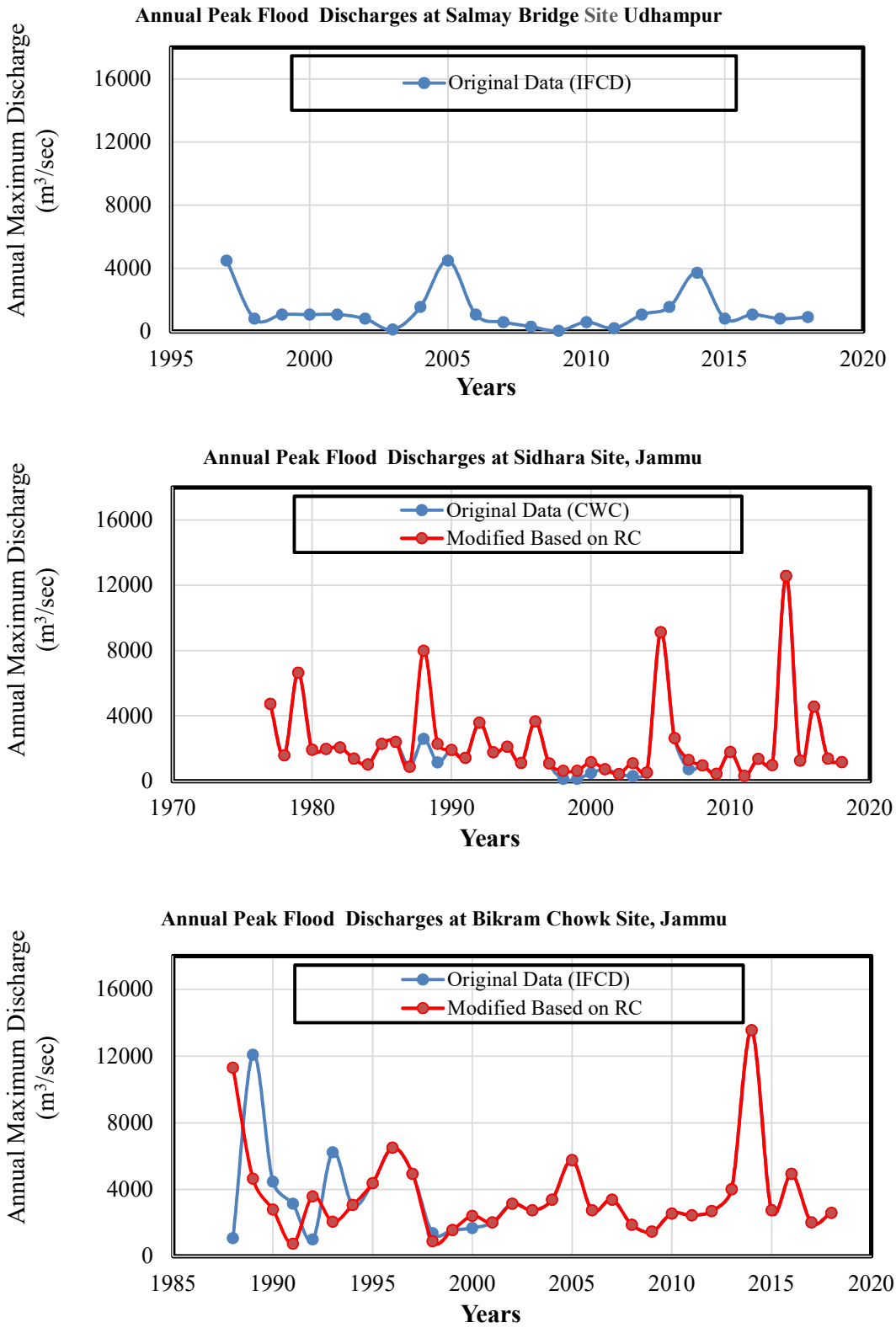

Figure 5.29 Annual maximum flood discharge values at various G&D sites on the Tawi River.

5.5.1 Quality analysis of annual maximum flood timeseries data

Prior to FFA, it is necessary to check the quality of the data using various standard statistical tests. In the study, the following data quality check techniques has been used.

1. **Test for outliers**: to detect inconsistence in data and possible outliers
   - **USWRC (U. S. Water Resources Council, 1981) method** – This method is recommended by the CWC (2001). If the station skewness is greater than 0.4, then the test for outlier should be performed based on following equation

$$X_H = X + K_N S \text{ --- for High outlier} \quad (4.1)$$

$$X_L = X - K_N S \text{ --- for Low outlier}$$

     If the logarithms of peak value > X_H it is high outlier; If the logarithms of peak value < X_L it is lower outlier
   - **Dixon test** – it is used test whether an extreme value observation is statistical outlier. It has two parameters critical value and p-value. If the computed p-value is lower than the significance level alpha=0.05, one should reject the null hypothesis H0, and accept the alternative hypothesis, Ha.
2. **Homogeneity and consistency checks** - It checks if the two or more populations have the same distribution of a single categorical variable.
   - **Student t-test** – If parameter $t\,stat < t\,critical$, the flood time series is assumed homogeneous at 5% significance level.
   - **Wald-Wolfowitz test** - The null hypothesis at the 0.05 level will be rejected if the p-value is lower than 0.05
3. **Randomness check** – This check is used to analyze the distribution of a set of data to check whether it can be described as random.
   - **Spearman test** – In this method the Spearman's Rho Table to find the critical value. If the absolute value of rho is larger than the critical value, the null hypothesis will be rejected which suggest that there is no correlation at 5% significance level.
   - **Non-parametric Mann-Kendall test** – this test is used to detect monotonic trends in series of hydrological time series data. If the p-value greater than z-stat, the hypothesis is rejected which mean there is no trend in the time-series.
   - **Turning point test** – If the test statistic, $z < 1.96$, the annual maximum flood series may be considered random at 5% significance level.

The annual maximum time series data at three G& D sites were used the check the quality of the data using the above three checks using various recommended method. The test to check outliers in the data for these three G&D sites is presented in the Table 5.5. Base on the estimated X_H and X_L by USWRC method as shown in Table 5.5, it was found that there is higher outlier for the Jammu (Bikram Chowk) G&D site in the year 2014. However, looking at the discharge at nearby Sidhara G&DS site, the observed discharge value checked and found to be reasonably correct. Further, the lower outlier identified in the Udhampur (Salmay Bridge) G&D site in the year 2009. Therefore, the rainfall records are checked and found that this discharge value was results of very low rainfall in this catchment area. Further, the results of the Dixon test for these three G&D sites suggests that as the computed p-value is lower than the significance level alpha=0.05, one should reject the null hypothesis that there is no outlier in the data. As per Dixon test, in case of Udhampur (Salmay Bridge) G7D site maximum outlier exists in year 1997 and 2014. Similarly, for the Sidhara (Jammu) the outlier observed in year 1988, 2005 and 2014 and for the Jammu (Bikram Chowk) outlier observed in 2014. All these outliers checked using the rainfall characteristics in the catchment area and if necessary, it was corrected by using rating curve available at gauge site.

Table 5.5 Outlier tests results for three G&D sites on the Tawi River basin

Parameters	Udhampur (Salmay Bridge)	Sidhara (Jammu)	Jammu (Bikram Chowk)
USWRC) method			
Mean	2.91	3.21	3.48
Std. Deviation	0.47	0.36	0.26
No. of years	22.00	42.00	31.00
Skewness	-0.93	0.50	0.22
K_N	2.43	2.70	2.58
X_H	0.66	4.56	4.06
X_L	1.77	2.25	2.80
Dixon test			
Observed value)	0.687	0.378	0.645
Critical value	0.480	0.369	0.413
p-value (Two-tailed)	0.000	0.041	< 0.0001
alpha	0.05	0.05	0.05

In order to check the homogeneity and consistency of the annual maximum flood timeseries data at these three-gauge sites, Student t-test and Wald-Wolfowitz test were used and the results are presented in Table 5.6. As shown in Table 5.6, Student t-test for all three

G&D sites suggests that as $t\ stat\ <\ t\ critical$, the flood time series at these three gauging sites can be assumed homogeneous at 5% significance level. Further, results of the Wald-Wolfowitz test suggests that as the p-value is higher than 0.05, the null of the annual maximum flood series at these gauges sites can be accepted. It means that the considered annual maximum time series are homogeneous and consistent.

Table 5.6 Homogeneity and consistency tests results for three G&D sites on the Tawi River basin

Parameters	Udhampur (Salmay Bridge)	Sidhara (Jammu)	Jammu (Bikram Chowk)
Student t-test			
Mean	1561.91	2566.22	3614.44
Variance	2232569.69	3425431.54	7017380.00
Observations	11.00	21.00	15.00
Pearson Correlation	-0.32	-0.26	-0.27
Hypothesized Mean Difference	0.00	0.00	0.00
df	10.00	20.00	14.00
t Stat	0.90	0.48	-0.13
P(T<=t) one-tail	0.20	0.32	0.45
t Critical one-tail	1.81	1.72	1.76
P(T<=t) two-tail	0.39	0.64	0.89
t Critical two-tail	2.23	2.09	2.14
Wald-Wolfowitz test			
n1	11	21	15
n2	11	21	16
n	22	42	31
runs	10	20	15
mean	12.00	22.00	16.48
var	5.24	10.24	7.48
stddev	2.29	3.20	2.73
alph	0.05	0.05	0.05
z	0.87	0.62	0.54
tails	2	2	2
p-value	0.38	0.53	0.59
z-crit	1.96	1.96	1.96
significance	No	No	No

The results of the Spearman test, Non-parametric Mann-Kendall test and Turning point test used to check the randomness are presented in the table 5.7. the results of the Spearman test suggest that the absolute value of rho is lower than the rho critical value, the null hypothesis (of no trend) will be accepted and there is correlation at 5% significance

level. Similarly, the results of the Non-parametric Mann-Kendall test suggests that as the p-value greater than z-stat, the hypothesis is rejected which mean there is no trend in the time-series. The results of the Turning point test as shown in Table 5.7 suggests that the test statistic, $z < 1.96$, the considered annual maximum flood series may be considered random at 5% significance level. Therefore, final it is concluded that with presented results to check the quality of annual maximum flood timeseries data at these three gauging sites was successfully cheeked for stationarity, homogeneity and independence and therefore, they are considered adequate for conducting the FFA.

Table 5.7 Randomness check tests results for three G&D sites on the Tawi River basin

Parameters	**Udhampur (Salmay Bridge)**	**Sidhara (Jammu)**	**Jammu (Bikram Chowk)**
Spearman test			
r	-0.32	-0.26	-0.27
rho	0.00	0.00	0.00
n	11.00	21.00	15.00
df	9.00	19.00	13.00
Sr	0.32	0.22	0.27
t	-1.00	-1.15	-1.01
alph	0.05	0.05	0.05
t-crit	2.26	2.09	2.16
p-value	0.35	0.26	0.33
sig	No	No	No
rho-crit	0.62	0.54	0.52
Non-parametric Mann-Kendall test			
alpha	0.05	0.05	0.05
MK-stat	-26	-178	-25
s.e.	35.06	92.27	58.78
z-stat	-0.71	-1.92	-0.41
p-value	0.48	0.06	0.68
trend	no	no	no
Turning point test			
p	12	28	17
N	22	42	31
E(p)	13.33	26.67	19.33
var(p)	351.68	671.68	495.68
z	-0.07	0.05	-0.10

5.5.2 Flood Frequency Analysis at Gauging Stations

By applying annual maximum discharge data at Udhampur (Salmay bridge), Sidhara (Jammu) and Jammu (Bikram Chowk), the FFA has been carried to estimate the magnitude of the extreme floods for different returned periods of 2, 5, 10, 20, 50, 100, 500 years. The probability distributions used in the present study are Normal, Log Normal (2p), LogNormal (3p), Gumbel, General Extreme Values Distribution (GEV), Gamma (2p), Log Pearson 3, Goodrich, and Weibull (2p) as available in FFD 2.1 MATLAB program. The results of these distribution are tested by using goodness of fit method such as Kolmogorov-Smirnov (K-S), Chi-square and Anderson and Darling (A-D) tests, for the confidence level of 95% or significance level of 5%.

5.5.2.1 Udhampur (Salmay Bridge) gauging station

For the Udhampur (Salmay Bridge) gauging station, the annual maximum flood discharge timeseries data from 1997 to 2019 is used. The flood frequency distribution plot using various probability distribution functions at Udhampur (Salmay Bridge) gauging station is presented in Figure 5.30. The summary of goodness of fit tests for selecting best fitting probability distribution function at Udhampur (Salmay Bridge) gauge station is presented in Table 5.8.

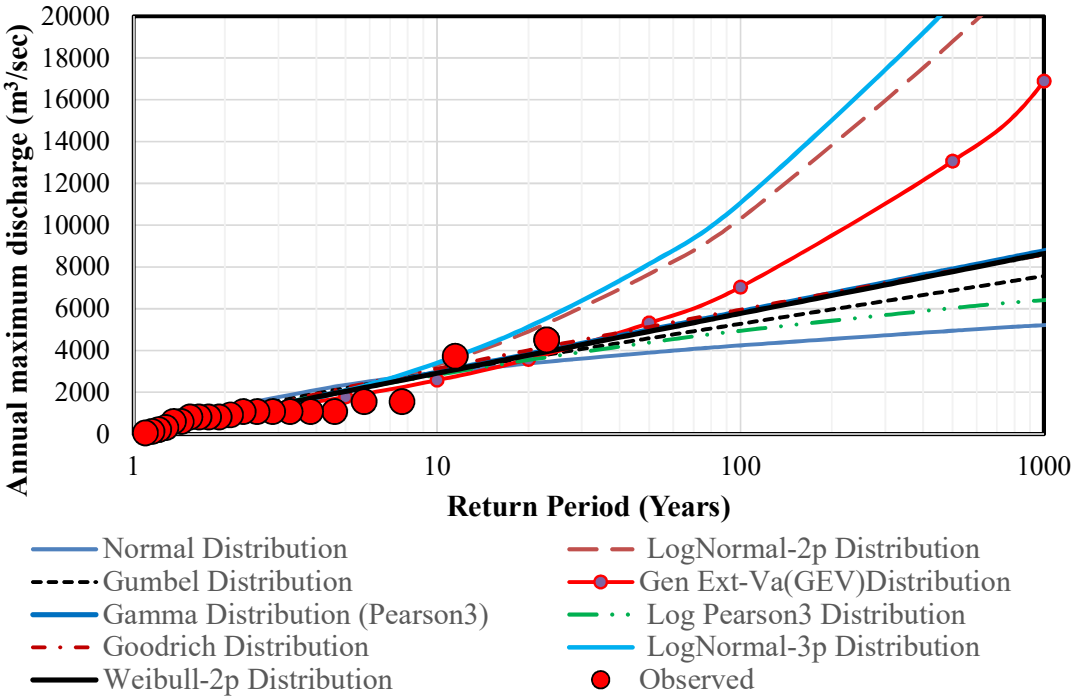

Figure 5.30 Flood frequency distribution plot at Udhampur (Salmay Bridge) gauging station on the Tawi River.

Table 5.8 Summary of the goodness of fit tests at Udhampur (Salmay Bridge) gauge station on the Tawi River basin

Probability Distribution	Kolmogorov Smirnov test	Chi square test	Anderson -Darling test	Correlation	RMSE	Rank
	Confidence level =95 %	Confidence level =95 %	Confidence level =95 %	Observed/ Quantile	Observed/ Quantile	
Normal	Reject	Accept	Reject	0.84	682.35	8
Log Normal-2p	Accept	Accept	Reject	0.94	420.03	5
Gumbel	Reject	Accept	Reject	0.90	549.09	7
General Extreme Value (GEV)	Accept	Accept	Accept	0.94	534.63	4
Gamma (Pearson3)	Accept	Accept	Accept	0.93	482.49	1
Log Pearson-3	Accept	Accept	Accept	0.92	523.99	3
Goodrich	Reject	Reject	Reject	0.92	489.89	9
Log Normal-3p	Accept	Accept	Reject	0.94	434.22	6
Weibull-2p	Accept	Accept	Accept	0.93	488.37	2

Table 5.9 Summary of the results of the Flood Frequency Analysis at Udhampur (Salmay Bridge) gauging station on the Tawi River.

Return Period (Years)	Non-Exceedance probability	Gamma (Pearson -3)	Weibull-2p	Log Pearson-3	General Extreme Value (GEV)
		Quantile (%)	Quantile (%)	Quantile (%)	Quantile (%)
2	0.5	898.7	904.2	966.1	892
5	0.8	2066	2044	2069.1	1772.2
10	0.9	2945.7	2906.2	2838	2579.3
20	0.95	3823.8	3768.4	3545.5	3580.2
50	0.98	4983.4	4908.2	4384.3	5312.5
100	**0.99**	**5859.8**	**5770.4**	**4947.1**	**7035.2**
500	0.998	7893.3	7772.4	6032.9	13062.9

Based on the results of the summary of the goodness of fit tests, correlation and RMSE at Udhampur (Salmay Bridge) gauge station (as shown in Table 5.8), the rank of best fitted frequency distribution is decided. According to this ranks, Gamma (Pearson3), Weibull-2p and Log Pearson-3 are the best fitting frequency distribution function for annual maximum discharge data at Udhampur (Salmay Bridge) gauge station. Accordingly, the summary of the results of the Flood Frequency Analysis (best fitted first four frequency distributions) at Udhampur (Salmay Bridge) gauging station is given in Table 5.9.

5.5.2.2 Sidhara (Jammu) gauging station

For the Sidhara (Jammu) gauging station, the annual maximum flood discharge timeseries data from 1977 to 2019 is used. The flood frequency distribution plot using various probability distribution functions at Sidhara (Jammu) gauging station is presented in Figure 5.31. The summary of goodness of fit tests for selecting best fitting probability distribution function at Udhampur (Salmay Bridge) gauge station is presented in Table 5.10.

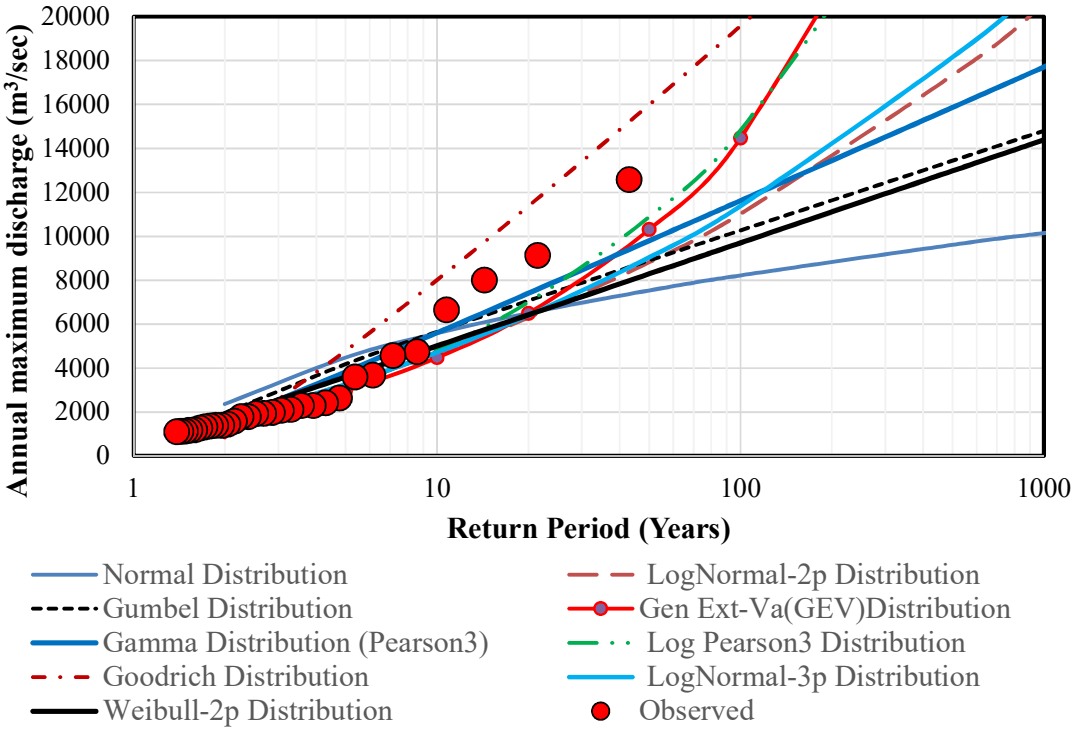

Figure 5.31 Flood frequency distribution plot at Sidhara (Jammu) gauging station on the Tawi River.

Table 5.10 Summary of the goodness of fit tests at Sidhara (Jammu) gauge station on the Tawi River basin

Probability Distribution	Kolmogorov Smirnov test	Chi square test	Anderson-Darling test	Correlation	RMSE	Rank
	Confidence level =95 %	Confidence level =95 %	Confidence level =95 %	Observed/ Quantile	Observed/ Quantile	
Normal	Reject	Reject	Reject	0.81	1488.13	8
Log Normal-2p	Accept	Accept	Accept	0.97	929.28	4
Gumbel	Reject	Accept	Reject	0.90	1074.46	7
General Extreme Value (GEV)	Accept	Accept	Accept	0.99	799.20	**2**
Gamma (Pearson3)	Reject	Reject	Reject	0.96	743.03	6
Log Pearson-3	Accept	Accept	Accept	0.99	649.13	**1**
Goodrich	Reject	Reject	Reject	0.97	1546.85	9
Log Normal-3p	Accept	Accept	Accept	0.98	894.42	**3**
Weibull-2p	Accept	Reject	Accept	0.95	969.11	5

Table 5.11 Summary of the results of the Flood Frequency Analysis at Sidhara (Jammu) gauging station on the Tawi River.

Return Period (Years)	Non-Exceedance probability	Log Pearson-3	General Extreme Value (GEV)	Log Normal-3p	Log Normal-2p
		Quantile (%)	Quantile (%)	Quantile (%)	Quantile (%)
2	0.5	1527.2	1517.5	1616.4	1634
5	0.8	3169.4	2987.3	3254.2	3260
10	0.9	4833.4	4481	4707.6	4677
20	0.95	6999.5	6491.9	6393.2	6301
50	0.98	10880	10314.7	9030.1	8813
100	0.99	14815	14473.7	11372	11022
500	0.998	28717	31170	18149	17335

Based on the results of the summary of the goodness of fit tests, correlation and RMSE at Sidhara (Jammu) gauge station (as shown in Table 5.8), the rank of best fitted frequency distribution is decided. According to this ranks, Log Pearson-3, General Extreme Value (GEV), and Log Normal-3p are the best fitting frequency distribution function for annual maximum discharge data at Sidhara (Jammu) gauge station. Accordingly, the ssummary of the results of the Flood Frequency Analysis (best fitted first four frequency distributions) at Sidhara (Jammu) gauge station is given in Table 5.11.

5.5.2.3 Jammu (Bikram Chowk) gauging station

For the Jammu (Bikram Chowk) gauging station, the annual maximum flood discharge timeseries data from 1977 to 2019 is used. The flood frequency distribution plot using various probability distribution functions at Jammu (Bikram Chowk) gauging station is presented in Figure 5.32. The summary of goodness of fit tests for selecting best fitting probability distribution function at Jammu (Bikram Chowk) gauge station is presented in Table 5.12.

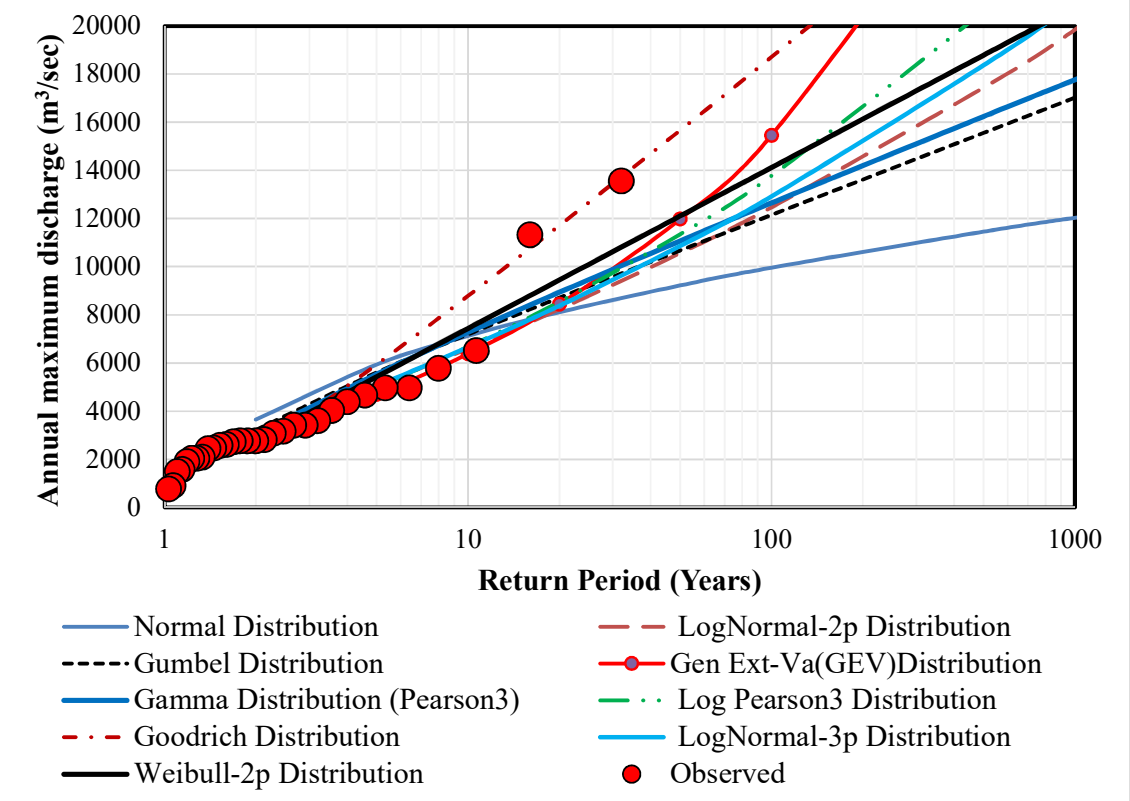

Figure 5.32 Flood frequency distribution plot at Jammu (Bikram Chowk) gauging station on the Tawi River.

Table 5.12 Summary of the goodness of fit tests at Jammu (Bikram Chowk) gauge station on the Tawi River basin

Probability Distribution	Kolmogorov Smirnov test	Chi square test	Anderson-Darling test	Correlation	RMSE	Rank
	Confidence level =95 %	Confidence level =95 %	Confidence level =95 %	Observed/ Quantile	Observed/ Quantile	
Normal	Accept	Reject	Reject	0.84	1459.93	8
Log Normal-2p	Accept	Accept	Accept	0.95	1025.00	5
Gumbel	Reject	Accept	Reject	0.91	1094.22	7
General Extreme Value (GEV)	Accept	Accept	Accept	0.97	910.72	**1**
Gamma (Pearson3)	Accept	Accept	Reject	0.93	995.29	6
Log Pearson-3	Accept	Accept	Accept	0.96	927.15	**2**
Goodrich	Accept	Reject	Reject	0.96	1124.16	9
Log Normal-3p	Accept	Accept	Accept	0.95	983.01	**3**
Weibull-2p	Accept	Reject	Accept	0.95	857.53	4

Table 5.13 Summary of the results of the Flood Frequency Analysis at Jammu (Bikram Chowk) gauging station on the Tawi River.

Return Period (Years)	Non-Exceedance probability	Gen Extreme Value (GEV)	Log Pearson- 3	Log Normal-3p	Weibull-2p	Log Normal-2p
		Quantile (%)	Quantile (%)	Quantile (%)	Quantile (%)	Quantile (%)
2	0.5	2850.1	2954.4	2994.3	2766.8	3022.5
5	0.8	4700.6	5006.2	5050.6	5425	5046
10	0.9	6378.7	6682.8	6660.2	7435.9	6596.2
20	0.95	8441.2	8542.6	8379.8	9446.7	8229.5
50	0.98	11974.9	11347.9	10863.1	12104.9	10556.3
100	**0.99**	**15455.1**	**13775.7**	**12921.5**	**14115.7**	**12462.6**
500	0.998	27454.3	20628.5	18376.7	18784.8	17439.9

Based on the results of the summary of the goodness of fit tests, correlation and RMSE at Jammu (Bikram Chowk) gauge station (as shown in Table 5.12), the rank of best fitted frequency distribution is decided. According to this ranks, General Extreme Value (GEV), Log Pearson-3, and Log Normal-3p are the best fitting frequency distribution function for annual maximum discharge data at Jammu (Bikram Chowk) gauge station. Accordingly, the summary of the results of the Flood Frequency Analysis (best fitted first five frequency distributions) at Jammu (Bikram Chowk) gauge station is given in Table 5.13.

5.5.2.4 Overall summary

The summary of the results of the flood frequency analysis for choosing the best fitting probability distribution function is given in Table 5.14. From the analysis of results of flood frequency analysis at Udhampur (Salmay Bridge), Sidhara (Jammu) and Jammu (Bikram Chowk) gauging stations, it can be revealed that the General Extreme Value (GEV) distribution gives higher estimate of the magnitude of extreme flood discharge value for respective return period as compared those at the Jammu (Bikram Chowk) gaging station.

As shown in Table 5.14, the magnitude of extreme discharges at Udhampur (Salmay Bridge) gauging station ranges between approximately 900 m^3/s for 2-year return period and 7800 m^3/s for 500 returned period. Similarly, the average magnitude of the extreme flood discharge ranging from around 1554 m^3/s for 2-year return period to 26012 m^3/s for 500-year return period. At the Jammu (Bikram Chowk) gauging station, the average magnitude of the extreme flood discharge ranges between 2933 m^3/s for 2-year return period and 22153 m^3/s for 500-year return period.

Further, it can be noted from the results of flood frequency analysis for Tawi river basin as shown in Table 5.14, the magnitude of flood discharges for 100-year return flood based on flood frequency analysis are very close to those values during 3-6 September 2014 high flood event. During 3-6 September 2014 high flood event, the maximum flood discharge observed at Jammu (Bikram Chowk), Sidhara (Jammu) and Udhampur (Salmay Bridge) were 13552 m^3/s, 12559 m^3/s and 3724 m^3/s. Further, the maximum discharge observed at Udhampur (Salmay Bridge) gauging station during year 1997 and 2005 flood was 4498 m^3/s. Further, Figure 5.33 represents the estimated floods at these three different gauging stations on the Tawi River basin by using IAHS (3003) and WMO (2009) maps. It can be inferred from Figure 5.33 that the estimated flood for Tawi basin at Bikram chowk G&D gauging station were about 20739 m^3/s (by using Figure 5.33a) and 13604 m^3/s (using Figure 5.33b).

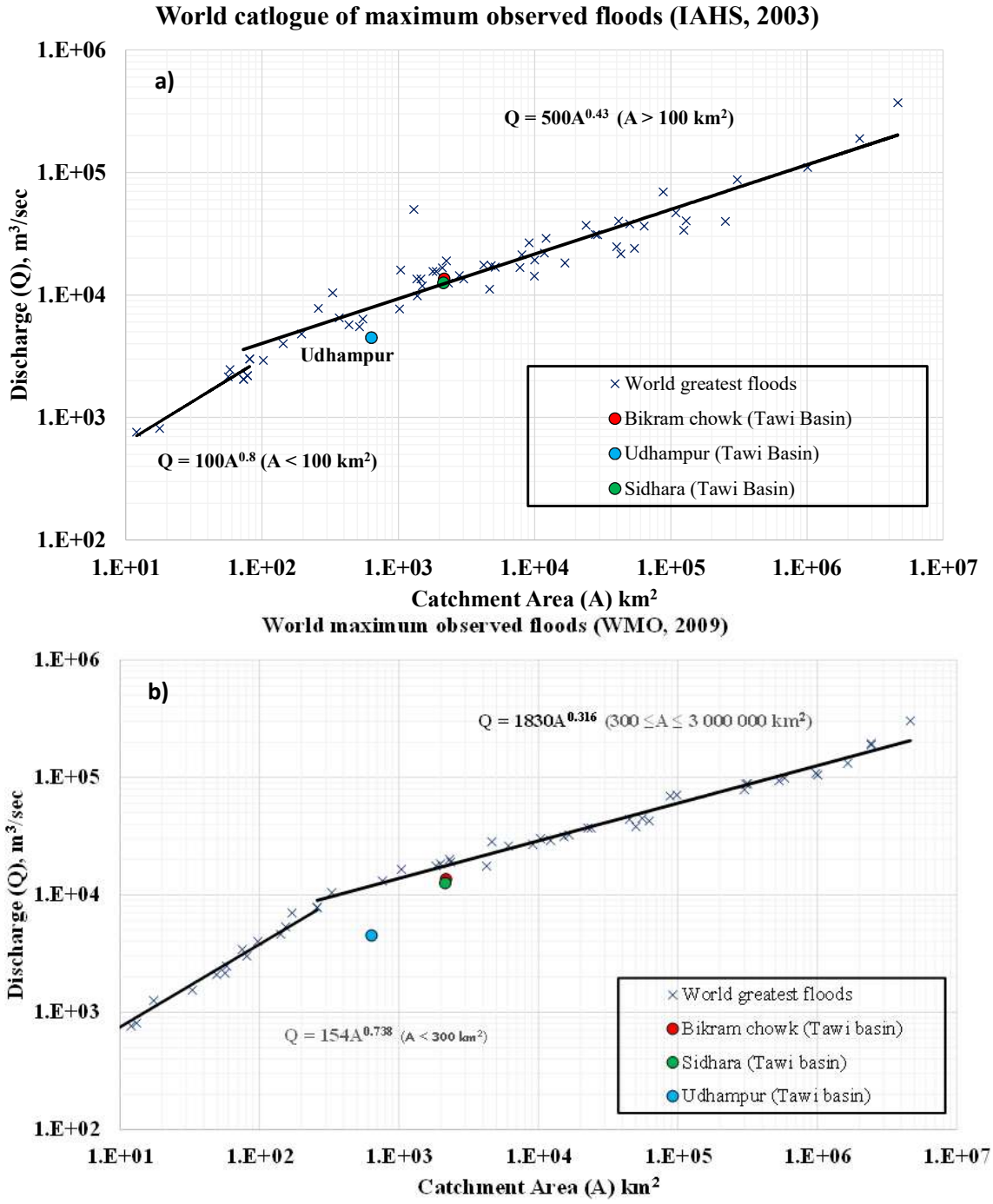

Figure 5.33 Estimated maximum flood for the Tawi River basin at various G&D site by using WMO (2009) and IAHS (2013) maps.

Table 5.14 Summary of the results of the Flood Frequency Analysis at Udhampur (Salmay Bridge), Sidhara (Jammu) and Jammu (Bikram Chowk) gauging stations on the Tawi River.

Return Period (Years)	Non-Exceedance probability	Udhampur (Salmay Bridge)				Sidhara (Jammu)				Jammu (Bikram Chowk)			
		Gamma (Pearson3)	Weibull-2p	Log Pearson-3	Average	Log Pearson-3	General Extreme Value (GEV)	Log Normal-3p	Average	Gen Extreme Value (GEV)	Log Pearson - 3	Log Normal-3p	Average
		Quantile (%)	Quantile (%)	Quantile (%)	Quantile (%)	Quantile (%)	Quantile (%)	Quantile (%)	Quantile (%)	Quantile (%)	Quantile (%)	Quantile (%)	Quantile (%)
2	0.5	898.7	904.2	966.1	923.0	1527.2	1517.5	1616.4	1553.7	2850.1	2954.4	2994.3	2932.9
5	0.8	2066	2044	2069.1	2059.7	3169.4	2987.3	3254.2	3137.0	4700.6	5006.2	5050.6	4919.1
10	0.9	2945.7	2906.2	2838	2896.6	4833.4	4481	4707.6	4674.0	6378.7	6682.8	6660.2	6573.9
20	0.95	3823.8	3768.4	3545.5	3712.6	6999.5	6491.9	6393.2	6628.2	8441.2	8542.6	8379.8	8454.5
50	0.98	4983.4	4908.2	4384.3	4758.6	10880	10314.7	9030.1	10074.9	11974.9	11347.9	10863.1	11395.3
100	**0.99**	**5859.8**	**5770.4**	**4947.1**	**5525.8**	**14815**	**14473.7**	**11372**	**13553.6**	**15455.1**	**13775.7**	**12921.5**	**14050.8**
500	0.998	7893.3	7772.4	6032.9	7232.9	28717	31170	18149	26012.0	27454.3	20628.5	18376.7	22153.2

5.7 Analysis of Regional Climate Model-predicted Future Climate

5.7.1 Climate data preparation

To assess the future possible floods under climate change scenarios, the hydrologic models HEC-HMS and steady State HECRAS-1D were forced with future precipitations. Future climate scenarios as output from the Regional Climate Model (RCM) were procured through the CORDEX web source <https://cordex.org/data-access/esgf/>. Total 17 number of RCM simulations, viz., ACCESS1-0, BCC-CSM1-1, BNU-ESM, CCSM4, CESM1-BGC, CNRM-CM5, CSIRO-Mk3-6-0, CanESM2, GFDL-CM3, GFDL-ESM2M, INMCM4, IPSL-CM5A-LR, IPSL-CM5A-MR, MIROC 5, MPI-ESM-LR, MPI-ESM-MR, MRI-CGCM3, NorESM1-M were downloaded and processed for analysis. As RCMs give output at coarse resolution, to get fine resolution output, statistical downscaling was performed by perturbation approach inbuilt with the climate perturbation tool (Ntegeka et al., 2014). The future forcings of climate models were perturbed based on the statistical relationship between the observed and RCM output for the control period 1961-1990. Quantile-perturbation based approach (Willems and Vrac, 2011) was used for downscaling the future precipitation datasets. In this method, the observed (ground station-based) precipitation values are perturbed by a perturbation factor, φ, expressed as:

$$\varphi(p) = \frac{Q_f(p)}{Q_c(p)} \tag{5.3}$$

where $\varphi(p)$ = perturbation factor associated with the probability of exceedance, (p). $Q_f(p)$ and $Q_c(p)$ = future and present precipitation quantiles, respectively.

The scenario (future) period considered was 2020-2039 (near future), 2040-2069 (mid future), and 2070-2099 (far future). Two different representative concentration pathway (RCP) scenarios, RCP4.5 and RCP8.5 were considered for analysis of future precipitation. Out of total 17 RCMs, based on the performance in reproducing the historical precipitation, best eight were chosen for studying the impact of future climate on floods which are BCC-CSM-1-1, ACCESS1-0, CCSM4, BNU-ESM, CAN-ESM2, CSIRO, CNRM and CESM.

5.7.2 **Future climate change scenarios**

For the eight RCMs chosen, for designing the percentage change scenarios, it can be inferred from Figure 5.34 that the future monthly average precipitation is expected to increase for most of the months and RCP combinations. Further, the increase in case of RCP 8.5 is

higher than that of RCP 4.5. Although, all the RCMs predicted increase in monsoon precipitation, higher increase in monsoon precipitation was predicted by BNU-ESM, ACCESS1-0 and CCSM4. As the monthly scale analysis only gives crude idea of climate change, the future climate forcings were analysed based on well-established indices (Venkata Rao et al., 2020) such as the total annual precipitation, *PRCPTOT* (mm); number off consecutive wet days, *CWD* (-); change in number of very heavy precipitation days with daily precipitation exceeding 20 mm, *R20mm* (-) that are discussed subsequently.

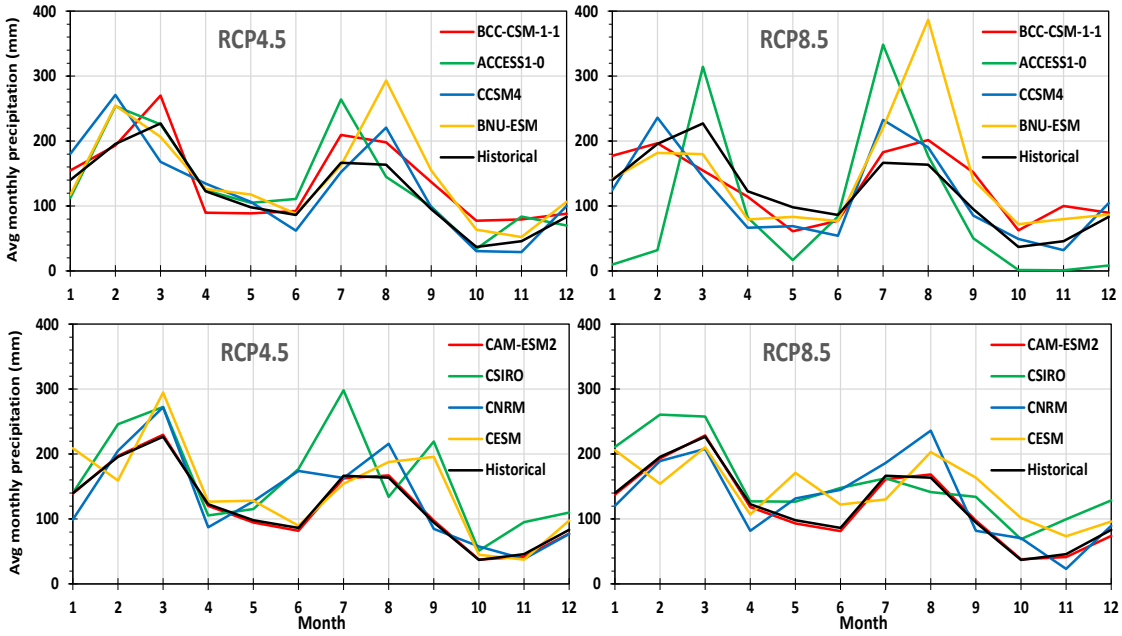

Figure 5.34 Regional Climate Model simulated future average monthly precipitation and temperature over the Tawi River basin for different RCP scenarios.

The total annual precipitation gives information on the future water budget. As can be inferred from Fig. 2, the future annual precipitation is going to increase as predicted by most of the RCMs except for ACCESS-1-0 and RCP8.5 combination. Figure 5.35. illustrates the typical case of location (Lat = 32.75 °N; Lon = 74.75 °N) in the northern part of the basin. Similar observations were obtained for all the other part of the Tawi River basin. The positive trend in slope for RCP 4.5 scenario as predicted by ACCESS1-0, BCC-CSM-1-1, and BNU-ESM are 2.469, 1.826, and 3.299, respectively.

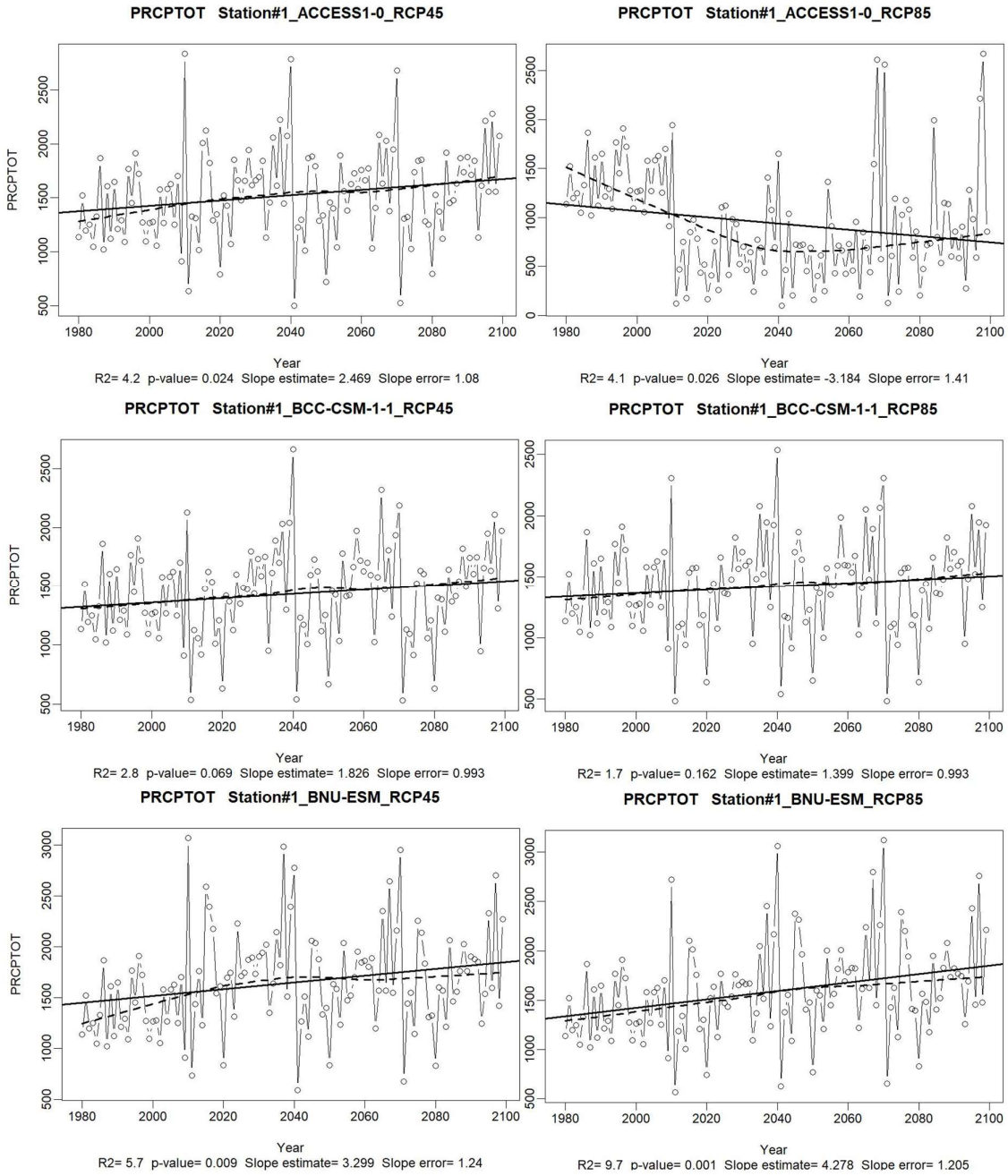

Figure 5.35 Trend in total annual precipitation, PRCPTOT (mm) at the location (Lat = 32.75 °N; Lon = 74.75 °N) as predicted by the different climate models for the scenarios of RCP 4.5 and 8.5.

Further, as the number of consecutive wet days, CWD determines the chance of onset and severity of flood, the trend in CWD was estimated for the different RCPs for different RCM output. A positive trend is predicted for all the RCP and RCM combinations as envisaged in Figure 5.36. The slope range was in the range 0.01-0.06. A comparison between Figures 5.35 and 5.36 brings possibility of one-to-one relationship between increase in

PRCPTOT and CWD. The highest change in the CWD was predicted for the RCP-RCM combination: RCP8.5-BNU-ESM, wherein the CWD increased from 6-18.

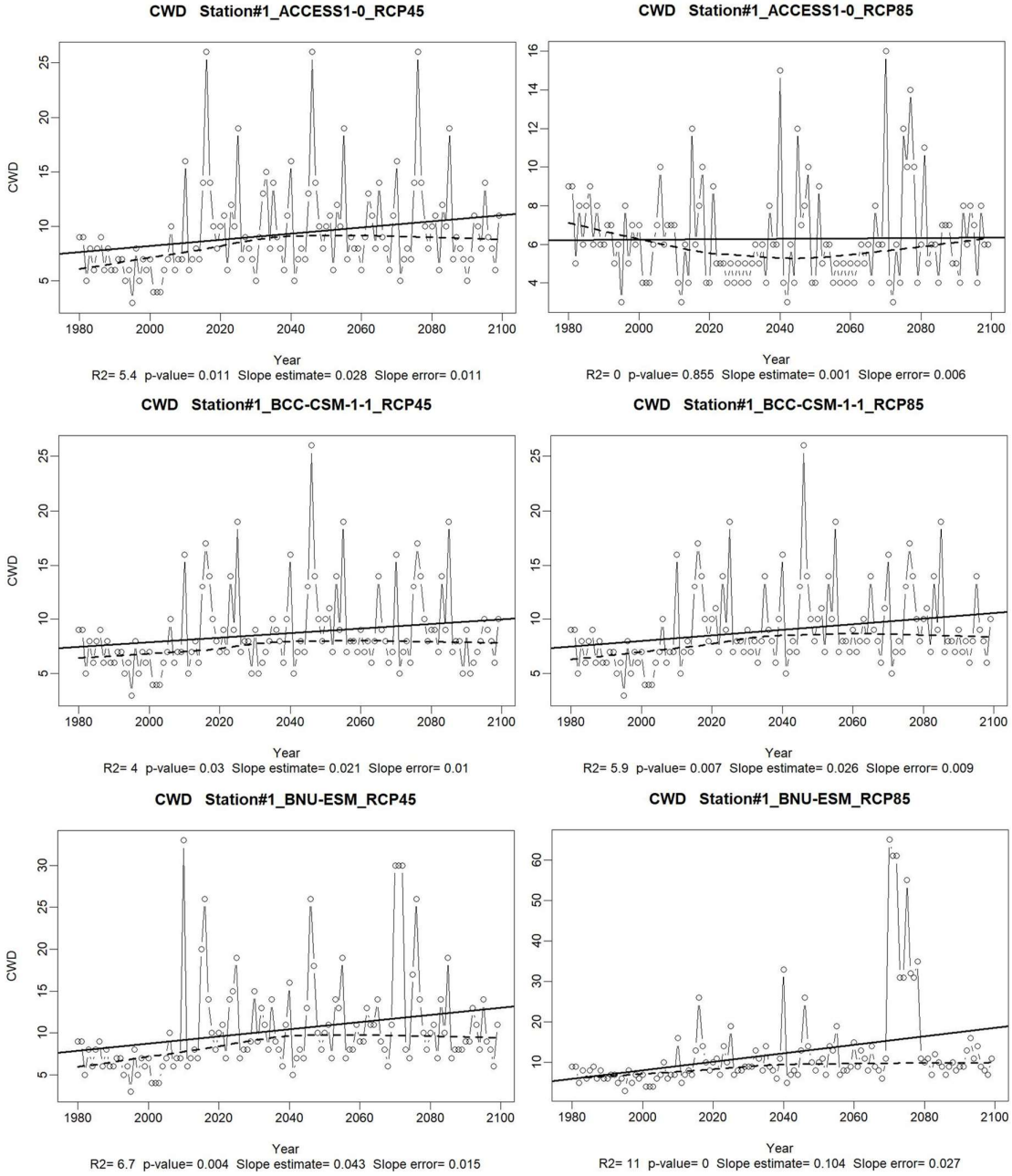

Figure 5.36 Trend in the number off consecutive wet days, CWD at the location (Lat = 32.75 °N; Lon = 74.75 °N) as predicted by the different climate models for the scenarios of RCP 4.5 and 8.5.

In addition to the CWD, the number of very heavy precipitation days, R20 is the important determinant for flood occurrence (Figure 5.37). As depicted in Fig. 5.37, R20 is

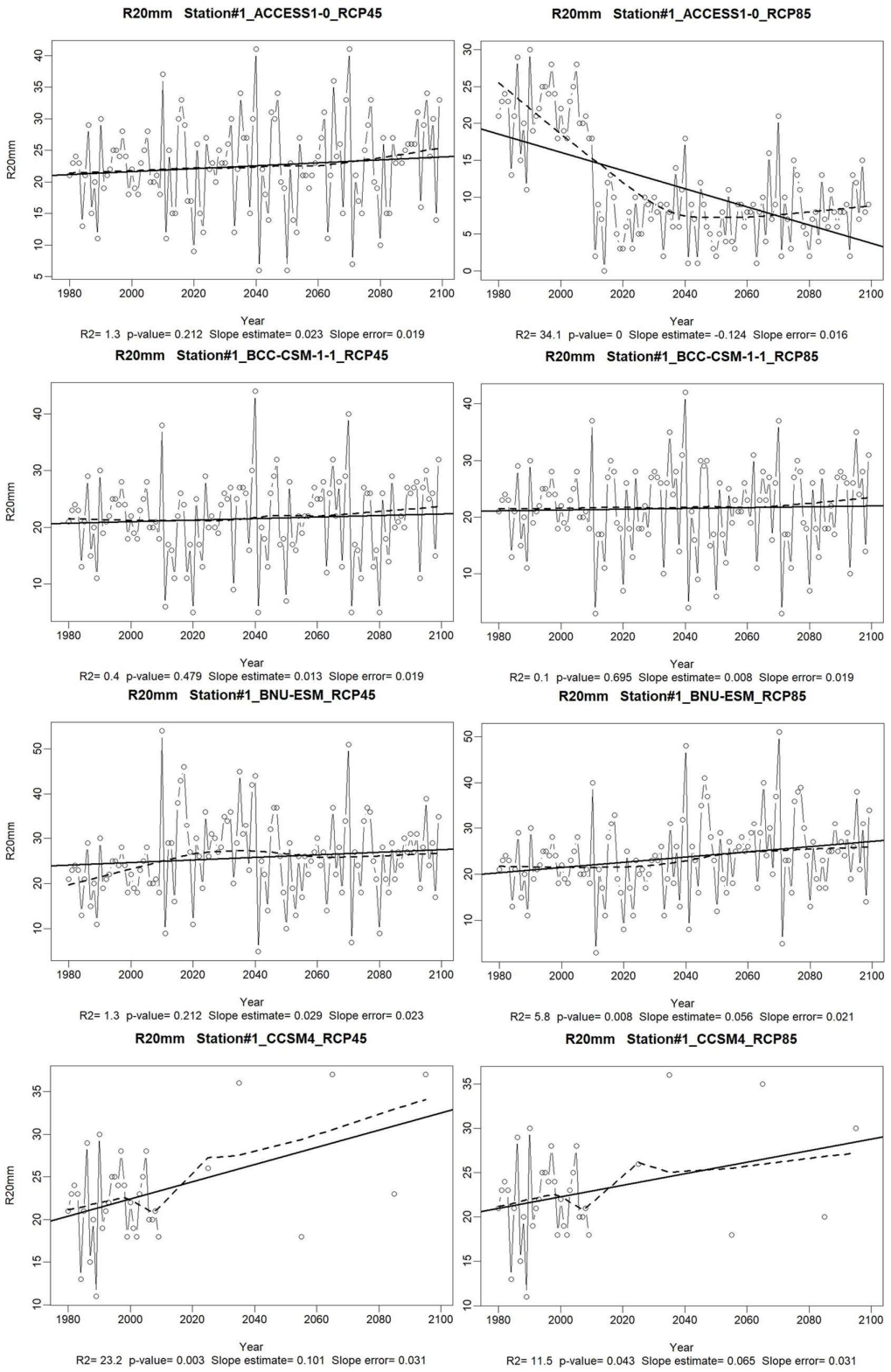

Figure 5.37 Trend in the number of very heavy precipitation days, R20 at the location (Lat = 32.75 °N; Lon = 74.75 °N) as predicted by the different climate models for the scenarios of RCP 4.5 and 8.5.

predicted to increase for all the RCP-RCM combinations except for ACCESS1-0-RCP8.5 combination, wherein the R20 is predicted first decrease from 25 to 8 around 2035 and then increase slightly. From the bias-corrected future climate data, although the increase in R20 is negligible to naked eye, rising trend is observed when analysing the data statistically. The highest increase in R20 was predicted by CCSM4 that is about 50% increase in the number of rainy days.

5.8 Flood Hazard Mapping

Flood hazard mapping is an exercise to define the area which are at risk of flooding due to extreme climatic conditions. Its primary aim is to reduce the impact of the extreme flooding on society and economy. Flood hazard mapping is flood management tool which is used identify area at risks, and consequently to improve the flood disaster management and preparedness activities. Flood assessment usually look at expected depth and extent based on the design flood scenarios based on flood frequency analysis and climate change projections (Demir and Kisi, 2016). In this study flood hazard map generated based on the design floods for different return period using flood frequency analysis and also based on climate change scenario based generated design floods using HEC-HMS model.

5.8.1 Based on the flood frequency analysis

The design floods for 2-year, 5-year, 10-year, 20-year, 50-year, 100-year and 500-year return periods estimated at Sidhara (Jammu) gauging station using **General Extreme Value (GEV) flood** frequency analysis method (see Table 5.14) are used as an input in the HEC-RAS model for the lower Tawi river basin. Accordingly, the flood inundation depth maps simulated for various return periods are shown in Figure 5.38.

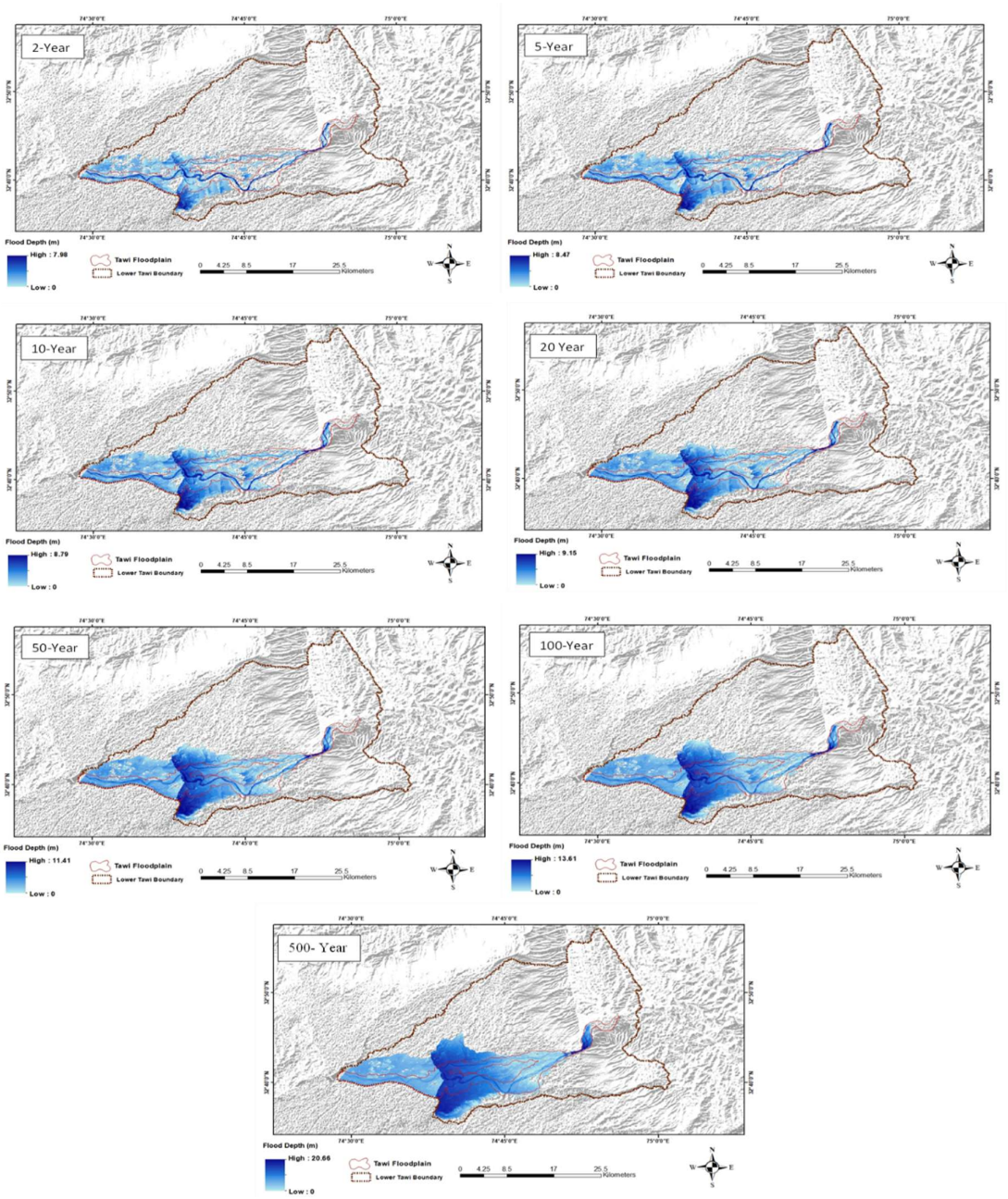

Figure 5.38 Flood inundation depth maps of the lower Tawi basin for the design floods of various return period.

The flood hazard map generated for September 2014 high flood event from HEC-RAS model output for lower Tawi river basin shown in Figure 5.39. Similarly, Flood hazard maps of the lower Tawi basin developed by Irrigation and Flood Control Department based on actual field visits during September 2014 high flood event is shown in Figure 5.40. Based HEC-RAS based food hazard map (see Figure 5.39), total area affected due to flood in lower Tawi is 223.20 km^2 (22320 ha) out of which 120.96 km^2 (12096 ha) area in Indian territory. And affected villages ae 105 as per 2001 census data with 25 villages having zero population.

Considering village population more than 100 people, the total villages affected during September 2014 may be around 67. Interestingly, from Figure 5.40 it can be seen that ICFCD reported affected villages due to flood were 66. Thus, it can be revealed that the flood hazard map is closely matching the ground situations during September 2014 flood.

The flood hazard maps generated for design floods of different return period are shown in 5.41. Using the flood inundation depth maps for different frequency floods, demographic data for Indian part, land use and land cover map for the study area, the future flood hazard information is summarized in Table 5.15. Based on the information presented in Table 5.15, it is revealed that the total flood inundated area ranges between 10591 ha to 26305 ha (for Indian part, it is 4063 ha to 15163 ha) for design floods of 2-year to 500-year return periods, respectively. In Indian part of lower Tawi basin, total villages and population affected due flood will ranges between 83 to 117 and 8.07 to 8.16 Lakh, respectively for design floods of 2-year to 500-year return periods at present conditions. The total affected agricultural and residential area will ranges between 2059 ha to 8719 ha and 83 to 371, respectively for design floods of 2-year to 500-year return periods under present conditions.

Table 5.15 Summary of flood hazard related information in lower Tawi basin based on design flood of different returned period

Return period of design flood	**Total flood inundated area (ha)**	**Flood inundated area in India (ha)**	**Total affected Indian Villages**	**Total affected agricultural area (ha)**	**Total affected residential area (ha)**	**Population (2021)**
2-Year	10591	4063	83	2059	83	807496
5-Year	14775	6286	89	3289	130	813064
10-Year	17155	7889	95	4202	162	813664
20-Year	19296	9539	98	5162	195	814161
50-Year	21672	11353	103	6268	244	815128
100-Year	23318	12646	108	7098	287	818594
500-Year	26305	15163	117	8719	371	830688
Sep-14 flood	22620	12096	105	6740	268	816000

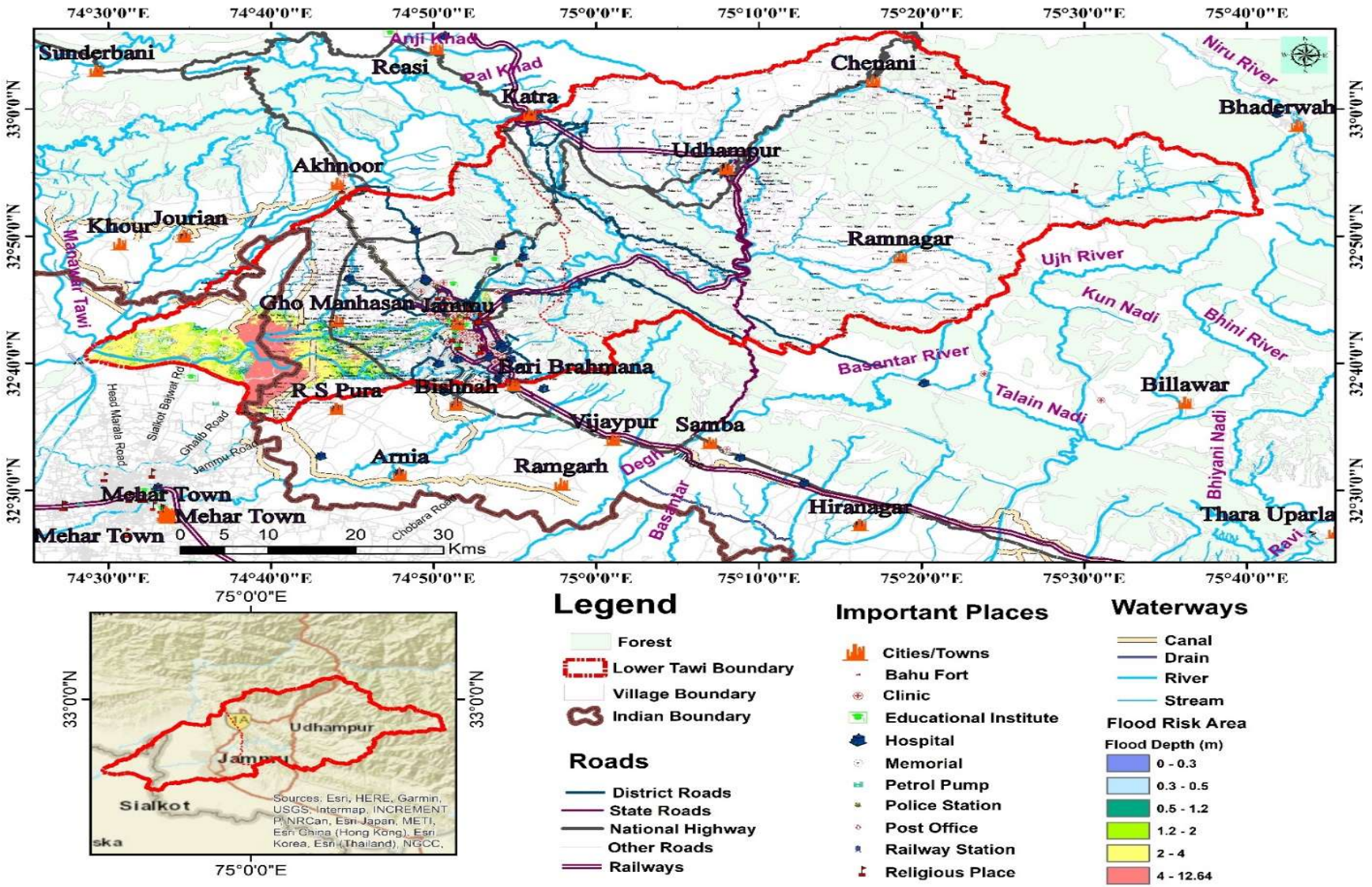

Figure 5.39 Flood hazard maps of the lower Tawi basin for September 2014 high flood event.

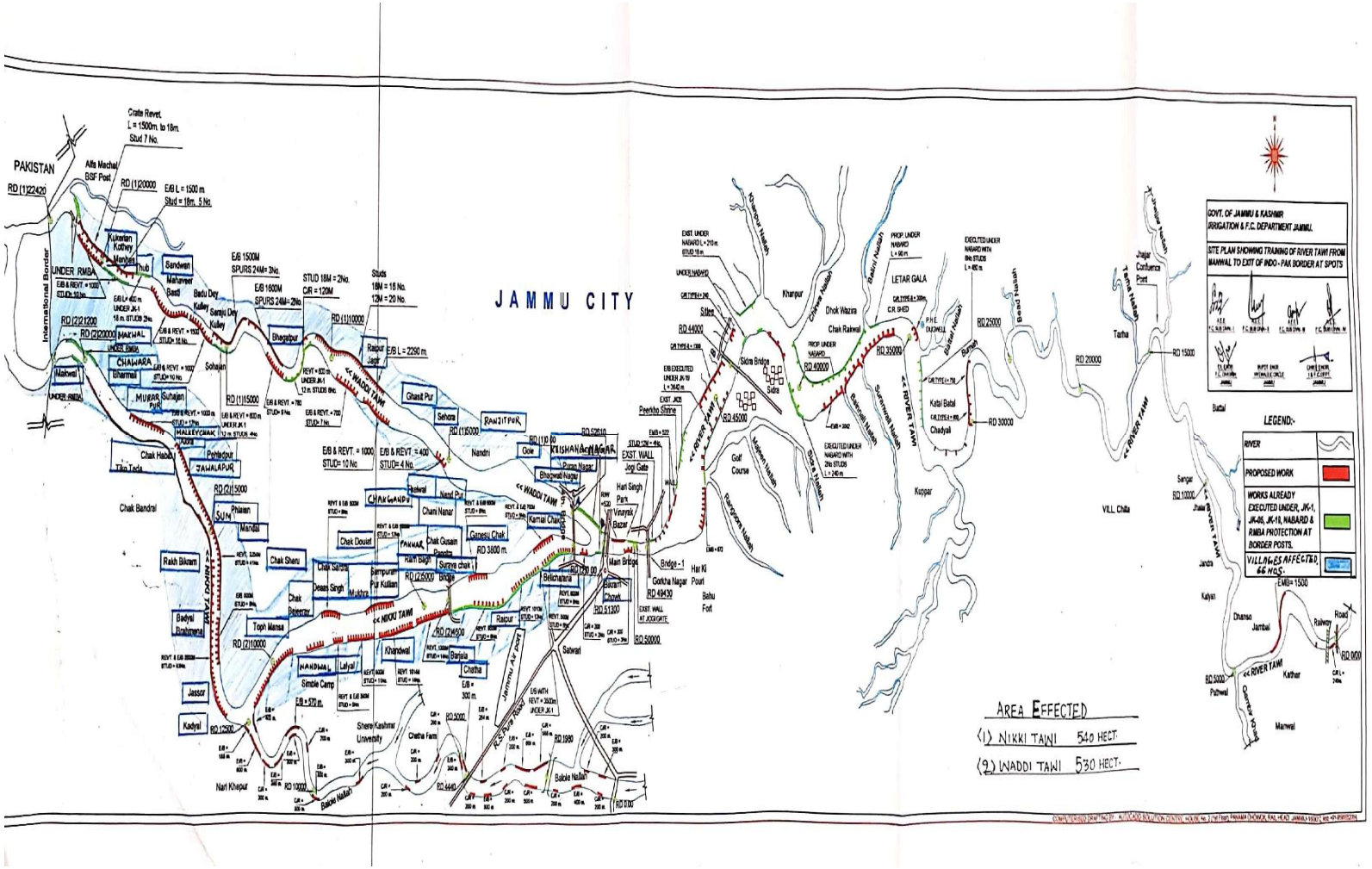

Figure 5.40 Flood hazard maps of the lower Tawi basin developed by Irrigation and Flood Control Department based on actual field visits during September 2014 high flood event

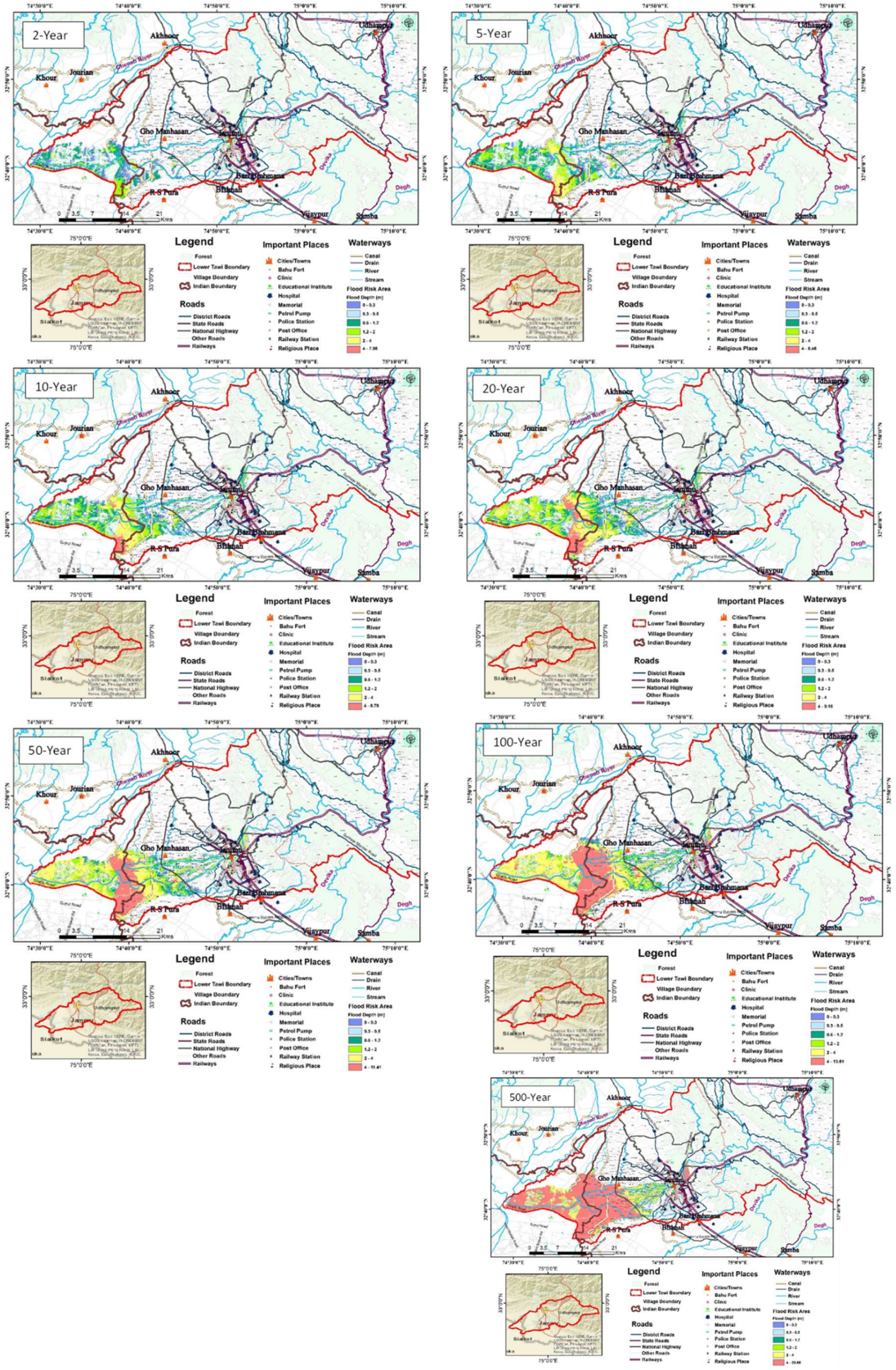

Figure 5.41 Flood hazard maps of the lower Tawi basin based on Flood Frequency analysis

5.8.2 Based on the climate change scenarios

Stephens et al. (2018) have attempted to analyse the feasibility of calibrated loss values in the event-based hydrological model to be used for future prediction under climate change impact by comparing the results of the event and continuous hydrological models. As the antecedent conditions at the calibration of the event-based hydrological model are likely to change in future. According to Stephens et al. (2018), greater uncertainty in event-based hydrological model results encounters when it is applied in drier climatic condition attributed to greater antecedent conditions. However, when the event-based hydrological model applied to simulate extreme flood event due to high rainfall intensities (high rainfall events and generally wetter antecedent conditions) wetter, the impact of changing antecedent conditions is less important than the models' representations of catchment nonlinearity. This statement suggests that changing antecedent conditions are not always the key source of potential model performance degradation. In similar way, Devi et al (2015) have attempted to use the vent-based HEC-HMS model to simulate future flood hydrographs with increased (scaled-up baseline rainfall) scenarios. Similarly, in this study, the event-based calibrated HEC-HMS model with baseline data of September 2014 used to simulate future flood hydrographs Sidhara (Jammu), Jammu (Bikram Chowk) and Udhampur (Salmay Bridge) gauging stations. The future flood hydrographs were generated for four scenarios of 5%, 15%, 25% and 35% increase in the baseline extreme rainfall event (September 2014 high flood event) and are shown in Figure 5.42. The simulated peak discharges based on these four climate change scenarios are presented in Table 5.16. These peak discharges are used as an input to the HEC-RAS hydraulic model for simulation of possible future flood inundation pattern in the lower Tawi River basin. The simulated flood inundation depths for these four climate change scenarios maps are presented in Figure 5.43 and flood hazard maps are presented in Figures 5.44 – 5.47.

Table 5.16 Simulated peak discharge for the different climate change scenarios.

G&D Stations	Simulated Peak Discharge (m^3s)				
	Observed (Sep 2014)	**CC5**	**CC15**	**CC25**	**CC35**
Udhampur (Salmay Bridge)	3724	3537.5	4071.9	4513.4	5989.7
Sidhara (Jammu)	12569	13430.2	15957.1	17977.8	19874.9
Jammu (Bikram Chowk)	13552.4	13579	16125.2	18165.9	20081

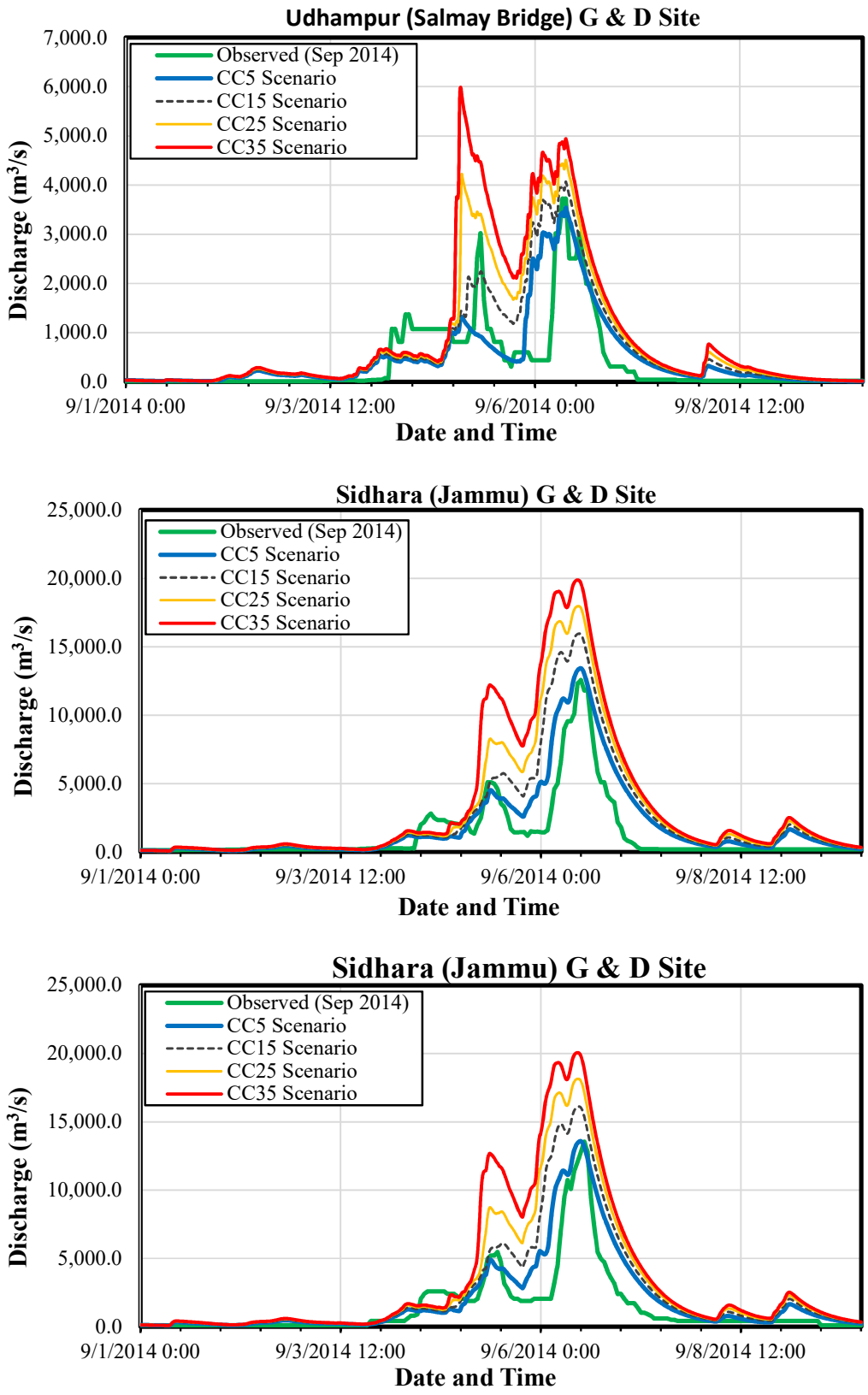

Figure 5.42 Simulated flood hydrographs for different climate change scenarios

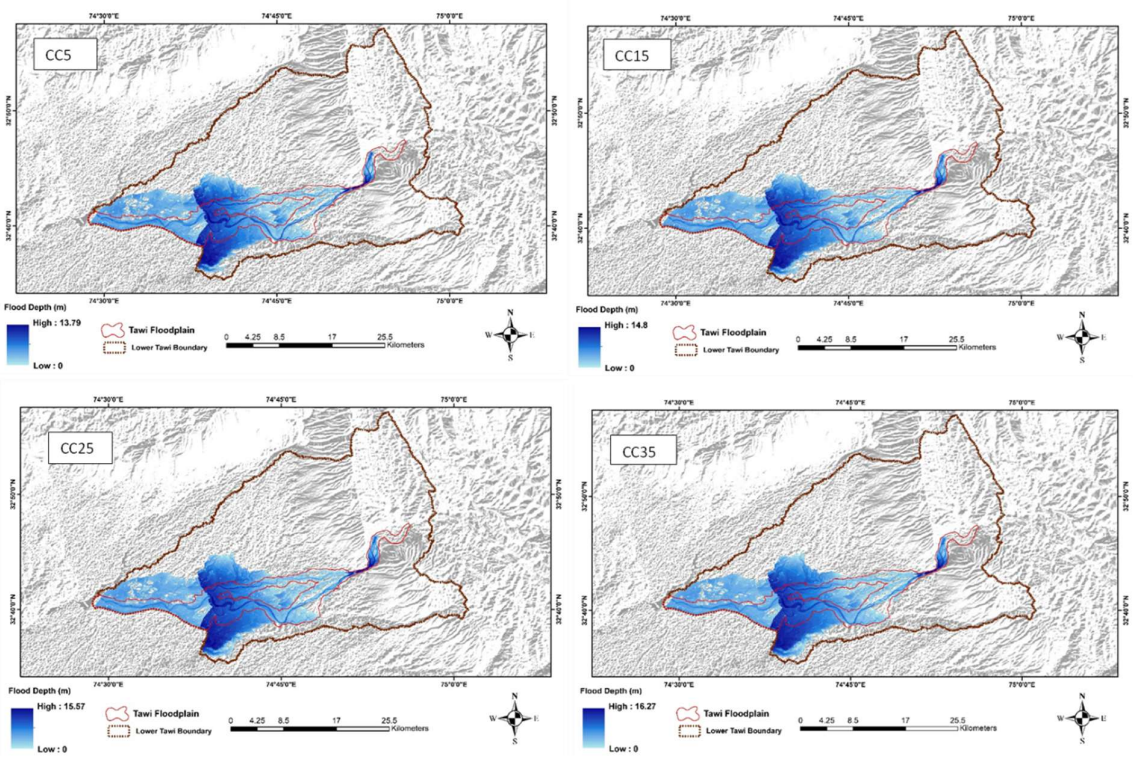

Figure 5.43 Flood inundation depth maps of the lower Tawi basin for the design floods of various return period.

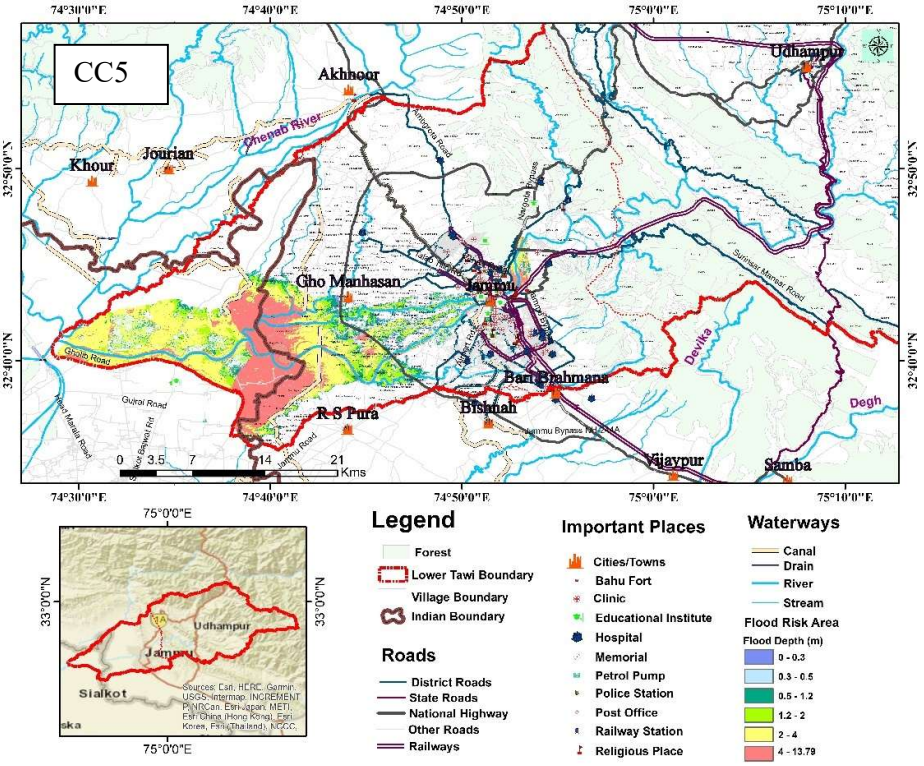

Figure 5.44 Flood hazard maps of the lower Tawi basin for climate change scenarios CC5.

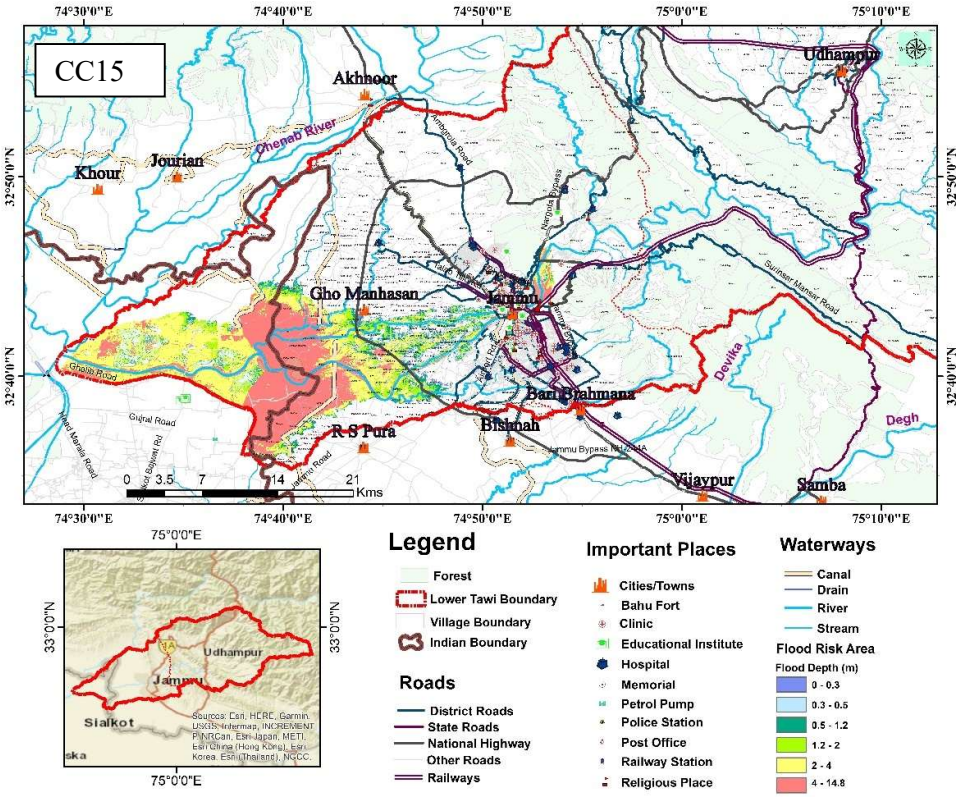

Figure 5.45 Flood hazard maps of the lower Tawi basin for climate change scenarios CC15.

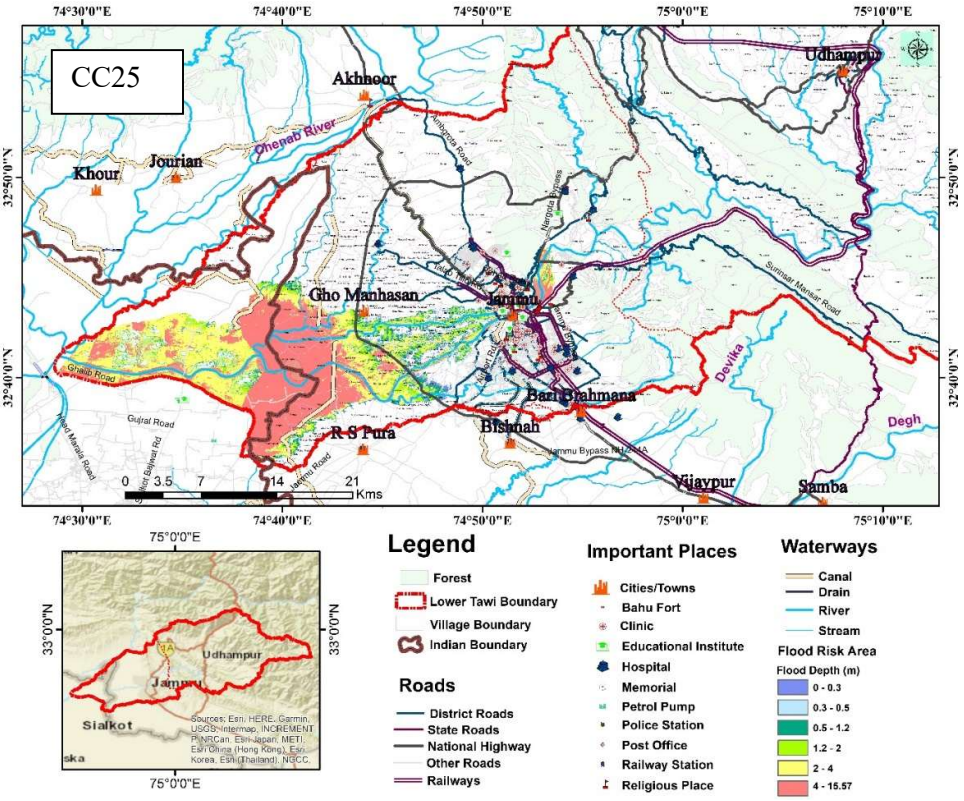

Figure 5.46 Flood hazard maps of the lower Tawi basin for climate change scenarios CC25.

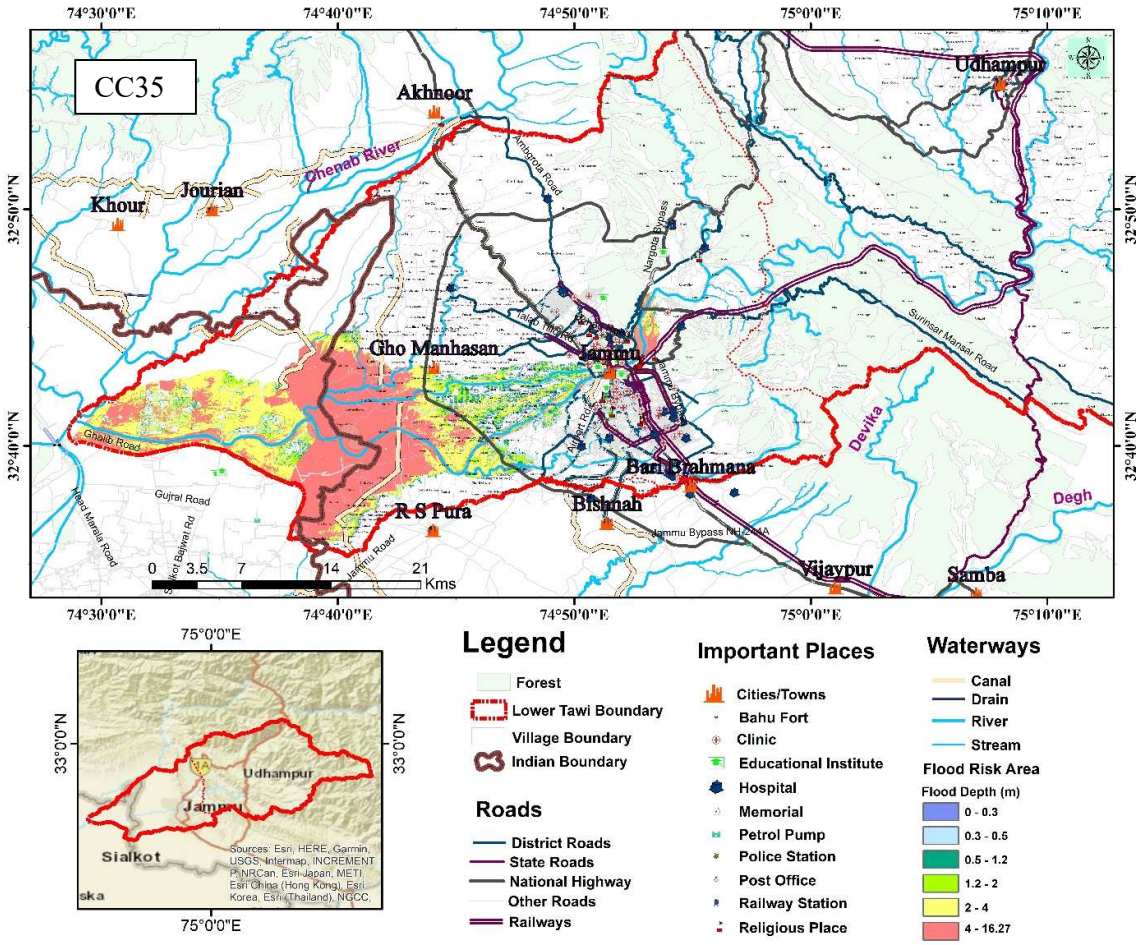

Figure 5.47 Flood hazard maps of the lower Tawi basin for climate change scenarios CC35.

Using the flood inundation depth maps for these four climate change scenarios, demographic data for Indian part, land use and land cover map of the study area, the future flood hazard information is summarized in Table 5.17. Based on the information presented in Table 5.17, it is revealed that the total flood inundated area ranges between 22574 ha to 24348 ha (for Indian part, it is 12342 ha to 13746 ha) for the four climate change scenarios (CC5, CC15, CC25 and CC35). In Indian part of lower Tawi basin, total villages and population affected due flood will ranges between 107 to 114 for climate change scenario CC5 and CC35 under present conditions. The total affected agricultural and residential area will ranges between 6899 ha to 7841 ha and 278 to 268, respectively for climate change scenario CC5 and CC35 under present conditions. Therefore, it can be concluded that based on climate change scenarios of CC35 (35% increase in baseline rainfall event of September 2014), the flood affected area, agricultural and residential areas in the Indian

Table 5.17 Summary of flood hazard related information in lower Tawi basin based on climate change scenarios

Climate change scenario	Total flood inundated area (ha)	Flood inundated area in India (ha)	Total affected Indian Villages	Total affected agricultural area (ha)	Total affected residential area (ha)
CC5	22574	12342	107	6899	278
CC15	23382	12982	109	7313	302
CC25	23939	13449	111	7616	317
CC35	24348	13796	114	7841	329
Sep-14	22620	12096	105	6740	268

territory in lower Tawi basin will increase by around 1700 ha, 1101 ha and 61 ha over the affected these areas during baseline period (September 2014), if the proper flood management activities will not be undertaken.

6 CONCLUSIONS AND RECOMMENDATIONS

Floods are the most common natural disasters that often cause significant economic losses, and human and social tragedies. In the recent years, the flood management challenges have been raised multidimensionally with unprecedented climate change and land use change issues. Staggered development in flood plain and changing climate pattern resulting in the exponential increase in inundation of flood plain and associated risks due to increased potential floods. Many studies are reporting that under changing climate conditions, the Himalayan region likely to impact more in terms of devasting water-related disasters in future. In last 20 years, the Himalayan region is already witnessing increased extreme hydro-meteorological events. Particularly, the Tawi River basin located in Western Himalayan region is continuously subjected to water related disaster such as heavy torrential rainstorms, frequent cloud bursts along with its high precipitous relief. The record suggest that the extreme events are grown in frequency and intensity during last 20 years in this basin. The recent high flood event of September 2014 was a triggering event which triggered government and civil organizations to plan better flood assessment and management as well reduction strategies to fight water-related disasters in the Tawi River basin under glooming future climate change scenarios. Therefore, this study was undertaken with objectives: (i) To set-up HEC-HMS model for the Tawi River basin for the rainfall-runoff simulation (ii) To set-up HEC-RAS model for the Tawi River basin for flood inundation mapping (iii) Flood frequency analysis for the Tawi River basin under current climatic conditions (iv) Assessment of flood inundation under current and changing climatic conditions.

The hydrologic, hydraulic, geomorphologic and ecohydrological modelling studies are necessary to analyze the impact of climate change on water resources as well as the integrated management of the water resources. However, the accuracy of the digital elevation model (DEM) datasets plays a prominent role in these modelling studies. Now-a-days, open-access global digital elevation datasets are extensively used due to their cost-effectiveness and sparse coverage of sources at relatively high resolution. As these DEM datasets are created using the data captured by various types of onboard sensors at the different time periods and are processed using different algorithms, thus, the accuracy of each DEM dataset differs from others. Therefore, the researcher always faces the problem of using appropriate DEM datasets in the modelling studies. Therefore, this study deals with the assessment of the

accuracies of the available different types of DEMs (ASTER 30 m, SRTM 30 m, ALOS (AW3D30) 30 m, CartoDEM 30 m and ALOS PALSAR – RTC 12.5 m) with different resolutions based on drainage morphometric analysis for the Tawi river basin. This evaluation of the different DEMs derived from various sources provides insight into terrain and morphological characteristics analysis which are useful for hydro-ecological modelling studies.

The rainfall-runoff modelling in the Upper Tawi River basin up to the Jammu (Bikram Chowk Bridge) gauging station is carried by setting-up event-based HEC-HMS model. The HEC-HMS modelling schematic is prepared to simulate the runoff at three G&D stations namely Udhampur (Salmay Bridge), Sidhara (Jammu) and Jammu (Bikram Chowk) stations as well as other subbasins up to the Jammu (Bikram Chowk bridge) G&D station. Tawi basin is subjected to flash floods due to its topographic and climatological setting. Therefore, disaggregation of daily rainfall into hourly rainfall is necessary, in order to simulate high rainfall-runoff event. The disaggregation of daily rainfall depth at IMD grids covering the Tawi catchment river basin up to Jammu (Bikram Chowk) has been carried out using "Bivariate Satellite Ratio Disaggregation method". The calibration and validation of event-based HEC-HMS model is accomplished using the high flood event of 1-10 September, 2014 and 1-10 August, 2016, respectively. Various performance criteria such as Nash-Sutcliffe Efficiency (NSE), Percentage Biased Error in observed and simulated data (PBIAS), Coefficient of determination (R^2), Error in peak discharge (E_p) and Error in time to peak discharge (E_{pt}) were used to calibrate and validate the HEC-HMS model for the Tawi basin.

The steady state HEC-RAS model was set-up to obtain flood inundation mapping in lower Tawi basin downstream of the Sidhara G&D site up to its confluence with Chenab just upstream of Marla Barrage using Energy Equations. Total 406 cross has been used and four bridges as well as under construction Tawi barrage also included in the analysis. The obtained peak discharges using HEC-HMS model are provided as an input to the steady State HEC-RAS1D model to generate flood inundation and flood hazard maps. The flood inundation maps by HEC-RAS for the September 2014 event are validated with satellite data (Landsat 8, LISS-III and LISS-IV) during flood period.

The Flood Frequency Analysis (FFA) were conducted at Jammu (Bikram Chowk), Sidhara (Jammu) and Udhampur (Salmay Bridge) G&D stations using nine types of the frequency distribution recommended in the CWC guidelines. The bested fitted distribution

functions were chosen based Kolmogorov-Smirnov, Chi square, and Anderson-Darling tests. The design floods for the return period of 2, 5, 10, 20, 50, 100 and 500 years were estimated.

Further, NEX-GDDP and COREDEX RCM datasets were used to generate future scenarios using Climate Perturbation Tool. To analyze future flood under climate change impact, four scenarios with 5% (CC5), 15% (CC15), 25% (CC25) and 35% (CC35) increase in the extreme rainfall event assuming baseline period event of September 2014 were considered for simulation of flood hydrographs using event-based HEC-HMS model. The obtained future extreme floods for climate change scenarios CC5, CC15, CC25 and CC35 were used as input in the HEC-RAS model to generate future flood inundation depth map and flood hazard maps for lower Tawi basin downstream of the Sidhara gauging station. Based on analysis following conclusions were drawn:

- The comparison of the drainage morphometric parameters derived from the selected five DEMs (ASTER 30 m, SRTM 30 m, ALOS (AW3D30) 30 m, CartoDEM 30 m and ALOS PALSAR – RTC 12.5 m) with different resolutions is suggesting that the AW3D30 DEM performed very well as compared to other DEM datasets. Therefore, it was concluded that the use of the ALOS World 3D 30 m (AW3D30) DEM is most suited for the conduction of hydrological modelling study.
- Further, the comparison based on the hypsometric analysis (HI) for 14 sub-watersheds of the Tawi river basin using the selected above five DEM datasets are suggesting that the HI values of the Tawi basin up to the Sidhara gauging site were approximately the same.
- From the computed HI values, it can be concluded that the Ramnagar, Sardhan, Upper Tawi, Balini and Lower Tawi sub-watersheds are in the late mature stage of erosion ($0<HI<0.4$). The remaining sub-watersheds are in the old stage of the erosion ($0<HI<0.3$), representing a more incisive fluvial process. The sub-watersheds at the old stage are in equilibrium and thus less prone to further erosion.
- The application of Bivariate Satellite Ratio Disaggregation method to transform daily rainfall depths at IMD grid points to hourly rainfall depths and conversion of these disaggregated hourly rainfall into subbasin average rainfall provides reasonably well hourly rainfall depths timeseries by maintaining the rainfall intensities IMD grid points as well as for the subbasins considered for the HEC-HMS model set-up.

- The event-based HEC-HMS model set to upper Tawi River basin up to the Jammu (Bikram chowk) gauging shows a very good and acceptable hydrograph shape and also responding very well to the rainfall occurrence in the Tawi river basin catchment.
- During calibration of the event-based HEC-HMS model using September 2014 event, the observed and computed peak discharges were 3724 m^3/s & 3214.7 m^3/s (with E_p= 15.8% & E_{pt}= -1.0 hr, NSE = 0.63, R^2 = 0.65, RMSE = 0.61 and PBIAS = 11.47%), 12569 m^3/s & 12201 m^3/s (E_p= 3.9% & E_{pt}= -0.16%, NSE = 0.79, R^2 = 0.86, RMSE = 0.47 and PBIAS = 36.48%), and 13552.4 m^3/s and 12232 m^3/s (E_p= 10.8%, E_{pt}= -0.83 hr, NSE = 0.82, R^2 = 0.87, RMSE = 0.42 and PBIAS = 28.55%), respectively at Udhampur (Salmay Bridge), Sidhara (Jammu) and Jammu (Bikram Chowk) gauging stations.
- During calibration of the event-based HEC-HMS model using September 2014 event, the observed and computed peak stages during calibration using September 2014 flood event were 9 m & 8.6 m (E_p= 4.7% & E_{pt}= -1.0 hr, NSE = 0.61, R^2 = 0.72, RMSE = 0.6 and PBIAS = 25.46%), 8.85 m & 8.9 m (E_p= -0.6%, E_{pt}= 0.16 hr, NSE = 0.57, R^2 = 0.75, RMSE = 0.7 and PBIAS = 10.37%), and 10.08 m & 10.1 m (E_p= -0.2%, E_{pt}= -0.83 hr, NSE = 0.81, R^2 = 0.87, RMSE = 0.4 and PBIAS = 13.14%) respectively at Udhampur (Salmay Bridge), Sidhara (Jammu) and Jammu (Bikram Chowk) gauging stations.
- Based on the presented various performance evaluation criteria, the performance of HEC-HMS model for Tawi river basin up to Jammu (Bikram Chowk) gauging station is considered as very good at Jammu (Bikram Chowk) and Sidhara (Jammu) gauging stations for simulation of discharge and stage hydrograph. However, for Udhampur (Salmay Bridge) gauging station, it is considered as good model performance.
- During validation of the event-based HEC-HMS model using August 2016 flood event, the observed and computed peak discharges were 4559.7 m^3/s & 1860.8 m^3/s (with E_p= 145% & E_{pt}= -1.1 hr, NSE = 0.70, R^2 = 0.88, RMSE = 0.5 and PBIAS = 30.86%) at Sidhara (Jammu) gauging station.
- Similarly, the observed and computed peak stages during validation were 7.4 m & 6.1 m (E_p= 21.3% & E_{pt}= -1.1 hr, NSE = 0.63, R^2 = 0.77, RMSE = 0.6 and PBIAS = -6.62%) at Sidhara (Jammu) gauging station.

- The HEC-HMS model performance is considered good to very good during validation process.
- The calibrated HEC-HMS model for the Tawi River basin up to Jammu (Bikram Chowk) can be confidently used for flood inundation mapping under climate change.
- Comparison of the flood inundation extent by HEC-RAS for lower Tawi river basin with Landsat 8 imagery for September 2014 event were matching closely with the flood inundation extent on the Landsat 8 imagery of 10 September 2014.
- Comparison of the flood inundation extent for the part of lower Tawi basin by HEC-RAS with extracted flood extent from LISS-III and LISS-IV imagery for September 2014 event suggests that the error in the flood extent area by HEC-RAS model were -9.17 % and -4.08 % as compared to the those extracted from LISS-III and LISS-IV imagery.
- Comparison of the flood inundation depth map by HEC-RAS for lower Tawi river basin with photograph from the campus of Sher-e-Kashmir University of Agricultural Sciences and Technology of Jammu (SKUAST-Jammu) is suggest that the flood inundation depth at the campus is around 35 cm (from photograph) and those from HEC-Ras was around 44 to 60 cm.
- For the September 2014 high flood event, the total flood inundated area computed in the lower Tawi basin based on the HEC-RAS simulated flood inundation map is about 22251.4 hectors (Ha) out of which 12096 Ha (120.96 km2) in India.
- Based on flood frequency analysis, it is found that the magnitude of extreme discharges at Udhampur (Salmay Bridge) gauging station ranges between approximately 900 m^3/s for 2-year return period and 7800 m^3/s for 500 returned period. Similarly, the average magnitude of the extreme flood discharge ranging from around 1554 m^3/s for 2-year return period to 26012 m^3/s for 500-year return period. At the Jammu (Bikram Chowk) gauging station, the average magnitude of the extreme flood discharge ranges between 2933 m^3/s for 2-year return period and 22153 m^3/s for 500-year return period.
- The estimated floods at Jammu (Bikram Chowk) gauging station were about 20739 m^3/s and 13604 m^3/s by using IAHS (2003) and WMO (2009) maps, respectively.
- The climate change impact study suggests that in terms of percentage change in wet day frequency, there could be an increase of 22-100% increase during the month of

June; whereas, there could be nearly 30% decrease during the month of November for al RCMs and RCP scenarios.

- For far future (2070-2099) and RCP8.5 scenario, the highest change in the mean monthly precipitation is predicted by BNU-ESM (≈100%) followed by ACCESS1-0 (120%) for the months July and August.
- Increasing trend in number of heavy rainy days is predicted by all the models across the basin in the range 15 to 35%. The total annual precipitation is also expected to increase in the range of 15-35%. Hence, for future flood assessment the historical observation could be perturbed in this range.
- Based on flood frequency analysis, total flood inundated area ranges between 10591 ha to 26305 ha (for Indian part, it is 4063 ha to 15163 ha) for design floods of 2-year to 500-year return periods, respectively. Similarly, total villages and population affected due flood will ranges between 83 to 117 and 8.07 to 8.16 Lakh, respectively. Further, the total affected agricultural and residential area will ranges between 2059 ha to 8719 ha and 83 to 371, respectively.
- The simulated peak discharges for four climate change scenarios (CC5, CC15, CC25 and CC35) were 13430.2, 15957.1, 17977.8 and 19874.9 m^3/s, respectively. Those value close to obtained based on the flood frequency analysis.
- Based climate change scenarios (CC5, CC15, CC25 and CC35), the total flood inundated area ranges between 22574 ha to 24348 ha (for Indian part, it is 12342 ha to 13746 ha). Similarly, the total affected agricultural and residential area will ranges between 6899 ha to 7841 ha and 278 to 268, respectively.
- It can be concluded that based on climate change scenarios of CC35 (35% increase in baseline rainfall event of September 2014), the flood affected area, agricultural and residential areas in the Indian territory in lower Tawi basin will increase by around 1700 ha, 1101 ha and 61 ha as compared to those during baseline period (September 2014), if the proper flood management activities will not be undertaken.

REFERENCES

Afshari, S., Tavakoly, A. A., Rajib, M. A., Zheng, X., Follum, M. L., Omranian, E., & Fekete, B. M. (2018). Comparison of new generation low-complexity flood inundation mapping tools with a hydrodynamic model. *Journal of Hydrology*, *556*, 539–556. https://doi.org/10.1016/j.jhydrol.2017.11.036.

Alganci, U., Besol B., and Sertel. E(2018). Accuracy assessment of different digital surface models. ISPRS Int. J. Geo-Inf., 7, 114; doi:10.3390/ijgi7030114.

Angelica L. Gutierrez-Magness, A. L., and McCuen, R. H. (2004) Accuracy Evaluation of Rainfall Disaggregation Methods. *J. Hydrolog. Engg*., 9(2), 71.78. DOI: 10.1061/(ASCE)1084-0699(2004)9:2(71).

Asadi, A. (2013). Application of HEC-HMS for Flood Forecasting in Kabkian Basin and Delibajak Subbasin in Iran. *IOSR Journal of Engineering*, *03*(09), 10–16. https://doi.org/10.9790/3021-03931016

Azmat, M., Qamar, M., & Umair, M. (2017). *Application of HEC-HMS for the event and continuous simulation in high-altitude scarcely-gauged catchment under changing climate*.

Ball, J. E. (1994). The influence of storm temporal patterns on catchment response. J. of Hydrol., 158, 285-303.

Bhat, M.S., Ahmad, B., Alam, A., Farooq, H. and Ahmad, S., (2019) Flood hazard assessment of the Kashmir Valley using historical hydrology. *Journal of Flood Risk Management*, *2.19:12 (Supply. 1:e12521,* https://doi.org/10.1111/jfr3.12521.

Bhat, M.S., Alam, A., Ahmad, B., Kotlia, B.S., Farooq, H., Taloor, A.K., Ahmad, S., (2019) Flood frequency analysis of river Jhelum in Kashmir basin. *Quaternary International*, *507*, 288-294.

Bhatt, S., and Ahmed. S. A. (2014), Morphometric analysis to determine floods in the Upper Krishna basin using Cartosat DEM, Geocarto Int., 29 (8): 878-894, DOI:10.1080/10106049.2013.868042.

Bhuiyan, H. A. K. M., McNairn, H., Powers, J., & Merzouki, A. (2017). Application of HEC-HMS in a cold region watershed and use of RADARSAT-2 soil moisture in initializing the model. *Hydrology*, *4*(1), 1–19. https://doi.org/10.3390/hydrology4010009

Bomers, A., Schielen, R. M. J., and Hulscher, S. J. M. H.: Decreasing uncertainty in flood frequency analyses by including historic flood events in an efficient bootstrap approach, Nat. Hazards Earth Syst. Sci., 19, 1895–1908, https://doi.org/10.5194/nhess-19-1895-2019, 2019.

Burian, S. and Durrans, S. (2002) Short Time-Interval Rainfall Disaggregation for Continuous Hydrologic Simulation. Journal of Water Management Modeling, R208-04. doi: 10.14796/JWMM.R208-04.

CGWB (2014). Ground Water Information Booklet Udhampur district, Jammu & Kashmir. http://cgwb.gov.in/District_Profile/JandK/Udhampur.pdf.

Chu, X., & Steinman, A. (2009). Event and Continuous Hydrologic Modeling with HEC-HMS. *Journal of Irrigation and Drainage Engineering*, *135*(1), 119–124. https://doi.org/10.1061/(asce)0733-9437(2009)135:1(119)

Clark, C. O. (1945) Storage and the Unit Hydrograph, Am. Soc. Civil Engg., Paper No. 2261, 1419-1488.

Clarke, J. I. (1996) Morphometry from Maps. Essays in geomorphology. Elsevier publication. Co., New York. 1996, pp 235-274.

Costabile, P., Costanzo, C., Ferraro, D., Macchione, F., & Petaccia, G. (2020). Performances of the new HEC-RAS version 5 for 2-D hydrodynamic-based rainfall-runoff simulations at basin scale: Comparison with a state-of-the art model. *Water (Switzerland)*, *12*(9), 1–19. https://doi.org/10.3390/W12092326

Courty, L. G, Soriano-Monzalvo, J. C., and Pedrozo-Acuña, A. (2018) Evaluation of open-access global digital elevation models (AW3D30, SRTM and ASTER) for flood modelling purposes, Journal of Flood Risk Reduction

Cunnane, C. (1987). Review of statistical models for flood frequency estimation. In Hydrologic frequency modeling (pp. 49-95). Springer, Dordrecht.

CWC (2001) Manual on Estimation of Design Flood", Hydrology Studies Organization, Central Water Commission, New Delhi.

Darji, K., Khokhani, V., Prakash, I., Mehmood, K., & Pham, B. T. (2019). Rainfall-Runoff Modelling Using HEC-HMS Model : An Application of Regression Analysis . *Journal of Emerging Technologies and Innovative Research (JETIR)*, *6*(5), 226–234.

Demir, V. and Kisi, O. (2016) Flood Hazard Mapping by Using Geographic Information System and Hydraulic Model: Mert River, Samsun, Turkey. Advances in Meteorology, Hindawi, Volume 2016, Article ID 4891015, 9 pages http://dx.doi.org/10.1155/2016/4891015.

Derdour, A., Bouanani, A., & Babahamed, K. (2018). Modelling rainfall runoff relations using HEC-HMS in a semi-arid region: Case study in Ain Sefra watershed, Ksour Mountains (SW Algeria). *Journal of Water and Land Development*, *36*(1), 45–55. https://doi.org/10.2478/jwld-2018-0005

Devi, N. N., Sridharan, B., Kuiry, S. N. (2015) Impact of urban sprawl on future flooding in Chennai city, India. J. Hydrol., 574 (2019), 486–496. https://doi.org/10.1016/j.jhydrol.2019.04.041.

Dikpal, R. L., Renuka Prasad, and Satish, T. J. K (2017). Morphometric analysis and sub-watershed prioritization of Welmal watershed, Ganale-Dawa River Basin, Ethiopia: implications for sediment erosion. Appl. Water. Sci., 7: 4399–4414.

Dragut, L., Schauppenlehner, T., Muhar, A., Strobl, J., and Blaschke. T (2009). Optimization of scale and parametrization for terrain segmentation: an application to soil-landscape modeling. Comput. Geosci., 35 (9):1875–1883.

Girish, G., Ambili, G. K., Jesiya, N. P., and Lemoon, K. (2016), Hydro-hypsometric analysis of tropical river basins, southwest coast of India using geospatial technology. J. Mt. Sci., 13 (5), 939-946.

Gopinath, G., Swetha, T. V., and Ashitha, M. K(2014). Automated extraction of watershed boundary and drainage network from SRTM and comparison with Survey of India toposheet. Arab. J. Geosci., 7 (7): 2625–2632.

Guhathakurta, P., Sreejith, O. P. & Menon, P.A. (2011) Impact of climate change on extreme rainfall events and flood risk in India. *J Earth Syst Sci* **120,** 359 (2011). https://doi.org/10.1007/s12040-011-0082-5.

Gupta HV, Sorooshian S, Yapo P. O. (1999) Status of automatic calibration for hydrologic models: comparison with multilevel expert calibration. J. Hydrolog. Eng., 4(2),135–143. doi:10.1061/(asce)1084-0699(1999) 4:2(135).

Halwatura, D., & Najim, M. M. M. (2013). Application of the HEC-HMS model for runoff simulation in a tropical catchment. *Environmental Modelling and Software*, *46*, 155–

162. https://doi.org/10.1016/j.envsoft.2013.03.006

Hjelmfelt, A. T. (1981). Overland flow from time-distributed rainfall. Journal of the Hydraulics Division, 107(2), 227-238.

Horritt, M.S., Bates, P.D. (2002) Evaluation of 1D and 2D numerical models for predicting river flood inundation, Journal of Hydrology, Volume 268, Issues 1–4, 87-99, https://doi.org/10.1016/S0022-1694(02)00121-X.

Horton, R. E. (1932). Drainage basin characteristics. Transactions, Am. Geop. Union. 14: 350-361.

Horton, R. E. (1945). Erosional development of streams and their drainage basins; hydrophysical approach to quantitative morphology. Bull. Geol. Soc. Am. 56: 275-370.

Hossain, S. Hewa, G. A. and Wella-Hewage, S. (2019). A Comparison of Continuous and Event-Based Rainfall–Runoff (RR) Modelling Using EPA-SWMM. *Water* 2019, 11, 611-635; doi:10.3390/w11030611.

Hurtrez, J. E., Sol, C., and Lucazeau, F (1999). Effect of drainage area on hypsometry from an analysis of small-scale drainage basins in the Siwalik hills (central Nepal). Earth Surf. Process. Landf., 24: 799–808.

Jain, A. O., Thaker, T. K., Chaurasia, A., Patel, P., and Singh. A. K (2017). Vertical Accuracy Evaluation of SRTMDEM-GL1, GDEM-V2, AW3D30, and CartoDEM-V3.1 of 30m resolution with Dual Frequency GNSS for Lower Tapi Basin India, Geocarto Int., , DOI: 10.1080/10106049.2017.1343392.

Lindsay, J. B., and Evans. M. G (2008). The influence of elevation error on the morphometrics of channel networks extracted from DEMs and the implications for hydrological modelling. Hydrol. Process., 22 (11):1588–1603.

Ma, H., Dong, X., Chang, W. (2018). Application of Synthetic Unit Hydrograph on HEC-HMS Model for Flood Forecasting. *MATEC Web of Conferences*, *246*. https://doi.org/10.1051/matecconf/201824601076

Magesh, N. S., Jitheshlal, K. V., Chandrasekar, N. K., Jini, V. (2012) GIS based morphometric evaluation of Chimmini and Mupily watersheds, parts of Western Ghats, Thrissur District, Kerala. India Earth Sc. Inform. 2012, 5(2): 111–121.

Mahala. A (2020). The significance of morphometric analysis to understand the hydrological and morphological characteristics in two different morpho-climatic settings. Appl. Water Sci., 10: 33. https://doi.org/10.1007/s13201-019-1118-2.

Majidi, a, & Shahedi, K. (2012). Simulation of Rainfall-Runoff Process Using Green-Ampt Method and HEC-HMS Model (Case Study: Abnama Watershed, Iran). *International Journal of Hydraulic …*, *1*(1), 5–9. https://doi.org/10.5923/j.ijhe.20120101.02

Merkel, W. H. (2002) Muskingum-Cunge Flood Routing Procedure in NRCS Hydrologic Models, Second Federal Interagency Hydrologic Modeling Conference on "Hydrologic Modelling for the 21st Century, July 28- August 1, 2002, Riviera Hotel, Las Vegas, Nevada.

Merwade, V., Olivera, F., Arabi, M., and Edleman, S. (2008) Uncertainty in flood inundation mapping: current issues and future directions, Journal of Hydrologic Engg., ASCE, 13(7), https://doi.org/10.1061/(ASCE)1084-0699(2008)13:7(608).

Miller. V. C(1953). A quantitative geomorphic study of drainage basin characteristics in the Clinch Mountain area, Virginia and Tennessee. Project NR, Technical Report 3, Columbia Univ., Department of Geology, ONR, Geography Branch, New York, , pp 389–042

Moradkhani, H. and Sorooshian, S. (2009), General review of rainfall-runoff modeling: model calibration, data assimilation, and uncertainty analysis, In Hydrological modelling and the water cycle, pp. 1-24. Springer, Berlin, Heidelberg.

Moriasi, D.N., Arnold, J.G., Van Liew, M.W., Bingner, R.L., Harmel, R.D., and Veith, T.L. (2007) Model evaluation guidelines for systematic quantification of accuracy in watershed simulations. Transactions of the American Society of Agricultural and Biological Engineers, 49350(3), 885−900.

Morris, D. G., and Heerdegen, R. G (1988). Automatically-derived catchment boundaries and channel networks and their hydrological applications. Geomorphology., 1:131–141.

Muller, J. E. (1968) An introduction to the hydraulic and topographic sinuosity indexes. Ann. Assoc. Am. Geogr., 58: 371–385.

Nash J. E., Sutcliffe J. V. (1970) River flow forecasting through conceptual models. Part I. A discussion of principles. J. Hydrol. 10:282–290.

Nautiyal. M. D., (1994) Morphometric analysis of a drainage basin, district Dehradun, Uttar Pradesh. J. Indian. Soc. Remote Sens. 22(4): 251–261.

Nikolakopoulos, K. G(2020). Accuracy assessment of ALOS AW3D30 DSM and comparison to ALOS PRISM DSM created with classical photogrammetric techniques. European J. of Rem. Sens., 1-14. DOI: 10.1080/22797254.2020.1774424.

Niyaji, B., Zaidi, S., and Masoud, M(2019). Comparative study of different types of digital elevation models on the basis of drainage morphometric parameters (Case Study of Wadi Fatimah Basin, KSA). Earth Sys. Env., DOI: 10.1007/s41748-019-00111-2.

Ntegeka V., Willems P., Roulin E. and Baguis P. (2014). Developing tailored climate change scenarios for hydrological impact assessments. Journal of Hydrology, 508, 307–321.

Oguchi, T(1997). Drainage density and relative relief in humid steep mountains with frequent slope failure. Earth Surf. Process. Landf., 22: 107–120.

Ohmori, H(1993). Changes in the hypsometric curve through mountain building resulting from concurrent tectonics and denudation. Geomorphology., 8: 263–277.

Oleyiblo, J. O., & Li, Z. J. (2010). Application of HEC-HMS for flood forecasting in Misai and Wan'an catchments in China. *Water Science and Engineering*, *3*(1), 14–22. https://doi.org/10.3882/j.issn.1674-2370.2010.01.002

Pike, R. J. (2002) A Bibliography of Terrain Modeling (Geomorphometry), the Quantitative Representation of Topography - Supplement 4.0. (USGS, Open File Report 02-465). Menlo Park, Calif.: US Department of the Interior, United States Geological Survey.

Pike, R. J., and Wilson, S. E. (1971). Elevation-relief ratio, hypsometric integral and geomorphic area—altitude analysis. Geol. Soc. Am. Bull., 82: 1079–1084.

Prabhakaran, A., and Jawahar Raj, N. (2018). Drainage morphometric analysis for assessing form and processes of the watersheds of Pachamalai hills and its adjoining, Central Tamil Nadu, India. App. Water Sci., 8-31.

Rahman, K. U., Balkhair, K. S. Almazroui, M. Masood, A. (2017) Sub-catchments flow losses computation using Muskingum–Cunge routing method and HEC-HMS GIS based techniques, case study of Wadi Al-Lith, Saudi Arabia, Model. Earth Syst. Environ. (2017) 3:4. DOI 10.1007/s40808-017-0268-1.

Rao, A.R., Hamed, K.H. (2000) Flood Frequency Analysis. CRC Press, Boca Raton, FL.

Ray, K., Bhan, S. C. and Bandopadhyay, B. K. (2015) The catastrophe over Jammu and Kashmir in September 2014: a meteorological observational analysis. *Current Science*, 109(3), 580-591.

Ritter, D. F., Kochel, R. C., and Miller, J. R(2002). Process geomorphology, McGraw Hill, Boston, USA.

Sahoo, A., and Ghose, D. K. (2021) Flood Frequency Analysis for Menace Gauging Station of Mahanadi River, India. *J. Inst. Eng. India Ser. A*, Springer, 1-12. https://doi.org/10.1007/s40030-021-00544-x.

Sampath, D. S., Weerakoon, S. B., & Herath, S. (2015). HEC-HMS model for runoff simulation in a tropical catchment with intra-basin diversions – case study of the Deduru Oya river basin, Sri Lanka. *Engineer: Journal of the Institution of Engineers, Sri Lanka*, *48*(1), 1. https://doi.org/10.4038/engineer.v48i1.6843

Saran, S., Sterk, G., Peters, P., and Dadhwal. V. K. (2010), Evaluation of digital elevation models for delineation of hydrological response units in a Himalayan watershed. Geocarto Int.. 25: 105–122. https://doi.org/10.1080/10106040903051967.

Schendel, T. and Thongwichian, R. (2017) Considering historical flood events in flood frequency analysis: Is it worth the effort?, Adv. Water Resour., 105, 144 – 153. https://doi.org/10.1016/j.advwatres.2017.05.002.

Schumm, S. A (1956). Evolution of drainage system and slope in badlands of Perth Amboy. New Jersey., 67: 597–546.

ShahiriParsa, A., Noori, M., Heydari, M., & Rashidi, M. (2016). Floodplain zoning simulation by using HEC-RAS and CCHE2D models in the Sungai Maka river. *Air, Soil and Water Research*, *9*, 55–62. https://doi.org/10.4137/ASWR.S36089

Sharma, S., and Mahajan. A. K (2020). GIS-based sub-watershed prioritization through morphometric analysis in the outer Himalayan region of India. Appl. Water Sci., 10:163. https://doi.org/10.1007/s13201-020-01243-x.

Shreve, R. W (1969). Stream lengths and basin areas in topologically random channel networks. J. Geol., 77: 397–414.

Singh, P., Gupta, A., and Singh. M (2014). Hydrological inferences from watershed analysis for water resource management using remote sensing and GIS techniques. The Egyp. J. Remote Sens. Sp. Sci., 17, 111–121.

Singh, P., Thakur, J. K., and Singh, U. C (2013). Morphometric analysis of Morar River Basin, Madhya Pradesh, India, using remote sensing and GIS techniques. Environ. Earth. Sci., 68 (7):.1966-1977.

Singh, W. R., & Jain, M. K. (2015). Continuous Hydrological Modeling using Soil Moisture Accounting Algorithm in Vamsadhara River Basin, India. *Journal of Water Resource and Hydraulic Engineering*, *4*(4), 398–408. https://doi.org/10.5963/jwrhe0404011

Stephens, C. M., Johnson, F. M., and Marshall L. A. (2018) Implications of future climate change for event-based hydrologic models, Advances in Water Resources 119 (2018) 95–110. https://doi.org/10.1016/j.advwatres.2018.07.004.

Strahler, A. N. (1952). Hypsometric analysis of erosional topography. Bull. Geol. Soc. Am., 63: 1117–1142

Strahler, A. N. (1964). Quantitative geomorphology of drainage basins and channel networks. In: Chow VT (ed) Handbook of applied hydrology. McGraw-Hill, New York., pp 439–476.

Summerfield, M. A., and Hulton, N. J(1994). Natural controls of fluvial denudational rates in major world drainage basins. J. Geophys. Res., 99 (B7): 13871–13883.

Szypuła, B. (2017) Digital Elevation Models in Geomorphology. 5th Chapter in: Hydro-Geomorphology - Models and Trends. Intech. pp. 81-112. http://dx.doi.org/10.5772/intechopen.68447.

Tarik Benkaci (2021). Flood Frequency Distribution (FFD 2.1) (https://github.com/TBenkHyd2/Flood_Freq_Matlab), GitHub. Retrieved May 20, 2021.

Teng, J., Jakeman, A.J., Vaze, J., Croke, B.F., Dutta, D. and Kim, S. (2017), Flood inundation modelling: A review of methods, recent advances and uncertainty analysis. Environmental Modelling & Software, 90, pp.201-216.

Thol, T., Kim, L., Ly, S., Heng, S., & Sun, S. (2016). Application of Hec-Ras for a Flood Study of a River Reach in Cambodia. *Proceedings of the 4th International Young Researchers' Workshop on River Basin Environment and Management*, *November*, 12–13.

Traore, V. B., Bop, M., Faye, M., & Giovani, M. (2016). *Using of Hec-ras Model for Hydraulic Analysis of a River with Agricultural Vocation : A Case Study of the Kayanga River Basin , Senegal*. *January 2015*. https://doi.org/10.12691/ajwr-3-5-2

Traore, V. B., Bop, M., Faye, M., Giovani, M., Gueye, E. H. O., Sambou, H., Dione, A. N., Fall, S., Diaw, A. T., Sarr, J., & Chedikh Beye, A. (2015). Using of Hec-ras Model for Hydraulic Analysis of a River with Agricultural Vocation : A Case Study of the Kayanga River Basin , Senegal. *Science and Education Publishing*, *3*(5), 147–154. https://doi.org/10.12691/ajwr-3-5-2

Tutorial; GIS and Water Resources Modeling Workshop, https://web.ics.purdue.edu/~vmerwade/tutorial.html.

U.S. Army Corps of Engineers (2000). Hydrologic modelling System (HEC-HMS): Technical Reference Manual. Institute for Water Resources. Davis: Hydrologic Engineering Center.

U.S. Army Corps of Engineers (2020). HEC-RAS Mapper User's Manual: Version 6.0.

U.S. Army Corps of Engineers (USACE) (2021a). HEC-HMS User's Manual: Version 4.7.1. Davis: Institute for Water Resources, Hydrologic Engineering Center.

U.S. Army Corps of Engineers (2021b). HEC-RAS User's Manual: Version 6.1.

Vaze, J., Jordan, P., Beecham, R., Frost, A. and Summerell, G. (2012), Guidelines for rainfall-runoff modelling. Australian Government Department of Innovation, Industry, science and Research.

Venkata Rao, G., Venkata Reddy, K., Srinivasan, R., Sridhar, V., Umamahesh, N. V., Pratap, D., 2020. Spatio-temporal analysis of rainfall extremes in the flood-prone Nagavali and Vamsadhara Basins in eastern India. Weather Clim. Extrem. 29, 100265. https://doi.org/10.1016/J.WACE.2020.100265

Verma, A. K., Jha, M. K., & Mahana, R. K. (2010). Evaluation of HEC-HMS and WEPP for simulating watershed runoff using remote sensing and geographical information system. *Paddy and Water Environment*, *8*(2), 131–144. https://doi.org/10.1007/s10333-009-0192-8.

Willems, P., Vrac, M., 2011. Statistical precipitation downscaling for small-scale hydrological impact investigations of climate change. J. Hydrol. 402, 193–205. https://doi.org/10.1016/J.JHYDROL.2011.02.030

Wilson, J. P., Aggett, G., Deng, Y., and Lam, C. S(2008). Water in the landscape: a review of contemporary flow routing algorithms. In: Zhou Q, Lees B, Tang G (eds) Advances in digital terrain analysis. Lecture notes in geoformation and cartography series, vol 3. Springer, Berlin., pp 213–236.

Woolhiser, D. A. and Goodrich, D. C. (1988). Effect of storm rainfall intensity patterns on surface runoff." J. of Hydrol., 102, 335-354.

Study Team

Director : Dr. Jaivir Tyagi

Head (WHRC, Jammu): Dr M. K. Goel, Scientist 'G'

STUDY GROUP

Principal Investigator (PI) : Dr. Ravindra Vitthal Kale, Scientist 'D', WHRC

Team (Co-PI) : Dr. P. G. Jose, Scientist 'D',